NASA

MEMORANDUM

ESTIMATION OF DIRECTIONAL STABILITY DERIVATIVES AT SMALL ANGLES AND SUBSONIC AND SUPERSONIC SPEEDS

By Frederick K. Goodwin and George E. Kaattari

Ames Research Center
Moffett Field, Calif.

NATIONAL AERONAUTICS AND SPACE ADMINISTRATION

WASHINGTON
December 1958
Declassified December 8, 1961

NASA MEMO 12-2-58A

NATIONAL AERONAUTICS AND SPACE ADMINISTRATION

NASA MEMO 12-2-58A

ESTIMATION OF DIRECTIONAL STABILITY DERIVATIVES AT SMALL ANGLES AND SUBSONIC AND SUPERSONIC SPEEDS

By Frederick K. Goodwin and George E. Kaattari

SUMMARY

Methods are presented for estimating the directional stability derivative increments contributed by the stabilizing surfaces of subsonic and supersonic aircraft. These methods are strictly applicable at zero angle of attack and small angles of sideslip. The procedure of totaling the incremental coefficients to obtain an estimation of the total empennage side-force and yawing-moment coefficient derivatives is also shown, together with numerical examples. A correlation is presented between estimated and experimental incremental coefficients which indicates that the methods of this report generally estimate the increment of side force gained by the addition of a panel to within ±10 percent of the experimental value while the yawing-moment increment is generally estimated to within ±20 percent. This is true for both subsonic and supersonic Mach numbers.

An example application of the methods to one of the problems in directional stability, that of minimizing the effect of Mach number on the side-force coefficient derivative of the empennage, is discussed.

INTRODUCTION

Flight through an increasingly large supersonic Mach number range and at the large angles of attack required for high altitude maneuvering has introduced a significant problem in maintaining directional stability. With increasing Mach number the side-force coefficients of the vertical stabilizing surfaces decrease. The high angles of attack introduce the nonlinear destabilizing effects of body vortices and reduced dynamic pressure in the region of the upper vertical stabilizing surface. These effects are briefly discussed by Nielsen and Kaattari in reference 1.

In this reference it is pointed out that the problem of determining the variation of the side-force and yawing-moment coefficients with angle of attack and angle of sideslip can be considered one of first determining the derivatives of these coefficients at zero angle of attack and small angles of sideslip and then determining the nonlinear effects of the vortices and the dynamic pressure associated with large angles of attack and sideslip. The purpose of this report is to consider in detail the first of these steps, and to present methods for estimating the derivatives of the side-force and yawing-moment coefficients at both subsonic and supersonic speeds. The second step, that of estimating the nonlinearities introduced at high angles, is considered by Kaattari in reference 2.

SYMBOLS

a	vertical semiaxis of body in region of the tail panels, in.
b	horizontal semiaxis of body in region of the tail panels, in.
B	body
c_r	exposed root chord of a panel, in.
C_n	yawing-moment coefficient, $\frac{\text{yawing moment}}{2s_W q_\infty S_W}$
C_{n_β}	rate of change of yawing-moment coefficient with angle of sideslip ($\beta \approx 0^\circ$), $\partial C_n/\partial\beta$, per radian
C_Y	side-force coefficient, $\frac{\text{side force}}{q_\infty S_W}$
C_{Y_β}	rate of change of side-force coefficient with angle of sideslip ($\beta \approx 0^\circ$), $\partial C_Y/\partial_\beta$, per radian
h	vertical distance of wing or horizontal tail above or below body center line, in.
H	horizontal tail
K	apparent mass ratio
$K_{H(B)}$	apparent mass ratio due to adding a horizontal tail to a body
$K_{V(B)}$	apparent mass ratio due to adding an upper vertical stabilizing surface to a body

$K_{V(BHU)}$ apparent mass ratio due to adding an upper vertical stabilizing surface to a combination of a body, horizontal tail, and lower vertical stabilizing surface

$K_{V(BU)}$ apparent mass ratio due to adding an upper vertical stabilizing surface to a combination of a body and lower vertical stabilizing surface

$K_{V(BW)}$ apparent mass ratio due to adding an upper vertical stabilizing surface to a combination of a body and wing

$K_{W(B)}$ apparent mass ratio due to adding a wing to a body

K' effective apparent mass ratio

l distance from the nose to the leading edge, body juncture of a panel, in.

$\bar{l}$ distance from the center of moments to the center of pressure of a panel, in.

l_m distance from the nose to the center of moments, in.

M_∞ free-stream Mach number

P added panel

q_∞ free-stream dynamic pressure, lb/sq in.

s panel span measured from the body center line, in.

s_H horizontal-tail semispan measured from the body center line, in.

s_U span of lower vertical stabilizing surface measured from the body center line, in.

s_V span of upper vertical stabilizing surface measured from the body center line, in.

s_W wing semispan measured from the body center line, in.

S_U exposed lower vertical stabilizing surface area, sq in.

S_V exposed upper vertical stabilizing surface area, sq. in.

S_W total wing area, sq. in.

U lower vertical stabilizing surface

V	upper vertical stabilizing surface
W	wing
Y	side force, lb
α	angle of attack, radians
β	angle of sideslip, radians
Δ	incremental coefficient due to the addition of a panel
λ	taper ratio
Λ_{LE}	sweep angle of leading edge of a panel, deg

THEORETICAL CONSIDERATIONS

The method presented here to estimate incremental values of the side-force coefficient derivative, ΔC_{Y_β}, is similar to that which is used to predict the lift characteristics of wing-body combinations in reference 3. Briefly, as stated in reference 1, the principle underlying the method is that the ratio of the change in side force due to the addition of a vertical stabilizing panel to the side force developed by the panel alone is the same as the ratio of the change in apparent mass of the cross section at the base of the empennage when the panel is added to the apparent mass of the panel alone. (The panel alone is taken as the exposed panel mounted on a reflection plane.) This principle is true only when the crossflow is two-dimensional, implying the configuration is "slender," and when the trailing edges of all the panels in the empennage lie in the base plane of the configuration (sketch (a)).

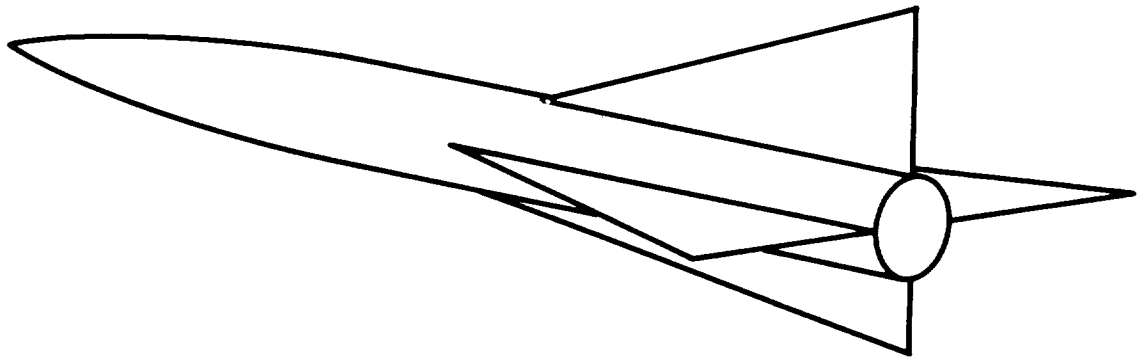

Sketch (a)

From the principle previously stated, the problem of estimating ΔC_{Y_β} resolves itself into the determination of two quantities, the apparent mass ratio, K, and the side-force curve slope of the added panel, $(C_{Y_\beta})_P$; that is,

$$\Delta C_{Y_\beta} = K(C_{Y_\beta})_P \tag{1}$$

The value of $(C_{Y_\beta})_P$ can be determined theoretically using, for example, reference 4, 5, or 6. For the greatest accuracy, an experimental value should be used if it is available.

To determine the apparent mass ratio, the work of Bryson, reference 7, has been used. In this work, a solution of the symmetric inertia coefficient tensor of the cross section of a body for the six apparent mass and apparent moment of inertia coefficients is presented. The only apparent mass that is necessary in determining ΔC_{Y_β} is that which is solely dependent on the potential due to a unit velocity in the lateral direction in the base plane of the model. In reference 7 this is referred to as m_{22}. Since K is the ratio of the change in apparent mass of the cross section at the base of the empennage when the panel is added to the apparent mass of the added panel alone, three apparent masses must be determined. These are: the apparent mass of the cross section of the complete empennage, the apparent mass of the cross section of the empennage without the panel, and the apparent mass of the exposed portion of the added panel mounted on an infinite reflection plane. The desired ratio, K, is then obtained by taking the difference of the first two of these three apparent masses and dividing by the third. Sketch (b) shows

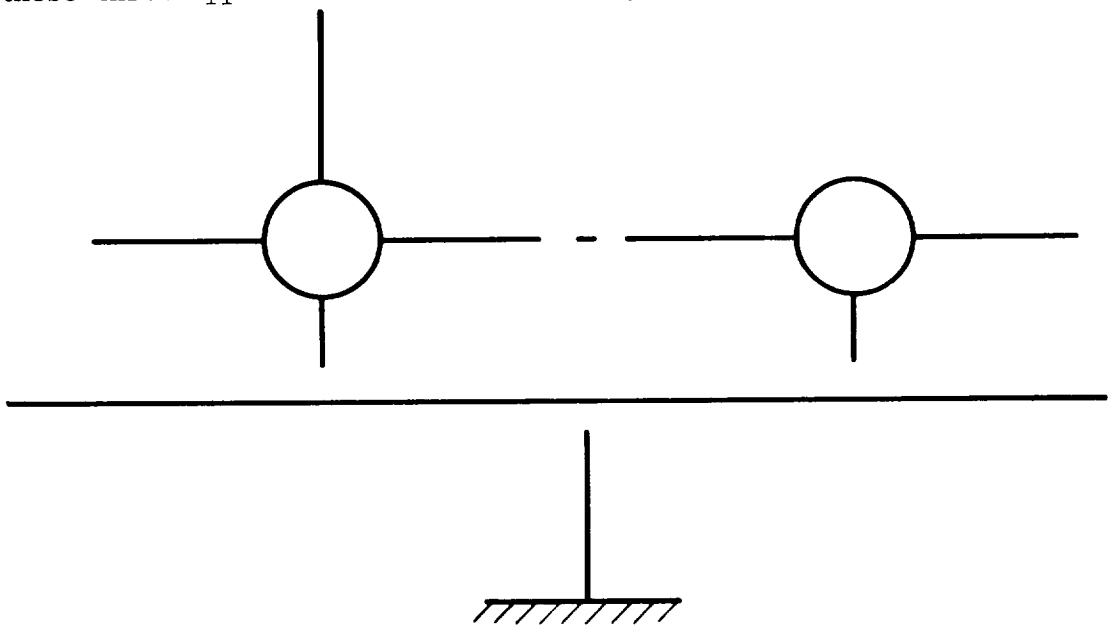

Sketch (b)

the cross sections whose apparent masses must be determined to obtain the value for K that would be used in estimating the increment, ΔC_{Y_β}, occurring when the upper vertical stabilizing surface is added to the combination of body, wing, and lower vertical stabilizing surface shown in sketch (a).

K Charts

The methods of references 7, 8, and 9 have been used to compute apparent mass ratios for various families of configurations and are presented as design charts in figures 1 through 13. The charts presented in figures 1 through 12 show apparent mass ratio as a function of a/s of the added vertical panel for various values of a/s of the existing vertical panel. Each chart is for a specific body cross-sectional shape, a/b ratio, and a specific body horizontal semiaxis - horizontal surface semispan ratio, b/s_H or b/s_W (i.e., the horizontal surface can be either the horizontal tail or the wing). A sketch of the typical cross section involved is shown on each chart with the added panel indicated by a dashed line. In utilizing these charts, it should be remembered that the added panel can be either the upper or lower vertical stabilizing surface; however, for convenience the sketches on the charts show only the upper vertical surface as the added panel. Special mention should be made of the K charts presented in figure 3. These charts are used in estimating ΔC_{Y_β} due to adding an upper vertical stabilizing surface to a body with a horizontal surface located in the high, tangent position. These charts also apply in estimating ΔC_{Y_β} due to adding a lower vertical stabilizing surface to a body with a horizontal surface located in the low, tangent position. Presented in figure 4 are K charts which are utilized in the same manner as figure 3, except that the horizontal surface is tangent to the body on the side opposite that to which the panel is added. An index of the K charts and the range of variables covered by each is presented in table I.

Estimation of Side-Force-Coefficient Derivative Increment ΔC_{Y_β}

Before presenting methods for estimating ΔC_{Y_β}, let us again look at the conditions of the method that were mentioned previously. They are that the crossflow be two-dimensional, that the configuration be "slender," and that the trailing edges of all the panels in the empennage be in the base plane of the model. A method that only applies to configurations which meet these conditions is quite limited in application. Therefore, to present a general method, it is necessary to determine some manner of handling cases which violate any or all of the conditions. In general,

it is found, as will be shown later, that good accuracy can be obtained for nonslender configurations where the crossflow is not strictly two-dimensional. It is also found that at subsonic speeds good accuracy can be obtained by determining the apparent mass ratio on the basis of the spans of the panels in the empennage regardless of longitudinal location.

In supersonic flow the components of a configuration give rise to numerous leading- and trailing-edge shock waves along its length. The characteristics of the longitudinal flow vary discontinuously in passing through these waves, thus creating a series of zones, each being characterized by a different apparent mass ratio. The supersonic interference problem thus requires a three-dimensional consideration. This three-dimensional effect is taken into account by determining the mean value of the apparent mass ratios from the various interference zones involved. This mean value, or the effective apparent mass ratio, K', gives good accuracy in determining the incremental directional coefficients.

Two methods for estimating ΔC_{Y_β} will now be presented in detail. The first is for subsonic speeds and the second is for supersonic speeds.

Subsonic speeds.- The method of determining $(C_{Y_\beta})_P$ will not be discussed in detail except to repeat that for the greatest accuracy the experimental value should be used. If this is not available, methods exist for determining this theoretically at subsonic speeds (e.g., refs. 4 and 5). To determine the apparent mass ratio, K, it is necessary to determine the ratios of body semiaxis to panel span for all the panels present in the empennage. For elliptical bodies, the body vertical semiaxis is used in conjunction with vertical stabilizing surface span, and the body horizontal semiaxis in conjunction with the horizontal surface semispan. If these semiaxes change length in the region of the panels in the empennage, the average lengths should be used. The ratio of the body vertical semiaxis to the body horizontal semiaxis, a/b, and the horizontal surface vertical position with respect to the body axis are also required. The value of K is determined by means of K charts appropriate to these parameters (or interpolation between charts if necessary). Then ΔC_{Y_β} is the product of these two quantities, $(C_{Y_\beta})_P$ and K. Appendix A presents a numerical example for a subsonic Mach number.

Supersonic speeds.- To clarify the method for estimating ΔC_{Y_β} at supersonic speeds, let us consider the empennage shown in sketch (c).

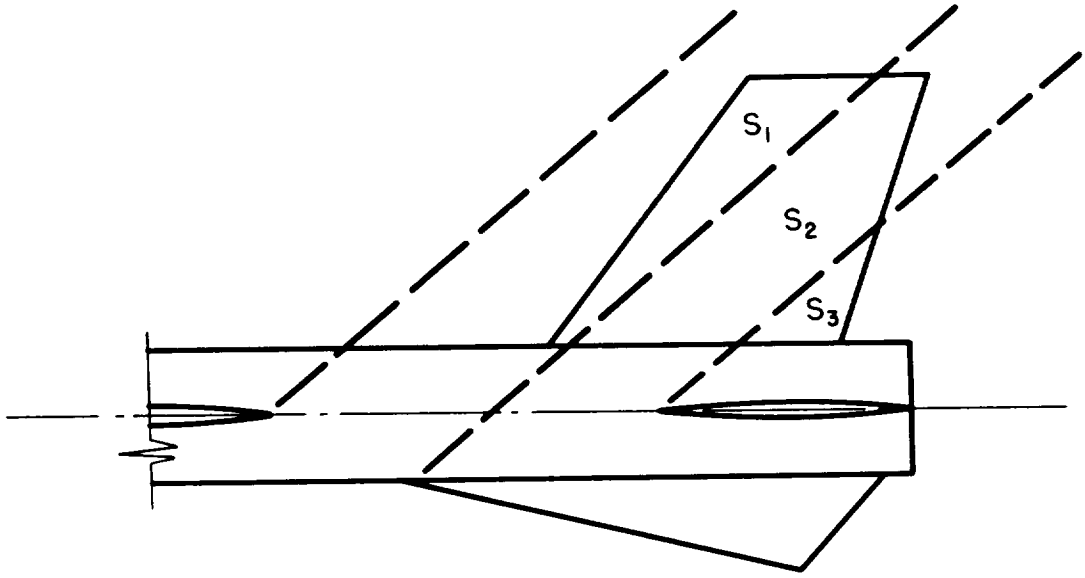

Sketch (c)

It is required to determine ΔC_{Y_β} due to adding the upper vertical stabilizing surface to the combination of body, wing, horizontal tail, and lower vertical stabilizing surface. To determine the effective apparent mass ratio, K', it is first necessary to draw in the Mach lines and trailing-edge shock waves emanating from the panels at zero angle of attack, as shown in sketch (c). Any point lying forward of the Mach line drawn from the leading-edge body juncture of a panel does not feel the presence of the panel, and it is assumed that any point lying behind the shock wave drawn from the trailing-edge body juncture of a panel does not feel the presence of the panel. With this in mind, it can be seen from sketch (c) that the upper vertical stabilizing surface is divided into three areas. Area S_1 senses only the presence of the body; area S_2, the body and lower vertical stabilizing surface; and area S_3, the body, horizontal tail, and lower vertical stabilizing surface. Since area S_1 senses only the body, the apparent mass ratio due to adding the upper vertical stabilizing surface to the body, $K_{V(B)}$, is determined from the K charts. In a similar manner, the apparent mass ratios due to adding the upper vertical stabilizing surface to the combinations of body and panels, S_2 and S_3, are also determined. The question arises as to whether the maximum spans of the areas affected by the different combinations or the total span should be used in determining these K's. For the sake of uniformity and simplicity in the calculations, the total spans are used in all cases. As will be shown later, this simplified procedure is justified on the basis of the degree of correlation which was obtained between the estimated and experimental values of ΔC_{Y_β}. It is assumed further that the contribution of each of these three apparent

mass ratios, $K_{V(B)}$, $K_{V(BU)}$, and $K_{V(BHU)}$, to K' is proportional to the percent of the total upper vertical stabilizing surface area, S_V, which senses each combination of body and panels. For the example shown in sketch (c), the expression for K' is

$$K' = K_{V(B)} \frac{S_1}{S_V} + K_{V(BU)} \frac{S_2}{S_V} + K_{V(BHU)} \frac{S_3}{S_V} \qquad (2)$$

This value of K' and the side-force curve slope of the added panel $(C_{Y_\beta})_P$ are used to determine ΔC_{Y_β} from equation (1) with K replaced by K'. In using this method for determining K', one can see from sketch (c) that for a sufficiently high Mach number it is possible for the wing, even though located forward of the upper vertical stabilizing surface, to affect this panel. This would add an additional term, the apparent mass ratio due to adding the upper vertical stabilizing surface to the body-wing combination, $K_{V(BW)}$, to the expression for K'. Appendix B presents a numerical example of the estimation of ΔC_{Y_β} for a supersonic Mach number.

Estimation of the Incremental Directional Coefficient ΔC_{n_β}

The method of estimating ΔC_{n_β} is simply that of multiplying the estimated value of ΔC_{Y_β} by the moment arm that equals the distance between the center of moments of the configuration and the center of pressure of the added vertical panel. Methods for estimating this center of pressure are given in reference 3 for plan forms having straight or sweptforward trailing edges. Additional considerations are necessary for configurations having sweptback trailing edges. In the present calculations the center of pressure was considered to be at the intersection of the mean aerodynamic chord and the quarter chord for subsonic speeds and at the centroid of area for supersonic speeds. The numerical examples presented in appendixes A and B show the determination of ΔC_{n_β} for these two cases.

Estimation of Directional Coefficient Derivatives of the Complete Empennage

A necessary extension of the method presented to estimate increments due to the addition of one panel to an empennage is to determine the total empennage side-force at zero angle of attack and small angles of sideslip which results from the addition of all the panels, both horizontal and vertical, to the body. The simplest method of doing this is to total the

increments gained by successive additions of the panels. For example, it is desired to find the side force gained by the addition of a horizontal tail, upper vertical stabilizing surface, and lower vertical stabilizing surface to a body. The first step is to find the increment gained by the addition of the horizontal tail to the body. Next, the increment gained by the addition of the upper vertical stabilizing surface to the combination of body and horizontal tail is found. Finally, the increment gained by the addition of the lower vertical stabilizing surface to the combination of body, horizontal tail, and upper vertical stabilizing surface is determined. This order of configuration build-up is usually used. An exception to this is the case at supersonic speeds where the vertical panels are staggered along the body so that their leading edges intersect the body at quite different locations. In this case, the panel whose leading edge intersects the body the farthest aft is added before the other panel, in order to obtain the most realistic estimate of the side force. If the panel lying the farthest forward is added first, the interference effects will be overestimated by the method presented here.

Discussion in the previous sections has been limited to determining increments due to the addition of a vertical panel. The method of estimating the increment due to the addition of a horizontal surface requires a somewhat different approach. The addition of a horizontal surface, either a horizontal stabilizer or a wing, in a low or high tangent location to a body, defines a ratio $K_{H(B)}$ or $K_{W(B)}$ which is defined as

$$K_{H(B)} = \frac{Y_{HB} - Y_B}{Y_B} \tag{3a}$$

or

$$K_{W(B)} = \frac{Y_{WB} - Y_B}{Y_B} \tag{3b}$$

In this apparent mass ratio, the side force developed by the body alone has been used to normalize the change in side force due to adding the horizontal surface to the body. This quantity, rather than the side force developed by the added surface which was used for the case of an added vertical panel, has been used, since a horizontal surface by itself develops no side force and would result in an infinite apparent mass ratio and an indeterminate solution for side force.

To estimate the increment gained by the addition of a horizontal surface, figure 13 is used to obtain the apparent mass ratio $K_{H(B)}$ or $K_{W(B)}$. This is then multiplied by the side-force curve slope of the body, as determined by experiment or slender-body theory. In coefficient form this increment is, therefore,

$$\Delta C_{Y_\beta} = K_{H(B)}(C_{Y_\beta})_B \tag{4a}$$

or

$$\Delta C_{Y_\beta} = K_{W(B)}(C_{Y_\beta})_B \tag{4b}$$

depending on whether it is the horizontal stabilizer or the wing which is added.

At subsonic speeds this increment is used as presented. However, at supersonic speeds it is necessary to use the Mach lines and shock waves from the horizontal surface to determine what portion of this incremental gain is realized. It is assumed that this gain through interference is felt over the area on the body defined by the Mach lines and shock waves from the leading- and trailing-edge body junctures. Sketch (d) shows two possibilities and the region of interference for each. The

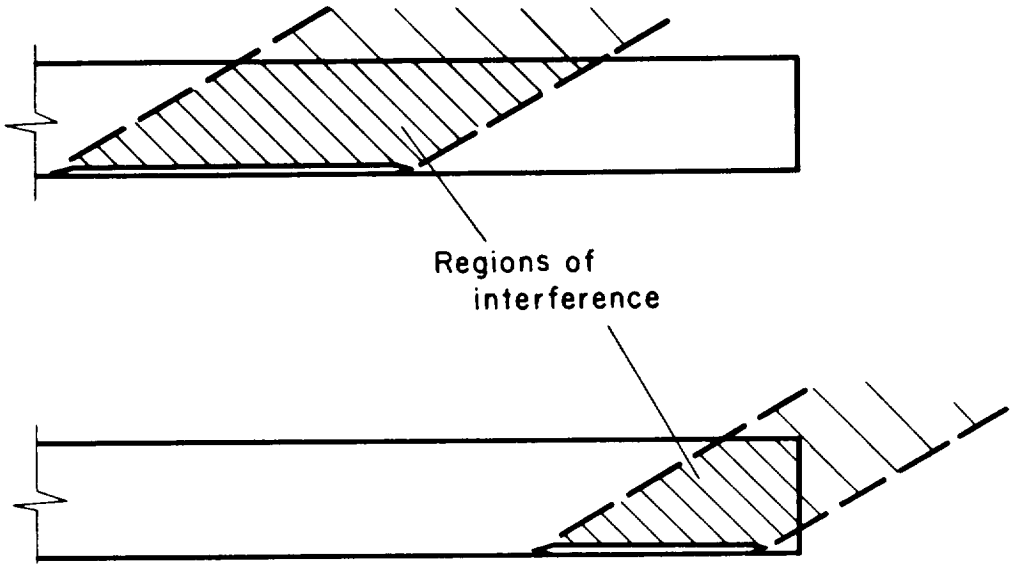

Sketch (d)

entire incremental gain is realized in the case of the top configuration. For the case presented in the lower part of sketch (d), the portion of the incremental gain that is realized is proportional to the ratio of the area of the actual region of interference to the area for a body extended indefinitely.

To determine the yawing-moment coefficient derivative of the complete empennage, the appropriate moment arms are applied to each of the incremental side-force quantities. The centroid of area of the region of interference approximates the moment arm in the case of the increment gained by adding the horizontal surface. For the other increments the methods presented previously are used.

Appendix C presents a numerical example showing the calculation of the side-force and yawing-moment coefficient derivatives of the complete empennage for a supersonic Mach number.

RESULTS AND DISCUSSION

Comparison Between Estimated and Experimental Values of the Stability Derivatives

To evaluate the methods presented in this report for estimating the directional coefficient derivative increment gained by the addition of a vertical stabilizing panel to an empennage, a series of calculations have been made for configurations for which experimental data exist. The geometric and aerodynamic characteristics of these configurations are presented in table II for the subsonic cases, and in table III for the supersonic cases. The correlation between the estimated and the experimental values of ΔC_{Y_β} is shown in figure 14. A 45° line denoting perfect agreement is shown, as are ±10-percent deviation lines. At subsonic Mach numbers (fig. 14(a)), the use of K to estimate ΔC_{Y_β} generally results in accuracy that is within ±10 percent of experiment. The same degree of correlation is also obtained when K' is used to estimate ΔC_{Y_β} for the supersonic Mach number cases (fig. 14(b)). The scatter in both correlations appears to be random about the line of perfect agreement.

The question arises as to whether sufficient accuracy could be obtained if K, at subsonic speeds, or K', at supersonic speeds, were ignored and the side-force curve slope of the added panel were used as an estimation of ΔC_{Y_β}. If the cases presented in tables II and III are examined, it can be seen that there are some where the value of K or K' is close to 1.00. If this quantity were ignored in these cases little effect on the correlation would result. However, there are a number of cases where K or K' is significantly larger than 1.00, so that ignoring this quantity in these cases would result in a considerable underestimation of ΔC_{Y_β}. Figure 15 is presented to show graphically the improvement in the over-all correlation through the use of K or K'. The open symbols show the comparison between estimated and experimental values when K or K' is ignored. Generally, ΔC_{Y_β} is underestimated. When K or K' is used to account for interference effects, the correlation shown by the solid symbols results.

The method presented for estimating the stability derivative increments at supersonic speeds requires the determination of an effective apparent mass ratio, K', to account for the three-dimensional nature of the flow. To justify the use of this effective apparent mass ratio, rather than the apparent mass ratio applying at subsonic speeds, let us

look at table III and figure 16. In table III the values of both K and K' are given, along with the stability derivatives determined by each. In a number of the cases K and K' are equal. This is true for cases where a vertical stabilizing surface is added to a body alone or to a body-wing combination where the wing is located far enough forward that its presence is not sensed by the added panel. The cases where K and K' are not equal are shown in figure 16. The open symbols show the correlation when K is used, and the solid symbols, the correlation when K' is used. As can be seen from this figure, there is a marked improvement in the correlation when K' is used in estimating ΔC_{Y_β} at supersonic speeds.

Figure 17 presents the correlation between the estimated and experimental values of ΔC_{n_β} for subsonic speeds (fig. 17(a)) and supersonic speeds (fig. 17(b)). For both speed ranges the method presented previously, that of applying a moment arm to the estimated value of ΔC_{Y_β}, generally estimated ΔC_{n_β} to within ±20 percent of experiment. At supersonic speeds there are some cases which are off by more than this amount. Since ΔC_{Y_β} includes, in addition to the side force developed on the added panel, the side force developed on the body and other panels in the empennage through interference with the added panel, the use of the center of pressure of the added panel does not result in a realistic moment arm. The method of this report for estimating ΔC_{Y_β} does not permit a breakdown of this increment into the portions developed on each of the surfaces present in the empennage. If this could be done, and the appropriate moment arm applied to each of these portions, a better estimate of ΔC_{n_β} should be obtained.

Effect of Stabilizing Surface Arrangement on the Side-Force Coefficient Derivative of the Complete Empennage

A useful application of the method for estimating the side-force coefficient derivative of the complete empennage at zero angle of attack is in comparing the effectiveness of various stabilizing surface arrangements on minimizing the effect of Mach number on C_{Y_β}. Two families of configurations have been investigated and the results are presented in figures 18 and 19. The two configurations chosen have the same total wing area and the same total exposed vertical stabilizing surface area. The example of figure 18 has an original upper vertical stabilizing surface of aspect ratio 4.5, while that of figure 19, an aspect ratio of 2.0. The necessary dimensions for making the calculations are presented in figures 18(a) and 19(a).

Let us first consider the effect of shifting a part of the original upper vertical stabilizing surface area to a lower vertical stabilizing surface with the same exposed root chord. Figures 18(b) and 19(b) show

the results of shifting approximately 29 percent of this area. The shift of area of the configuration of figure 18(a) results in a gain in side force throughout the Mach number range considered (fig. 18(b)). At a Mach number of 4.0, even though the aspect ratios of the panels of the $S_U/S_V = 0.4$ configuration are less than that of the panel of the $S_U/S_V = 0.0$ configuration, the leading edges remain supersonic and the lift per unit area is the same so that the gain in side force is brought about by an increase in interference. The area that is shifted from the original upper vertical stabilizing surface is moved from a region of low sidewash velocity to a region of higher sidewash velocity which increases the effectiveness of this area as a lifting surface. At a Mach number of 1.5, the percentage gain over the $S_U/S_V = 0.0$ configuration is not nearly as large as it is at a Mach number of 4.0. This lower percentage increase can be explained by comparing the average lift per unit area of the vertical panels of the two configurations. At this Mach number the leading edge of the panel on the $S_U/S_V = 0.0$ configuration is supersonic, while reducing the aspect ratio by shifting the area causes the leading edges of the two panels on the $S_U/S_V = 0.4$ configuration to be subsonic. This results in a lower lift per unit area for the $S_U/S_V = 0.4$ case which partially offsets the gain in sidewash interference obtained by shifting the area.

The result of shifting the same amount of area of the original upper vertical stabilizing surface of the configuration shown in figure 19(a) to a lower vertical stabilizing surface is shown in figure 19(b). A gain is realized at the higher Mach numbers, while there is a loss at the lower Mach numbers. As was the case with the aspect ratio 4.5 configuration, there is an increase in interference throughout the Mach number range because of the shifting of the area to a region of higher sidewash velocity. At a Mach number of 4.0, this gain is partially lost because of a lower average lift per unit stabilizer area. The lower vertical stabilizing surface of the $S_U/S_V = 0.4$ configuration has a subsonic leading edge, while the upper vertical stabilizing surfaces of the two configurations have supersonic leading edges. At a Mach number of 1.5, the vertical panels of both configurations have subsonic leading edges, but the average lift per unit stabilizer area of the $S_U/S_V = 0.4$ case is so much lower than that of the $S_U/S_V = 0.0$ case that the gain in interference by shifting the area is more than offset and the net result is a decrease in the side-force coefficient derivative of the empennage.

If figures 18(b) and 19(b) are now compared, it can be seen that the $S_U/S_V = 0.4$ configuration of figure 19(b) is desirable for several reasons in the design of aircraft for a Mach number of 4.0. Among these are that the value of this coefficient changes the least with Mach number, the wave drag can be reduced, and with the smaller spans involved, lighter structures can be used.

Figures 18(c) and 19(c) show the effect of horizontal-surface position on the side-force coefficient derivative of the complete empennage. The $S_U/S_V = 0.4$ configurations from figures 18(b) and 19(b) have been used as the basic configurations, since their characteristics are more desirable than those of the $S_U/S_V = 0.0$ cases (i.e., the percent decrease with increasing Mach number is less). Since the side-force curve slopes of the vertical panels alone do not change with the addition of a horizontal surface, the changes in side force result from the interference effects.

Let us first consider the case of adding a horizontal surface in the mid-position. Figures 18(c) and 19(c) both show the same result when this is done, a slight gain in side force throughout the Mach number range. This is brought about by small changes in sidewash over the two vertical panels. When the horizontal surface is added, a small amount of sidewash is diverted from the lower vertical tail to the upper vertical tail. Since the upper panel is a more effective lifting surface than the lower panel, a gain in side force results. When the horizontal surface is added in the high tangent position, a gain in side force throughout the Mach number range considered is again obtained. This gain is the net result of a gain in the side force developed by the body, a decrease in that developed by the addition of the upper vertical panel, and an increase in that developed by the addition of the lower vertical panel. Favorable wing-body interference, taken into account by $K_{W(B)}$, causes the increase on the body. The change in the side force developed by the addition of the panels is caused by the horizontal surface diverting sidewash from the upper panel to the lower panel. Also, the effect of Mach number is less on this configuration since a larger portion of the side force is developed on the body and the low-aspect-ratio lower vertical stabilizing surface. The side-force curve slopes of these surfaces are affected less by Mach number than that of the upper vertical stabilizing surface.

When the horizontal surface is located in the low tangent position, there is also a gain in side force throughout the Mach number range considered in figures 18(c) and 19(c). The side force developed by the body is not affected by shifting the horizontal surface from the high to the low tangent position. If the sidewash over the empennage of this configuration is compared to that over the configuration without the horizontal surface, it is found that when the surface is added, sidewash is diverted from the lower vertical stabilizing surface to the upper vertical stabilizing surface. This causes an increase in the side force developed by the upper panel and a decrease in that developed by the lower panel. Since the side-force curve slope of the upper panel is the most sensitive to Mach number changes, the variation in side force with Mach number is the greatest for this case, as the greater portion of the total side force is developed by this panel.

The yawing-moment coefficient derivative curves of the complete empennages for the configurations of figures 18 and 19 would generally show the same qualitative effects of shifting vertical stabilizing surface area and adding a horizontal surface as the side-force curves show. The percentage decrease in C_{n_β} with increasing Mach number would be approximately the same since the moment arms used to convert side force to yawing moment are affected very little by Mach number. The high or low tangent horizontal surface cases would not show the gain over the horizontal surface off or mid horizontal surface cases that is shown in side force. The region of wing-body interference is generally disposed in longitudinal location so that its centroid of area is relatively close to the center of moments of the configuration. The side-force increment gained by the addition of the wing to the body would contribute little to the total moment. The high horizontal surface configuration gives the yawing-moment curve which is the least sensitive to Mach number changes.

CONCLUSIONS

The methods presented for estimating the directional stability derivative increments gained by the addition of vertical stabilizing surfaces to airplane and missile configurations are utilized in a series of calculations for configurations for which experimental data exist. Comparisons are presented, between the calculated and the experimental increments, which indicate the following:

1. The methods presented generally predict the side-force coefficient derivative increment, ΔC_{Y_β}, at zero angle of attack and small angles of sideslip, to within ±10 percent of that of experiment.

2. The yawing-moment coefficient derivative increment, ΔC_{n_β}, generally can be estimated to within ±20 percent of that of experiment by the application of a moment arm determined by the center of pressure of the added panel to the estimated value of ΔC_{Y_β}.

An example application to one of the problems in directional stability, that of minimizing the effect of Mach number on the side-force coefficient derivative of the complete empennage, demonstrates that the method is useful for preliminary design studies.

Ames Research Center
National Aeronautics and Space Administration
Moffett Field, Calif., Sept. 12, 1958

APPENDIX A

A NUMERICAL EXAMPLE OF THE DETERMINATION OF ΔC_{Y_β} AND ΔC_{n_β} FOR A CONFIGURATION OPERATING AT A SUBSONIC MACH NUMBER

As a numerical example of this type, let us consider configuration number 3 of table II and determine ΔC_{Y_β} and ΔC_{n_β} due to adding the upper vertical stabilizing surface to the combination of body, wing, and horizontal tail. The Mach number considered here is 0.06. Table II presents the dimensions necessary to make the calculations.

The first step is to determine the side-force curve slope of the added panel. The exposed upper vertical stabilizing surface is approximated by one which is trapezoidal in plan form. From reference 4, $(C_{Y_\beta})_V$ is found to be

$$(C_{Y_\beta})_V = -0.522 \text{ per radian}$$

referenced to the total wing area, S_W.

Next, the apparent mass ratio must be found. The empennage in this example consists of the body, the horizontal tail, and the upper vertical stabilizing surface. The apparent mass ratio to be found is that due to adding the upper vertical stabilizer to the combination of body and horizontal tail, $K_{V(BH)}$. The sketch of the configuration shown in table II shows that the body is nearly square in cross section. Since apparent mass solutions for bodies of other than circular or elliptic cross section are not available, the assumption is made that the ratio of height to width, a/b, is the important parameter and that the details of the body contour are of secondary importance. This assumption was used for the cases of tables II and III where the body is other than circular or elliptic. As can be seen from these tables, the resulting correlation with experiment is as good as for the cases to which the K charts apply directly.

From table II the necessary ratios for this configuration are: $a/b = 1.000$, $(b/s)_H = 0.275$, and $(a/s)_V = 0.206$. The horizontal tail is located in the mid-position, $h/a = 0.000$. Since this example does not have a lower vertical stabilizing surface, $(a/s)_U$ is equal to 1.000. Table I indicates that for these values of the parameters an interpolation must be made to obtain $K_{V(BH)}$. From figure 2(b), $(b/s)_H = 0.200$, $K_{V(BH)}$ is found to be 1.35. Figure 2(c), $(b/s)_H = 0.400$, gives a value of 1.24 and figure 2(d), $(b/s)_H = 0.600$, a value of 1.17. Interpolating graphically gives, for $(b/s)_H = 0.275$,

$$K_{V(BH)} = 1.30$$

For these values of $(C_{Y_\beta})_V$ and $K_{V(BH)}$, the increment of side force gained by adding the upper vertical stabilizing surface is

$$\Delta C_{Y_\beta} = K_{V(BH)}(C_{Y_\beta})_V$$

$$= -0.678 \text{ per radian}$$

This estimate corresponds to an experimental value of -0.64 per radian.

Since the added upper vertical stabilizing surface has a sweptback trailing edge, the intersection of the quarter chord and the mean aerodynamic chord is used in determining ΔC_{n_β}. This is found to lie at 56.1 percent of the exposed root chord. Therefore, the moment arm, made dimensionless by dividing by the total wing span, is

$$\frac{\bar{l}}{2s_W} = \frac{l_m - l_V - 0.561\, c_r}{2s_W}$$

$$= -0.451$$

and

$$\Delta C_{n_\beta} = \frac{\bar{l}}{2s_W}(\Delta C_{Y_\beta})$$

$$= 0.306 \text{ per radian}$$

This estimate corresponds to an experimental value of 0.28 per radian.

APPENDIX B

A NUMERICAL EXAMPLE OF THE DETERMINATION OF ΔC_{Y_β} AND ΔC_{n_β} FOR A CONFIGURATION OPERATING AT A SUPERSONIC MACH NUMBER

As a numerical example of this type, let us consider configuration number 3 of table III and determine ΔC_{Y_β} and ΔC_{n_β} due to adding the upper vertical stabilizing surface to the combination of body, wing, horizontal tail, and lower vertical stabilizing surface. The Mach number for this example is 2.01. Table III presents the dimensions necessary to make the calculations.

If the exposed upper vertical stabilizing surface is approximated by one which is trapezoidal in plan form, reference 6 can be used to determine the side-force curve slope of the panel. This is found to be

$$(C_{Y_\beta})_V = -0.398 \text{ per radian}$$

with S_W as the reference area.

The next step is to take the approximate planar view of this configuration, sketch (e), and draw in the shock wave from the wing trailing edge,

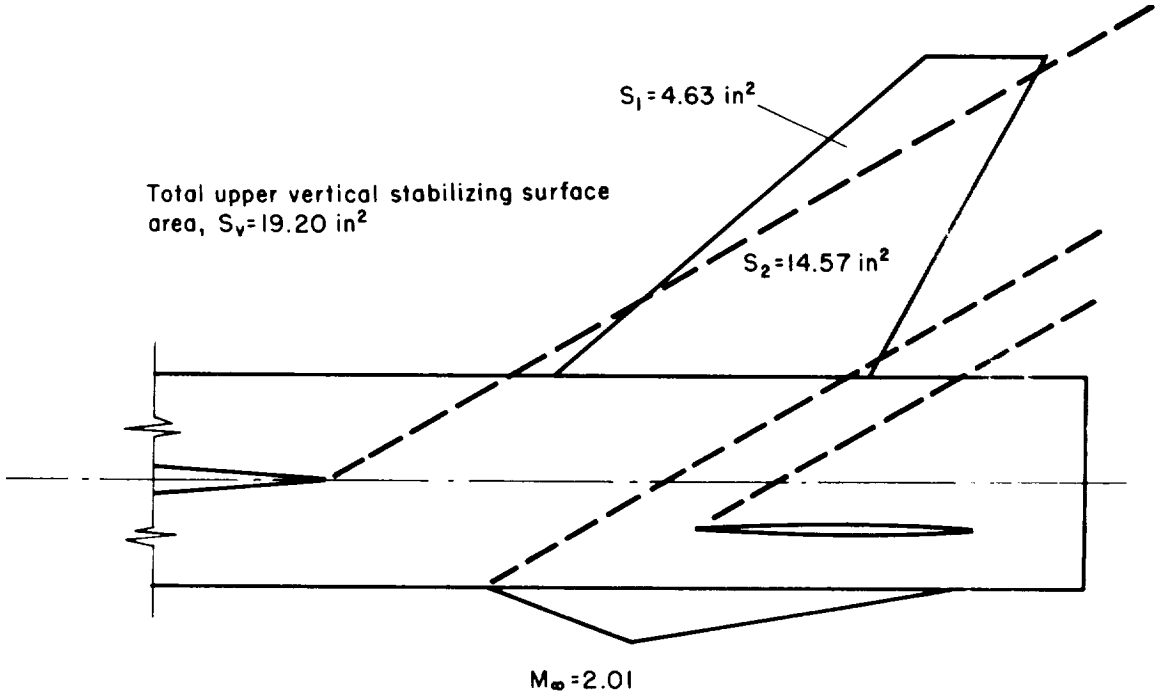

Sketch (e)

body juncture and the Mach lines from the leading edge, body junctures of the horizontal tail and the lower vertical stabilizing surface. This has been done in this sketch. Area S_1 senses the presence of the body and the wing. For this area the apparent mass ratio due to the addition of the upper vertical stabilizing surface to the body-wing combination, $K_{V(BW)}$, must be determined. Area S_2 senses only the body so that for this area $K_{V(B)}$ has to be determined. The contribution of each of these apparent mass ratios to the effective apparent mass ratio, K', is proportional to the percent of the total upper vertical stabilizing surface area which senses each combination. Therefore, the expression to be evaluated in order to determine K' is

$$K' = K_{V(BW)} \frac{S_1}{S_V} + K_{V(B)} \frac{S_2}{S_V}$$

To determine $K_{V(BW)}$, the following ratios have to be determined: a/b, $(b/s)_W$, and $(a/s)_V$. From table III a/b = 1.170, $(b/s)_W$ = 0.157, and $(a/s)_V$ = 0.247. The lower vertical stabilizing surface is not felt in this region, so that $(a/s)_U$ = 1.000. Since the wing is located in the mid-position, table I shows that a double interpolation will have to be made in order to obtain $K_{V(BW)}$ for a/b = 1.170 and $(b/s)_W$ = 0.157. Figures 8(a), 8(b), and 8(c) are used to determine $K_{V(BW)}$ for a/b = 0.667 and $(b/s)_W$ = 0.157. A graphical interpolation between these three figures gives $K_{V(BW)}$ = 1.48. For a/b = 1.000 figures 2(a), 2(b), and 2(c) are used and $K_{V(BW)}$ for $(b/s)_W$ = 0.157 is 1.49. Figures 10(a), 10(b), and 10(c) are used to determine $K_{V(BW)}$ for a/b = 1.500. This is found to be 1.45. Interpolating between these three values determines $K_{V(BW)}$ for a/b = 1.170, which is

$$K_{V(BW)} = 1.49$$

To determine $K_{V(B)}$ it is necessary to interpolate between figures 1, 7, and 9, since the region we are considering here does not sense the wing and, therefore, $(b/s)_W$ = 1.000. This interpolation gives

$$K_{V(B)} = 1.27$$

These apparent mass ratios, $K_{V(BW)}$ and $K_{V(B)}$, and the areas shown in sketch (e), determine K'.

$$K' = \frac{1.49(4.63)}{19.20} + \frac{1.27(14.57)}{19.20}$$

$$= 1.32$$

Since $(C_{Y_\beta})_V$ and K' are now known, we find

$$\Delta C_{Y_\beta} = K'(C_{Y_\beta})_V = -0.525 \text{ per radian}$$

This estimate corresponds to an experimental value of -0.52 per radian.

Since the upper vertical stabilizing surface has a sweptback trailing edge and we are considering a supersonic Mach number, the centroid of area of this panel is used in estimating ΔC_{n_β}. This is found to lie at 93.3 percent of the exposed root chord. Therefore, the moment arm made dimensionless by dividing by the total wing span is

$$\frac{\bar{l}}{2s_W} = \frac{l_m - l_V - 0.933\, c_r}{2s_W} = -0.575$$

and

$$\Delta C_{n_\beta} = \frac{\bar{l}}{2s_W}(\Delta C_{Y_\beta}) = 0.302 \text{ per radian}$$

This estimate corresponds to an experimental value of 0.30 per radian.

As another example in determining K', consider the case shown in sketch (f). This is the same configuration as was just considered;

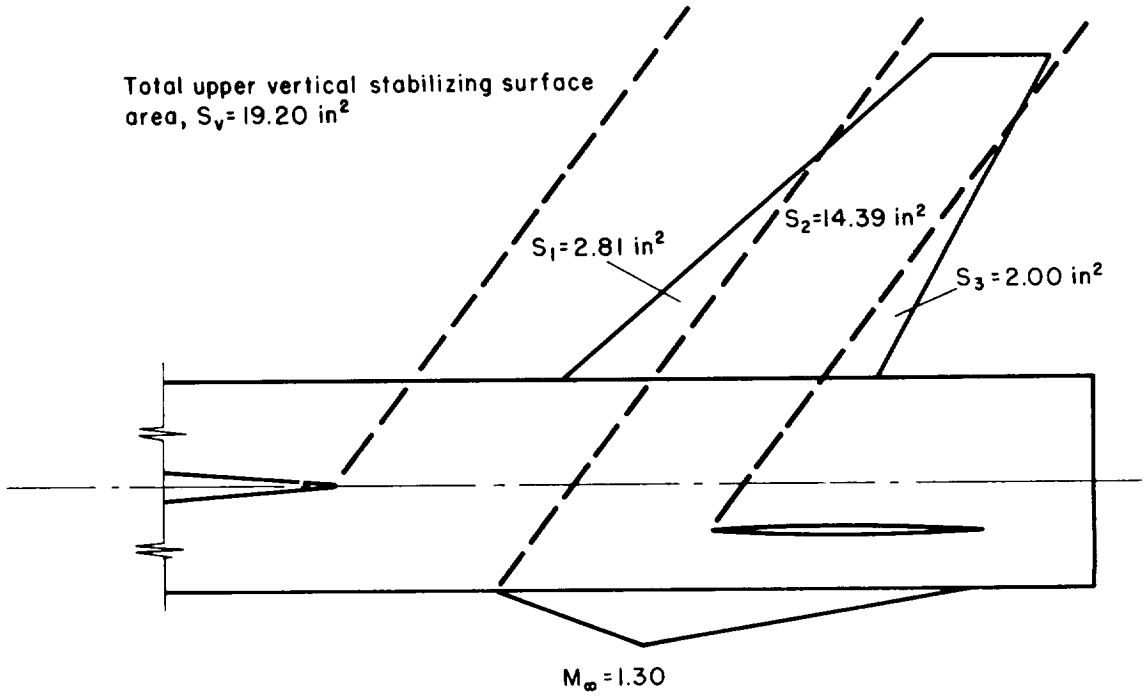

Sketch (f)

however, the Mach number is 1.30. If this sketch is compared with sketch (e), it can be seen that the upper vertical stabilizing surface now feels the presence of the horizontal tail and the lower vertical stabilizing surface over part of its area, and the wing is not sensed by any portion of the panel. The expression for the effective apparent mass ratio, K', for this case is,

$$K' = K_{V(B)} \frac{S_1}{S_V} + K_{V(BU)} \frac{S_2}{S_V} + K_{V(BHU)} \frac{S_3}{S_V}$$

The apparent mass ratio $K_{V(B)}$ has the same value as before; that is,

$$K_{V(B)} = 1.27$$

An interpolation between figures 1, 7, and 9 is made to determine $K_{V(BU)}$. From table III the necessary ratios are: $a/b = 1.170$, $(a/s)_U = 0.684$, and $(a/s)_V = 0.247$. A graphical interpolation gives

$$K_{V(BU)} = 1.30$$

The values of the ratios necessary to determine $K_{V(BHU)}$ are: $a/b = 1.170$, $(b/s)_H = 0.328$, $(a/s)_U = 0.684$, and $(a/s)_V = 0.247$. Since the horizontal tail is located below the body center line, $h/a = -0.480$, and the body is elliptical, we have a cross section for which K charts are not presented. To handle this case, either the body has to be considered circular in cross section and an interpolation made for horizontal-tail height, or the horizontal tail has to be assumed located in the mid-position and an interpolation performed between a/b ratios. A comparison of figures 2(c), 8(c), and 10(c) shows that a small variation from a body which is circular in cross section has little effect on the apparent mass ratio in the region in which this case falls, $(a/s)_V = 0.247$. Therefore, the interpolation for tail height will be made rather than for body shape. First, let us determine $K_{V(BHU)}$ for a combination of a body, high tangent horizontal tail ($h/a = 1.000$), and upper and lower vertical stabilizing surfaces. Figures 3(b), 3(c), and 3(d) are used and $K_{V(BHU)}$ for $(b/s)_H = 0.328$ is found to be 1.06. With the horizontal tail located in the mid-position ($h/a = 0.000$), figures 2(b), 2(c), and 2(d) give an interpolated value of $K_{V(BHU)} = 1.41$. Figures 4(b), 4(c), and 4(d) give a value of 1.68 for a low tangent horizontal tail ($h/a = -1.000$). An interpolation between these three values of $K_{V(BHU)}$ gives, for $h/a = 0.480$,

$$K_{V(BHU)} = 1.55$$

The values determined for $K_{V(B)}$, $K_{V(BU)}$, and $K_{V(BHU)}$ and the areas from sketch (f) yield

$$K' = \frac{1.27(2.81)}{19.20} + \frac{1.30(14.39)}{19.20} + \frac{1.55(2.00)}{19.20}$$

$$= 1.32$$

APPENDIX C

A NUMERICAL EXAMPLE OF THE DETERMINATION OF THE SIDE-FORCE AND YAWING-MOMENT DERIVATIVES OF THE COMPLETE EMPENNAGE

As a numerical example of this type, let us consider configuration number 3 of table III and determine C_{Y_β} and C_{n_β} due to adding the horizontal tail, upper vertical stabilizing surface, and lower vertical stabilizing surface to the body-wing combination. The Mach number for this case is 2.01 and the dimensions necessary for the calculations are presented in table III.

The first surface to be added to the body is the horizontal tail. The side-force curve slope of the body, as determined by slender-body theory and referenced to the total wing area, S_W, is

$$(C_{Y_\beta})_B = \frac{2\pi ab}{S_W}$$

$$= -0.147 \text{ per radian}$$

From table III the ratios necessary to determine $K_{H(B)}$ are $a/b = 1.170$, $(b/s)_H = 0.328$, and $h/a = -0.480$. Since K charts are not presented for the case where a horizontal surface is added to an elliptical body, the body will be considered circular and an interpolation made between the curves of figure 13 for horizontal surface height. From figure 13 we find that for $(b/s)_H = 0.328$, a surface mounted tangent to the body in either a high or low position gives a value of K equal to 1.06, and in the mid-position K is zero. In lieu of apparent mass solutions for adding a horizontal surface at an intermediate point on the body, it is assumed that small changes from a mid-position result in little additional interference. Therefore, rather than interpolating linearly a higher order interpolation is to be made. For the sake of simplicity the equation of an ellipse was used.

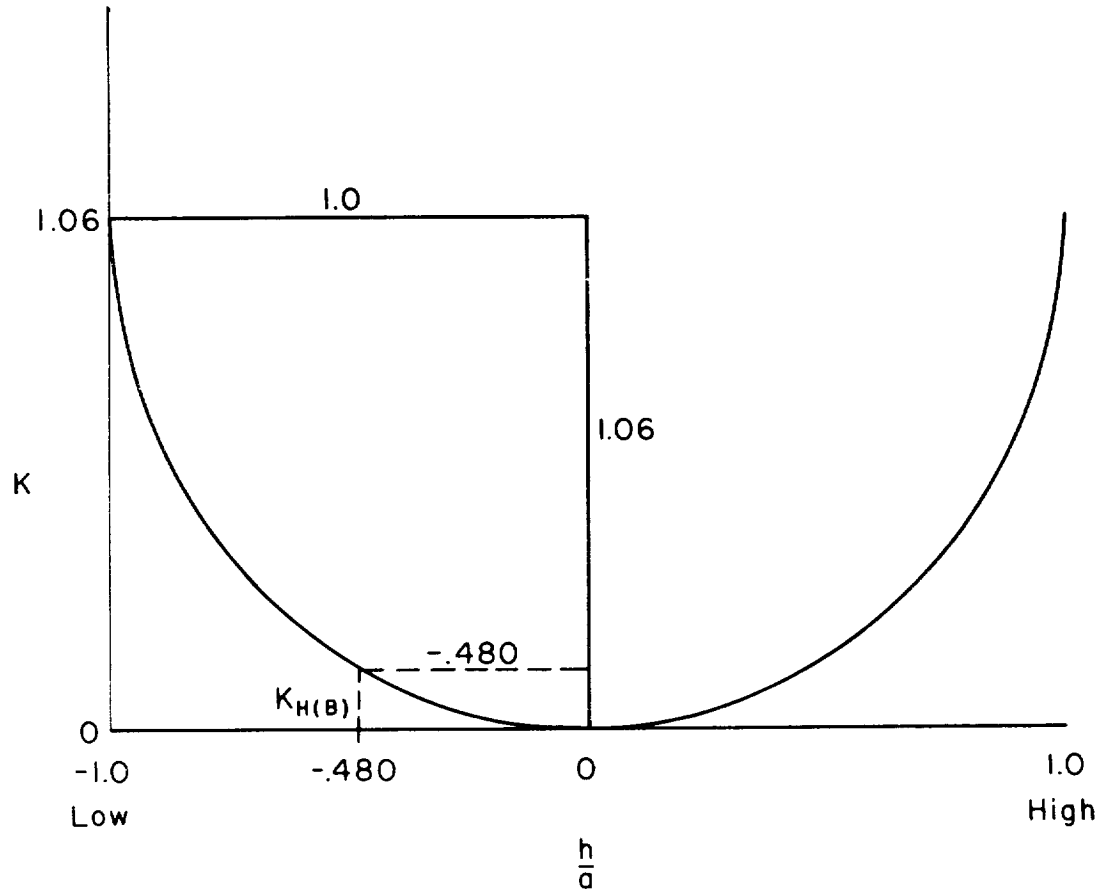

Sketch (g)

From sketch (g) the equation for $K_{H(B)}$ when $h/a = -0.480$ is

$$K_{H(B)} = K_{Low}\left[1 - \sqrt{1 - (h/a)^2}\right]$$

$$= 1.06\left[1 - \sqrt{1 - (-0.480^2}\right]$$

$$= 0.13$$

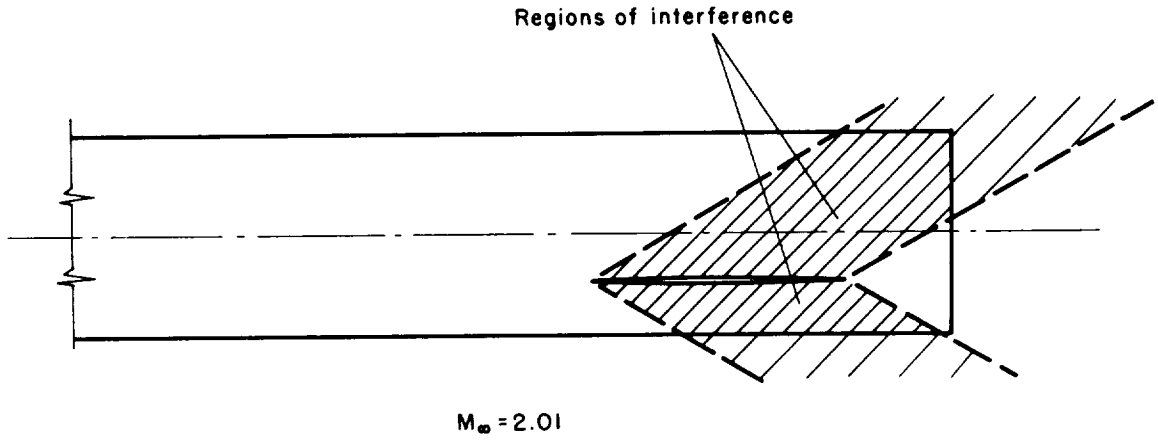

Sketch (h)

Sketch (h) shows that not all of the side-force increment gained by the addition of the horizontal surface to the body is realized, since a portion of the area determined by the shock waves and the body, if it were extended, lies behind the base of the actual body. Of the total area 87.5 percent lies on the body so that this percentage of the increment estimated by $K_{H(B)}$ and $(C_{Y_\beta})_B$ is realized.

$$(C_{Y_\beta})_{BWH} - (C_{Y_\beta})_{BW} = 0.875\, K_{H(B)} (C_{Y_\beta})_B$$

$$= -0.017 \text{ per radian}$$

The second increment to be determined is that due to adding the upper vertical stabilizing surface to the combination of body, wing, and horizontal tail. From reference 6 the side-force curve slope of this panel, referenced to the total wing area, S_W, is

$$(C_{Y_\beta})_V = -0.398 \text{ per radian}$$

Sketch (i) shows that part of this panel, area S_1, senses only the body-wing combination, while area S_2 senses only the body, so that the expression for the effective apparent mass ratio, K', when this panel is added, is

$$K'_{V(BWH)} = K_{V(BW)} \frac{S_1}{S_V} + K_{V(B)} \frac{S_2}{S_V}$$

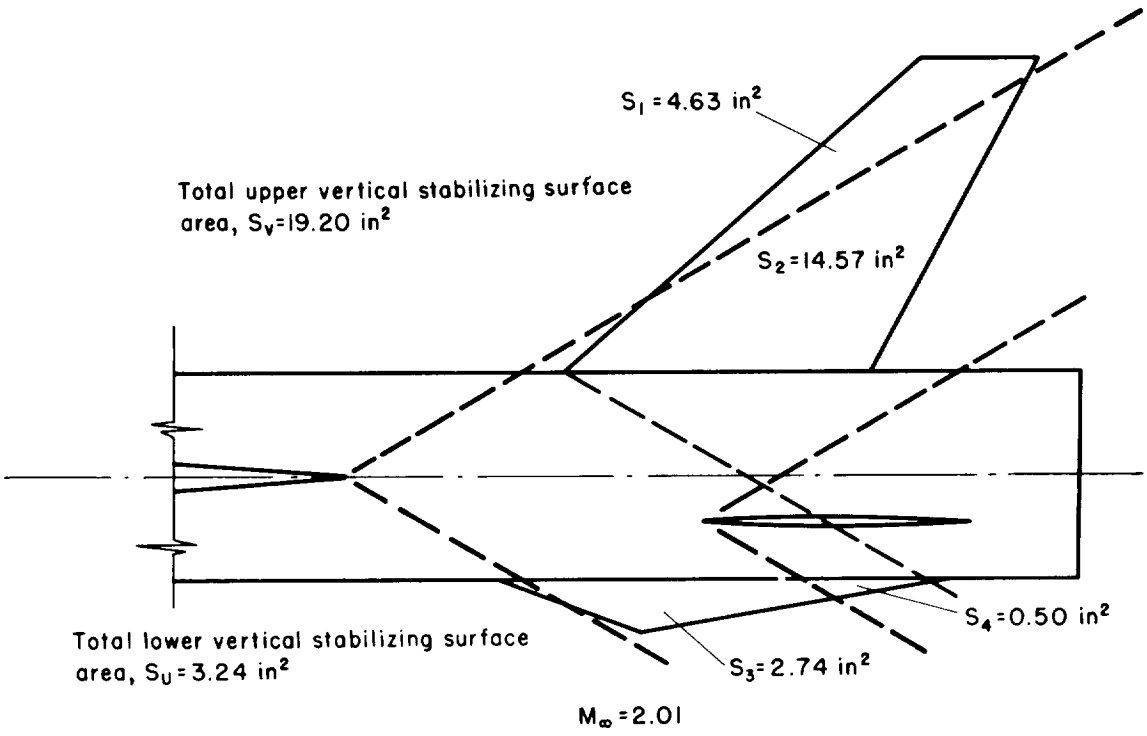

Sketch (i)

The use of the appropriate K charts for the dimensions given by table III, results in,

$$K'_{V(BWH)} = \frac{1.49(4.63)}{19.20} + \frac{1.27(14.57)}{19.20}$$

$$= 1.32$$

and, therefore,

$$(C_{Y_\beta})_{BWHV} - (C_{Y_\beta})_{BWH} = K'_{V(BWH)}(C_{Y_\beta})_V$$

$$= -0.525 \text{ per radian}$$

The third increment which must be found to determine the total empennage side force is that due to adding the lower vertical stabilizing surface to the combination of body, wing, horizontal tail, and upper vertical stabilizing surface. The slender-body value of the side-force curve slope of this panel, referenced to the total wing area, is determined and found to be

$$(C_{Y_\beta})_U = -0.021 \text{ per radian}$$

From sketch (i) it can be seen that area S_3 of the lower vertical stabilizing surface senses only the body, and area S_4, the body and horizontal tail. The expression for the effective apparent mass ratio is, therefore

$$K'_{U(BWHV)} = K_{U(B)} \frac{S_3}{S_U} + K_{U(BH)} \frac{S_4}{S_U}$$

The use of the appropriate K charts gives

$$K'_{U(BWHV)} = \frac{2.78(2.74)}{3.24} + \frac{2.18(0.50)}{3.24}$$

$$= 2.68$$

and, therefore,

$$(C_{Y_\beta})_{BWHVU} - (C_{Y_\beta})_{BWHV} = K'_{U(BWHV)}(C_{Y_\beta})_U$$

$$= -0.056 \text{ per radian}$$

The total of these three increments of side force due to adding the three surfaces gives us the side-force coefficient derivative of the complete empennage

$$(C_{Y_\beta})_{BWHVU} - (C_{Y_\beta})_{BW} = -0.598 \text{ per radian}$$

This estimate corresponds to an experimental value of -0.57 per radian.

To determine the yawing-moment coefficient derivative of the complete empennage, the appropriate moment arm is applied to each of the three incremental values of side force which make up the total. For the increment gained by adding the horizontal tail to the body, the centroid of area of the region of interference on the body is used. This is found to lie at 81.0 percent of the exposed root chord of the horizontal tail and, therefore,

$$\frac{\bar{l}}{2s_W} = \frac{l_m - l_H - 0.810\, c_r}{2s_W}$$

$$= -0.600$$

and

$$(C_{n_\beta})_{BWH} - (C_{n_\beta})_{BW} = \frac{\bar{l}}{2s_W}\left[(C_{Y_\beta})_{BWH} - (C_{Y_\beta})_{BW}\right]$$

$$= 0.010 \text{ per radian}$$

The centroid of area of the upper vertical stabilizing surface lies at 93.0 percent of the exposed root chord, so that

$$\frac{\bar{l}}{2s_W} = -0.575$$

and

$$(C_{n_\beta})_{BWHV} - (C_{n_\beta})_{BWH} = 0.304 \text{ per radian}$$

The centroid of area of the lower vertical stabilizing surface lies at 43.5 percent of the exposed root chord, so that

$$\frac{\bar{l}}{2s_W} = -0.439$$

and

$$(C_{n_\beta})_{BWHVU} - (C_{n_\beta})_{BWHV} = 0.025 \text{ per radian}$$

The addition of these three increments of yawing moment gives the yawing-moment coefficient derivative of the complete empennage gained by the addition of the horizontal tail, upper vertical stabilizing surface, and lower vertical stabilizing surface to the body-wing combination.

$$(C_{n_\beta})_{BWHVU} - (C_{n_\beta})_{BW} = 0.339 \text{ per radian}$$

This estimate corresponds to an experimental value of 0.37 per radian.

REFERENCES

1. Nielsen, Jack N., and Kaattari, George E.: The Effect of Vortex and Shock-Expansion Fields on Pitch and Yaw Stabilities of Supersonic Airplanes. IAS preprint 743, June 1957.

2. Kaattari, George E.: Estimation of Directional Stability Derivatives at Moderate Angles and Supersonic Speeds. NASA MEMO 12-1-58A, 1958.

3. Pitts, William C., Nielsen, Jack N., and Kaattari, George E.: Lift and Center of Pressure of Wing-Body-Tail Combinations at Subsonic, Transonic, and Supersonic Speeds. NACA Rep. 1307, 1957.

4. DeYoung, John, and Harper, Charles W.: Theoretical Symmetric Span Loading at Subsonic Speeds for Wings Having Arbitrary Plan Form. NACA Rep. 921, 1948.

5. Lawrence, H. R.: The Lift Distribution on Low Aspect Ratio Wings at Subsonic Speeds. Jour. Aero. Sci., vol. 18, no. 10, Oct. 1951, pp. 683-695. (Also available as IAS preprint 313, Feb. 1951, and Rep. AF-673-A-1, Cornell Aero. Lab., Inc., Aug. 1950)

6. Lapin, Ellis: Charts for the Computation of Lift and Drag of Finite Wings at Supersonic Speeds. Rep. SM-13480, Douglas Aircraft Co., 1949.

7. Bryson, Arthur E., Jr.: Evaluation of the Inertia Coefficients of the Cross Section of a Slender Body. Jour. Aero. Sci., vol. 21, no. 6, June 1954, pp. 424-427.

8. Bryson, Arthur E., Jr.: Stability Derivatives for a Slender Missile with Application to a Wing-Body-Vertical Tail Configuration. Jour. Aero. Sci., vol. 20, no. 5, May 1953, pp. 297-308.

9. Bryson, Arthur E., Jr.: The Aerodynamic Forces on a Slender Low (or High) Wing, Circular Body, Vertical Tail Configuration. Jour. Aero. Sci., vol. 21, no. 8, Aug. 1954, pp. 574-575.

10. Beam, Benjamin H., Reed, Verlin D., and Lopez, Armando E.: Wind-Tunnel Measurements at Subsonic Speeds of the Static and Dynamic-Rotary Stability Derivatives of a Triangular-Wing Airplane Model Having a Triangular Vertical Tail. NACA RM A55A28, 1955.

11. Buell, Donald A., and Tinling, Bruce E.: The Subsonic Lateral and Longitudinal Static Stability Characteristics Up to Large Angles of Sideslip for a Triangular-Wing Airplane Model Having a Ventral Fin. NACA RM A56H06, 1956.

12. Few, Albert G., Jr.: Investigation at High Subsonic Speeds of the Static Lateral and Directional Stability and Tail-Loads Characteristics of a Model Having a Highly Tapered Swept Wing of Aspect Ratio 3 and Two Horizontal-Tail Positions. NACA RM L56E29, 1956.

13. Paulson, John W., and Boisseau, Peter C.: Low-Speed Investigation of the Effect of Small Canard Surfaces on the Directional Stability of a Sweptback-Wing Fighter-Airplane Model. NACA RM L56F19a, 1956.

14. Sleeman, William C., Jr.: An Experimental Study at High Subsonic Speeds of Several Tail Configurations on a Model Having a 45° Sweptback Wing. NACA RM L57C08, 1957.

15. Moseley, William C., Jr.: Static Stability Characteristics of a Cambered-Delta-Wing Model at High Subsonic Speeds. NACA RM L56H13, 1956.

16. Wiggins, James W., Kuhn, Richard E. and Fournier, Paul G.: Wind-Tunnel Investigation to Determine the Horizontal- and Vertical-Tail Contributions to the Static Lateral Stability Characteristics of a Complete-Model Swept-Wing Configuration at High Subsonic Speeds. NACA TN 3818, 1956. (Supersedes NACA RM L53E19)

17. Goodman, Alex, and Thomas, David F., Jr.: Effects of Wing Position and Fuselage Size on the Low-Speed Static and Rolling Stability Characteristics of a Delta-Wing Model. NACA Rep. 1224, 1955. (Supersedes NACA TN 3063)

18. Letko, William, and Williams, James L.: Experimental Investigation at Low Speed of Effects of Fuselage Cross Section on Static Longitudinal and Lateral Stability Characteristics of Models Having 0° and 45° Sweptback Surfaces. NACA TN 3551, 1955.

19. Savage, Howard F., and Tinling, Bruce E.: The Static Lateral and Directional Subsonic Aerodynamic Characteristics of an Airplane Model Having a Triangular Wing of Aspect Ratio 3. NACA TN 4042, 1957. (Supersedes NACA RM A55B11)

20. Spearman, M. Leroy, and Driver, Cornelius: Longitudinal and Lateral Stability Characteristics of a Low-Aspect-Ratio Unswept-Wing Airplane Model at Mach Numbers of 1.82 and 2.01. NACA RM L56H06, 1957.

21. Spearman, M. Leroy: Static Lateral and Directional Stability and Effective Sidewash Characteristics of a Model of a 35° Swept-Wing Airplane at a Mach Number of 1.61. NACA RM L56E23, 1956.

22. Spearman, M. Leroy, Robinson, Ross B., and Driver, Cornelius: The Effects of the Addition of Small Fuselage-Mounted Fins on the Static Directional Stability Characteristics of a Model of a 45° Swept-Wing Airplane at Angles of Attack Up to 15.3° at a Mach Number of 2.01. NACA RM L56D16a, 1956.

23. Spearman, M. Leroy, and Robinson, Ross B.: Static Lateral Stability and Control Characteristics of a Model of a 45° Swept-Wing Fighter Airplane With Various Vertical Tails at Mach Numbers of 1.41, 1.61, and 2.01. NACA RM L56D05, 1956.

24. Spearman, M. Leroy, and Robinson, Ross B.: Investigation of the Aerodynamic Characteristics in Pitch and Sideslip of a 45° Swept-Wing Airplane Configuration With Various Vertical Locations of the Wing and Horizontal Tail. Static Lateral and Directional Stability; Mach Numbers of 1.41 and 2.01. NACA RM L57J25a, 1957.

TABLE I.- SUMMARY OF THE K CHARTS AND THE RANGE OF VARIABLES COVERED BY EACH

Figure no.	a/b	Horizontal surface position	$(b/s)_H$ or $(b/s)_W$	(a/s) Added vertical panel	(a/s) Existing vertical panel
1	1.000	---	---	0 to 1.0	0.1 to 1.0
2(a)	1.000	Mid	0.0	0 to 1.0	.0 to 1.0
(b)			.2		.1 to 1.0
(c)			.4		.1 to 1.0
(d)			.6		.1 to 1.0
(e)			.8		.1 to 1.0
3(a)	1.000	Tangent to body on same side as added panel	.0	0 to 1.0	.0 to 1.0
(b)			.2		.1 to 1.0
(c)			.4		.1 to 1.0
(d)			.6		.1 to 1.0
(e)			.8		.1 to 1.0
4(a)	1.000	Tangent to body on side opposite added panel	.0	0 to 1.0	.0 to 1.0
(b)			.2		.1 to 1.0
(c)			.4		.1 to 1.0
(d)			.6		.1 to 1.0
(e)			.8		.1 to 1.0
5	.333	---	---	0 to 1.0	.1 to 1.0
6(a)	.333	Mid	.0	0 to 1.0	.0 to 1.0
(b)			.2		.1 to 1.0
(c)			.4		.1 to 1.0
(d)			.6		.1 to 1.0
(e)			.8		.1 to 1.0
7	.667	---	---	0 to 1.0	.1 to 1.0
8(a)	.667	Mid	.0	0 to 1.0	.0 to 1.0
(b)			.2		.1 to 1.0
(c)			.4		.1 to 1.0
(d)			.6		.1 to 1.0
(e)			.8		.1 to 1.0
9	1.500	---	---	0 to 1.0	.1 to 1.0
10(a)	1.500	Mid	.0	0 to 1.0	.0 to 1.0
(b)			.2		.1 to 1.0
(c)			.4		.1 to 1.0
(d)			.6		.1 to 1.0
(e)			.8		.1 to 1.0
11	3.000	---	---	0 to 1.0	.1 to 1.0
12(a)	3.000	Mid	.0	0 to 1.0	.0 to 1.0
(b)			.2		.1 to 1.0
(c)			.4		.1 to 1.0
(d)			.6		.1 to 1.0
(e)			.8		.1 to 1.0
13	1.000	Mid or tangent position	.0 to ∞	1.0	1.0

TABLE II.- SUMMARY OF THE GEOMETRIC AND AERODYNAMIC CHARACTERISTICS OF THE CONFIGURATIONS STUDIED AT SUBSONIC SPEEDS

Configuration No.	Configuration Sketch	$S_{W,2}$, in.^{2}	$2s_W$, in.	l_m, in.	a, in.	a/b	Surface	s, in.	h, in.	l, in.	c_r, in.	λ	Λ_{LE}, deg
1	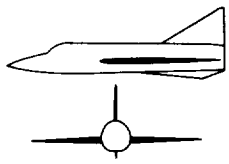	536.0	34.32	28.65	2.94	1.000	W	16.66	0.00	17.78	25.89	0.030	60.0
							V	10.66	---	30.91	13.09	.028	60.0
							U	4.32	---	28.65	15.35	.000	83.4
2	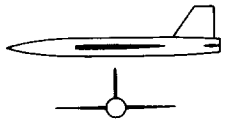	316.8	30.86	31.22	1.85	1.000	V	10.04	---	42.45	10.94	.461	35.8
3	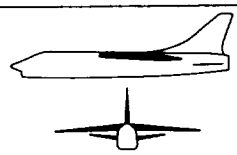	666.5	47.56	40.03	3.32	1.000	W	23.78	3.32	23.70	21.80	.280	47.0
							H	12.06	.00	58.51	8.72	.204	50.5
							V	16.11	---	52.35	16.30	.280	50.9
4	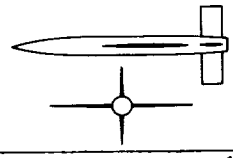	36.0	12.00	10.42	.64	1.000	W	6.00	.00	7.71	4.17	.332	48.6
							H	2.40	.00	16.00	1.80	1.000	.0
							V	2.40	---	16.00	1.80	1.000	.0
							U	2.40	---	16.00	1.80	1.000	.0
5	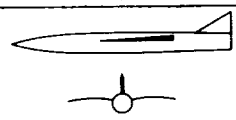	324.0	27.10	28.94	2.25	1.000	W	13.55	.80	21.52	19.12	.000	60.0
							V	9.30	---	42.51	12.21	.000	60.0
6	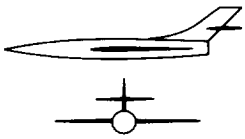	324.0	36.00	30.00	1.85	1.000	V	10.19	---	39.75	9.45	.610	55.2
7	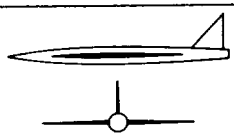	576.7	36.50	27.00	1.46	1.000	V_1	10.37	---	44.31	8.50	.000	42.5
							V_3	13.12	---	43.00	11.00	.000	42.5
8	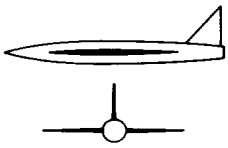	576.7	36.50	27.00	1.95	1.000	V_2	11.74	---	43.75	9.40	.000	42.5
							V_3	13.49	---	43.00	11.00	.000	42.5

TABLE II.- SUMMARY OF THE GEOMETRIC AND AERODYNAMIC CHARACTERISTICS OF THE CONFIGURATIONS STUDIED AT SUBSONIC SPEEDS - Continued

Configuration		M_∞	$\bar{l}/2s_W$	$(C_{Y_\beta})_P$	K	Estimation using K		Experiment		Ref. no.
No.	Panel added					ΔC_{Y_β}	ΔC_{n_β}	ΔC_{Y_β}	ΔC_{n_β}	
1	BWV-BW	0.25	-0.276	-0.244	1.58	-0.386	0.107	-0.42	0.11	10
	BWV-BW	.60	-.279	-.257	1.58	-.406	.113	-.46	.12	10
	BWV-BW	.80	-.281	-.276	1.58	-.436	.123	-.47	.13	10
	BWVU-BWV	.25	-.156	-.011	3.04	-.033	.005	-.046	.004	11
	BWVU-BWV	.80	-.156	-.011	3.04	-.033	.005	-.046	.007	11
2	BV-B	.80	-.508	-.585	1.07	-.626	.313	-.55	.29	12
3	BWHV-BWH	.06	-.451	-.522	1.30	-.678	.306	-.64	.28	13
4	BWV-BW	.60	-.502	-.224	1.34	-.300	.151	-.31	.15	14
	BWV-BW	.80	-.499	-.239	1.34	-.320	.160	-.34	.14	14
	BWHVU-BWHV	.60	-.502	-.224	1.74	-.390	.196	-.35	.17	14
	BWHVU-BWHV	.80	-.499	-.239	1.74	-.416	.208	-.38	.18	14
5	BWV-BW	.60	-.751	-.344	1.26	-.433	.325	-.40	.30	15
	BWV-BW	.80	-.754	-.365	1.26	-.460	.347	-.46	.31	15
6	BV-B	.40	[a]-.425	-.450	1.07	-.482	.205	-.44	.23	16
	BV-B	.50	[a]-.425	-.453	1.07	-.485	.206	-.45	.23	16
	BV-B	.60	[a]-.425	-.460	1.07	-.492	.209	-.46	.24	16
	BV-B	.70	[a]-.425	-.464	1.07	-.497	.211	-.47	.24	16
	BV-B	.80	[a]-.425	-.467	1.07	-.500	.213	-.48	.25	16
7	BV_1-B	.17	-.600	-.239	.94	-.225	.135	-.25	.14	17
	BV_3-B	.17	-.601	-.401	.85	-.341	.205	-.35	.21	17
8	BV_2-B	.17	-.598	-.293	1.01	-.296	.177	-.30	.18	17
	BV_3-B	.17	-.601	-.401	.95	-.381	.229	-.37	.24	17

[a]Intersection of mean aerodynamic chord and quarter chord of added panel used in determining moment arm.

TABLE II.- SUMMARY OF THE GEOMETRIC AND AERODYNAMIC CHARACTERISTICS OF THE CONFIGURATIONS STUDIED AT SUBSONIC SPEEDS - Continued

Configuration No.	Configuration Sketch	S_W, $in.^2$	$2s_W$, in.	l_m, in.	a, in.	a/b	Surface	s, in.	h, in.	l, in.	c_r, in.	λ	Λ_{LE}, deg
9	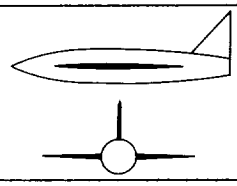	576.7	36.50	27.00	2.93	1.000	V_3	14.23	---	43.00	11.00	0.000	42.5
10	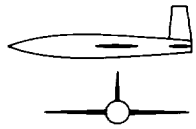	324.0	36.00	23.98	1.82	1.000	H	8.05	0.00	39.54	4.58	.660	3.6
							V	9.90	---	39.26	5.69	.647	2.8
11	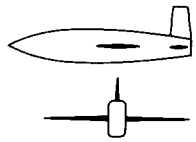	324.0	36.00	23.98	2.70	2.210	H	8.05	.00	39.50	4.73	.638	3.6
							V	9.90	---	39.32	5.43	.678	2.8
12	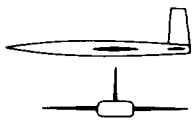	324.0	36.00	23.98	1.22	.451	H	8.05	.00	39.59	4.36	.693	3.6
							V	9.90	---	39.22	5.84	.630	2.8
13	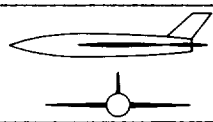	324.0	36.00	25.44	1.82	1.000	H	6.70	.00	39.55	5.39	.673	47.5
							V	8.25	---	38.50	6.72	.658	47.5
14	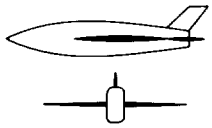	324.0	36.00	25.44	2.70	2.210	H	6.70	.00	38.89	5.61	.647	47.5
							V	8.25	---	39.46	6.41	.690	47.5
15	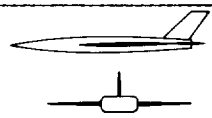	324.0	36.00	25.44	1.22	.451	H	6.70	.00	40.51	5.08	.714	47.5
							V	8.25	---	37.85	6.93	.638	47.5
16	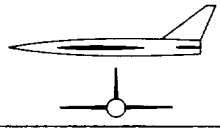	576.0	41.56	39.58	2.80	1.000	H	11.20	.00	64.24	7.05	.396	14.2
							V_S	13.28	---	59.99	12.48	.195	54.0
							V_L	15.23	---	57.75	14.72	.189	54.0

TABLE II.- SUMMARY OF THE GEOMETRIC AND AERODYNAMIC CHARACTERISTICS OF THE CONFIGURATIONS STUDIED AT SUBSONIC SPEEDS - Concluded

Configuration		M_∞	$\bar{l}/2s_w$	$(C_{Y_\beta})_p$	K	Estimation using K		Experiment		Ref. no.
No.	Panel added					ΔC_{Y_β}	ΔC_{n_β}	ΔC_{Y_β}	ΔC_{n_β}	
9	BV_3-B	0.17	-0.601	-0.401	1.15	-0.461	0.277	-0.42	0.26	17
10	BHV-BH	.13	-.464	-.400	1.26	-.504	.234	-.53	.22	18
11	BHV-BH	.13	-.464	-.331	1.53	-.506	.235	-.53	.21	18
12	BHV-BH	.13	-.464	-.448	1.11	-.497	.230	-.49	.20	18
13	BHV-BH	.13	[a]-.464	-.267	1.35	-.361	.168	-.39	.18	18
14	BHV-BH	.13	[a]-.464	-.208	1.71	-.356	.165	-.40	.17	18
15	BHV-BH	.13	[a]-.464	-.310	1.15	-.356	.165	-.39	.16	18
16	BV_S-B	.25	[a]-.620	-.370	1.16	-.429	.266	-.44	.31	19
	BV_S-B	.60	[a]-.620	-.389	1.16	-.451	.280	-.44	.32	19
	BV_S-B	.80	[a]-.620	-.415	1.16	-.482	.299	-.46	.34	19
	BV_L-B	.25	[a]-.599	-.514	1.07	-.550	.329	-.56	.39	19
	BV_L-B	.60	[a]-.599	-.541	1.07	-.579	.347	-.58	.41	19
	BV_L-B	.80	[a]-.599	-.577	1.07	-.617	.370	-.60	.44	19
	BHV_S-BH	.25	[a]-.620	-.370	1.34	-.496	.308	-.47	.32	19
	BHV_S-BH	.60	[a]-.620	-.389	1.34	-.522	.324	-.49	.33	19
	BHV_S-BH	.80	[a]-.620	-.415	1.34	-.556	.345	-.50	.37	19
	BHV_L-BH	.25	[a]-.599	-.514	1.25	-.642	.385	-.63	.41	19
	BHV_L-BH	.60	[a]-.599	-.541	1.25	-.676	.405	-.65	.44	19
	BHV_L-BH	.80	[a]-.599	-.577	1.25	-.721	.432	-.68	.48	19

[a]Intersection of mean aerodynamic chord and quarter chord of added panel used in determining moment arm.

TABLE III.- SUMMARY OF THE GEOMETRIC AND AERODYNAMIC CHARACTERISTICS OF THE CONFIGURATIONS STUDIED AT SUPERSONIC SPEEDS

Configuration No.	Configuration Sketch	S_W, in.^{2}	$2a_W$, in.	l_m, in.	a, in.	a/b	Surface	s, in.	h, in.	l, in.	c_r, in.	λ	Λ_{LE}, deg
1	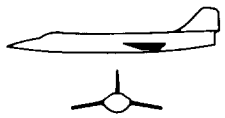	45.2	10.48	15.30	1.00	1.000	W	5.24	0.00	13.40	5.50	0.427	27.1
							V	3.80	---	20.67	4.50	.378	44.0
2	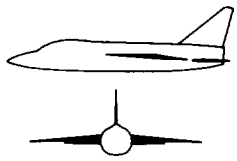	160.4	25.32	19.11	1.78	1.000	W	12.66	.00	14.33	7.83	.538	38.1
							H	6.06	.00	27.80	6.46	.541	38.5
							V	7.48	---	26.15	3.66	.192	50.4
3	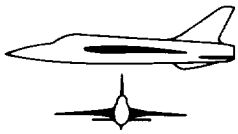	114.5	19.08	18.00	1.75	1.170	W	9.54	.00	12.49	7.92	.483	48.0
							H	4.56	-.84	26.53	3.60	.517	48.0
							V	7.08	---	24.12	5.20	.392	49.2
							U	2.56	---	22.89	8.00	.000	70.2
4	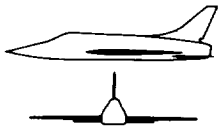	272.2	32.41	24.91	2.04	.940	W	16.21	-1.18	16.51	13.20	.313	49.7
							H	7.87	-1.37	33.62	5.89	.402	49.6
							V_o	7.20	---	32.80	6.69	.416	23.5
							V_{ext}	8.66	---	32.80	6.69	.260	23.5
							$V_{127\%}$	8.74	---	32.37	7.20	.290	23.5
5	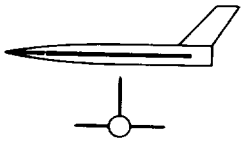	25.3	5.62	7.50	.63	1.000	W	2.81	.00	.00	11.25	.000	76.0
							V	3.12	---	10.36	2.10	.679	32.4
6	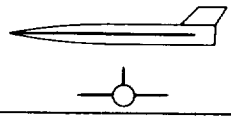	25.3	5.62	7.50	.63	1.000	W	2.81	.00	.00	11.25	.000	76.0
							V	1.88	---	10.36	2.10	.833	32.4
7	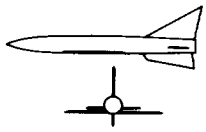	14.4	6.73	6.24	.54	1.000	W	3.37	-.54	3.81	4.22	.000	55.0
							H	1.80	-.18	10.73	1.44	.000	53.0
							V	2.75	---	9.03	3.42	.000	60.8
							a_U	1.57	---	9.03	3.36	.000	76.1

See footnotes to table, p. 41.

TABLE III.- SUMMARY OF THE GEOMETRIC AND AERODYNAMIC CHARACTERISTICS OF THE CONFIGURATIONS STUDIED AT SUPERSONIC SPEEDS - Continued

Configuration		M_∞	$\bar{l}/2s_w$	$(C_{Y_\beta})_P$	K	Estimation using K		K'	Estimation using K'		Experiment		Ref. no.
No.	Panel added					ΔC_{Y_β}	ΔC_{n_β}		ΔC_{Y_β}	ΔC_{n_β}	ΔC_{Y_β}	ΔC_{n_β}	
1	BWV-BW	1.82	-0.768	-0.418	1.33	-0.556	0.427	1.41	-0.589	0.453	-0.56	0.43	20
2	BV-B	1.61	[b]-.471	-.429	1.25	-.536	.253	1.25	-.536	.253	-.52	.22	21
	BHV-BH	1.61	[b]-.471	-.429	1.40	-.600	.283	1.29	-.553	.262	-.56	.23	21
3	BWHU-BWH	2.01	[b]-.439	-.021	2.14	-.045	.020	2.76	-.056	.025	-.057	.034	22
	BWHUV-BWHU	2.01	[b]-.575	-.398	1.55	-.617	.355	1.32	-.525	.302	-.52	.30	22
4	BWV_o-BW	1.61	[b]-.403	-.247	1.39	-.343	.138	1.45	-.358	.144	-.33	.14	23
	BWV_o-BW	2.01	[b]-.403	-.195	1.39	-.271	.109	1.72	-.335	.135	-.30	.12	23
	$BWHV_o$-BWH	1.61	[b]-.403	-.247	1.78	-.440	.177	1.49	-.368	.148	-.37	.15	23
	$BWHV_o$-BWH	2.01	[b]-.403	-.195	1.78	-.347	.140	1.72	-.335	.135	-.30	.12	23
	$BWHV_{ext}$-BWH	1.61	[b]-.414	-.321	1.57	-.504	.209	1.32	-.424	.176	-.41	.17	23
	$BWHV_{127\%}$-BWH	1.61	[b]-.410	-.349	1.57	-.548	.225	1.35	-.471	.193	-.44	.17	23
5	BV-B	2.94	[b]-.860	-.248	1.13	-.280	.241	1.13	-.280	.241	-.29	.26	(c)
	BWV-BW	2.94	[b]-.860	-.248	1.31	-.325	.279	1.31	-.325	.279	-.32	.26	(c)
6	BV-B	2.94	[b]-.780	-.121	1.55	-.188	.147	1.55	-.188	.147	-.18	.13	(c)
	BWV-BW	2.94	[b]-.780	-.121	1.71	-.207	.161	1.71	-.207	.161	-.19	.13	(c)
7	BV-B	2.94	[b]-.781	-.388	1.10	-.427	.333	1.10	-.427	.333	-.46	.30	(c)
	BU-B	1.97	[b]-.810	-.183	1.57	-.287	.230	1.57	-.287	.230	-.30	.23	(c)
	BWHVU-BWHV	2.94	[b]-.810	-.164	2.07	-.339	.275	1.60	-.262	.212	-.23	.14	(c)

See footnotes to table, p. 41.

TABLE III.- SUMMARY OF THE GEOMETRIC AND AERODYNAMIC CHARACTERISTICS OF THE CONFIGURATIONS STUDIED AT SUPERSONIC SPEEDS - Continued

Configuration		S_W, in.^{2}	$2s_W$, in.	l_m, in.	a, in.	a/b	Surface	s, in.	h, in.	l, in.	c_r, in.	λ	Λ_{LE}, deg
No.	Sketch												
8	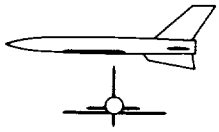	14.4	6.73	6.24	0.54	1.000	V	2.76	---	9.77	2.56	0.547	49.1
9	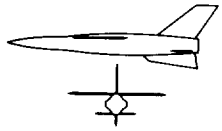	14.1	6.87	6.24	.55	1.170	H	1.50	-0.55	10.73	1.56	.000	53.0
							V	2.76	---	9.77	2.56	.547	49.1
							a_U	1.58	---	9.03	3.36	.000	76.1
10	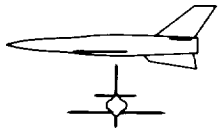	14.1	6.87	6.24	.55	1.170	H	1.50	.55	10.73	1.56	.000	53.0
							V	2.76	---	9.77	2.56	.547	49.1
							a_U	1.58	---	9.03	3.36	.000	76.1
11		144.0	24.00	20.81	1.47	1.000	W	12.00	.00	15.60	8.88	.225	49.4
							V	8.59	---	28.66	6.94	.235	20.6
12		144.0	24.00	20.81	1.47	1.000	W	12.00	.00	15.60	8.88	.225	49.4
							V	8.59	---	28.66	6.94	.235	41.6
13	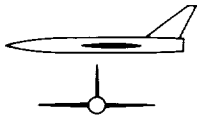	144.0	24.00	20.81	1.47	1.000	W	12.00	.00	15.60	8.88	.225	49.4
							V	8.59	---	28.66	6.94	.235	52.1
14	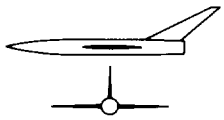	144.0	24.00	20.81	1.47	1.000	W	12.00	.00	15.60	8.88	.225	49.4
							V	8.59	---	28.66	6.94	.235	62.5

See footnotes to table, p. 41.

TABLE III.- SUMMARY OF THE GEOMETRIC AND AERODYNAMIC CHARACTERISTICS OF THE CONFIGURATIONS STUDIED AT SUPERSONIC SPEEDS - Concluded

Configuration		M_∞	$\bar{l}/2s_w$	$(C_{Y_\beta})_p$	K	Estimation using K		K'	Estimation using K'		Experiment		Ref. no.
No.	Panel added					ΔC_{Y_β}	ΔC_{n_β}		ΔC_{Y_β}	ΔC_{n_β}	ΔC_{Y_β}	ΔC_{n_β}	
8	BV-B	1.97	[b]-0.852	-0.672	1.09	-0.732	0.624	1.09	-0.732	0.624	-0.71	0.63	(c)
	BV-B	2.94	[b]-.852	-.444	1.09	-.484	.412	1.09	-.484	.412	-.48	.39	(c)
9	BV-B	1.97	[b]-.834	-.685	1.12	-.767	.640	1.12	-.767	.640	-.72	.60	(c)
	BU-B	1.97	[b]-.794	-.187	1.61	-.301	.239	1.61	-.301	.239	-.32	.23	(c)
	BVU-BV	1.97	[b]-.794	-.187	2.73	-.510	.405	1.88	-.352	.279	-.36	.13	(c)
	BUV-BU	1.97	[b]-.834	-.685	1.36	-.932	.776	1.18	-.808	.674	-.76	.50	(c)
	BHU-BH	1.97	[b]-.794	-.187	1.10	-.206	.164	1.38	-.258	.205	-.34	.27	(c)
	BHV-BH	1.97	[b]-.834	-.685	1.45	-.993	.828	1.12	-.767	.640	-.77	.64	(c)
	BHVU-BHV	1.97	[b]-.794	-.187	1.48	-.277	.220	1.52	-.284	.226	-.31	.19	(c)
	BHUV-BHU	1.97	[b]-.834	-.685	1.55	-1.062	.885	1.18	-.808	.674	-.75	.58	(c)
10	BHU-BH	1.97	[b]-.794	-.187	2.11	-.395	.314	1.61	-.301	.239	-.37	.23	(c)
	BHV-BH	1.97	[b]-.834	-.685	1.00	-.685	.571	1.09	-.746	.622	-.80	.60	(c)
	BHVU-BHV	1.97	[b]-.794	-.187	2.66	-.497	.395	1.79	-.335	.266	-.29	.14	(c)
	BHUV-BHU	1.97	[b]-.834	-.685	1.11	-.760	.634	1.11	-.760	.634	-.71	.52	(c)
11	BWV-BW	1.41	-.465	-.788	1.04	-.820	.381	1.06	-.836	.389	-.92	.37	24
	BWV-BW	2.01	-.469	-.470	1.04	-.489	.229	1.16	-.545	.256	-.65	.31	24
12	BWV-BW	1.41	[b]-.564	-.810	1.04	-.842	.475	1.04	-.842	.475	-.88	.42	24
	BWV-BW	2.01	[b]-.564	-.482	1.04	-.502	.283	1.12	-.540	.305	-.60	.30	24
13	BWV-BW	1.41	[b]-.630	-.761	1.04	-.792	.499	1.04	-.792	.499	-.85	.45	24
	BWV-BW	2.01	[b]-.630	-.512	1.04	-.532	.335	1.06	-.542	.342	-.53	.30	24
14	BWV-BW	1.41	[b]-.748	-.679	1.04	-.706	.528	1.04	-.706	.528	-.67	.36	24
	BWV-BW	2.01	[b]-.748	-.554	1.04	-.586	.438	1.04	-.586	.438	-.50	.32	24

[a]Approximated by triangular plan-form tail.

[b]Centroid of area of added panel used in determining moment arm.

[c]Unpublished data from Ames 1- by 3-foot supersonic wind tunnels.

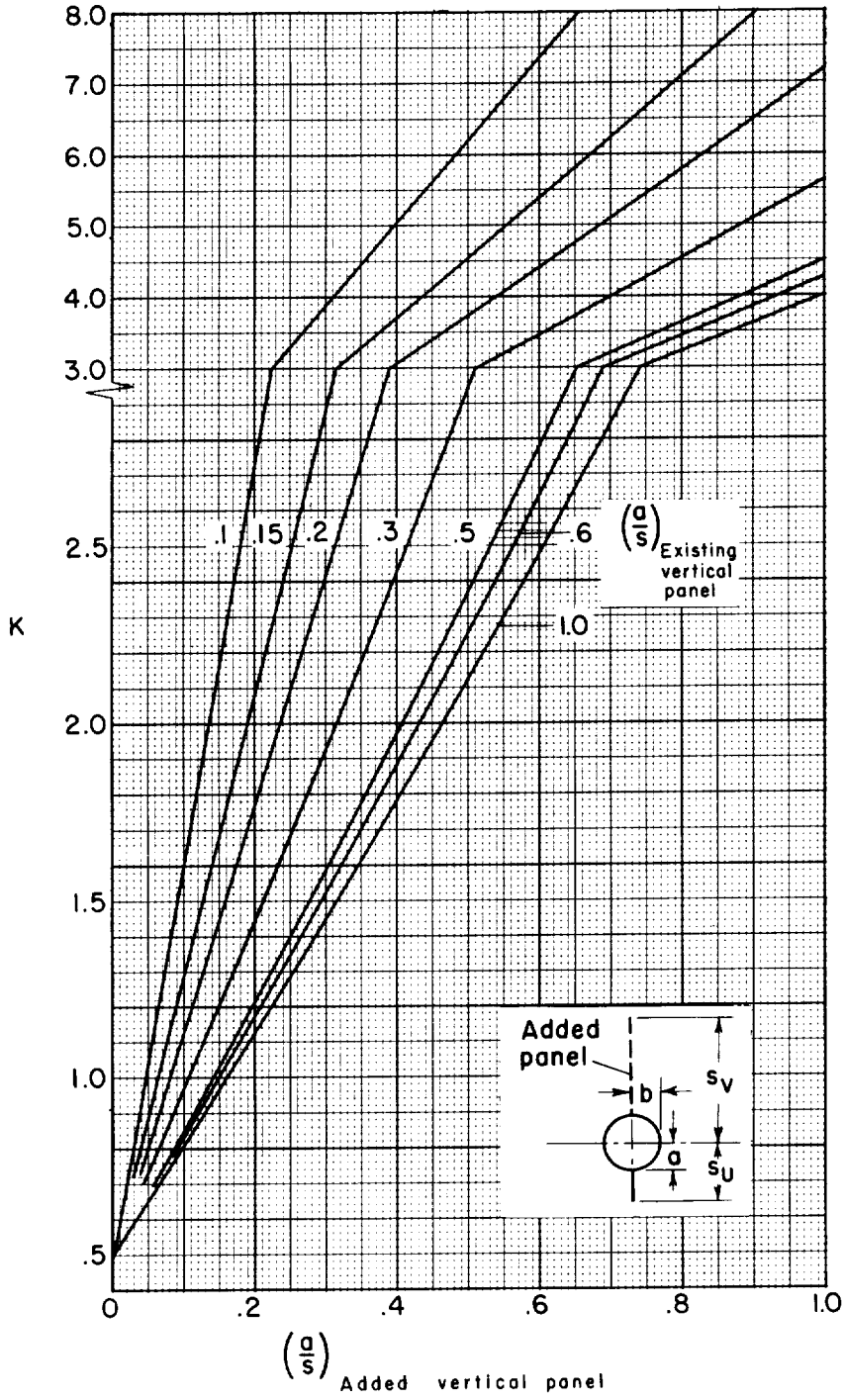

Figure 1.- Apparent mass ratio for various values of a/s of the existing vertical panel in the presence of a circular body.

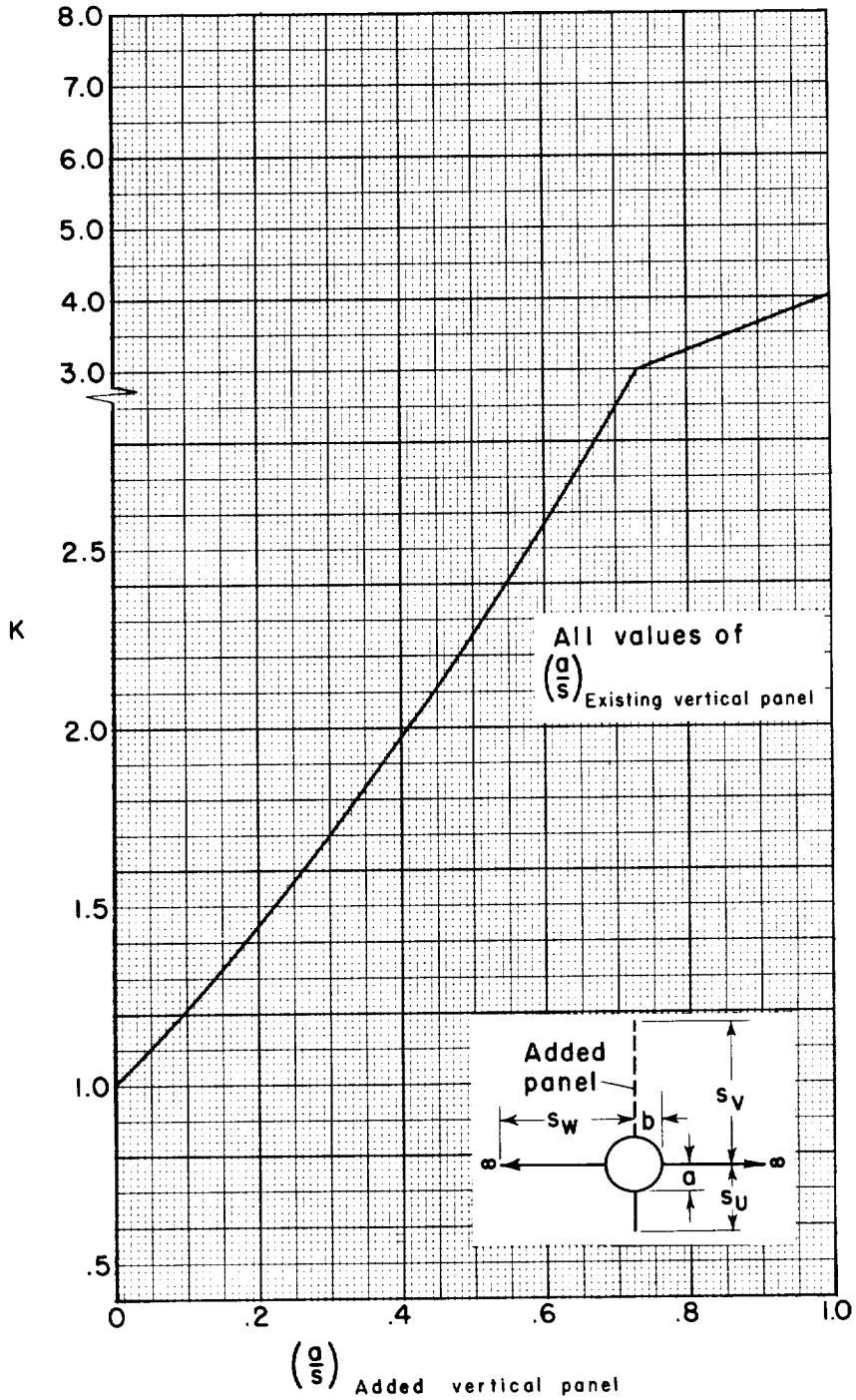

(a) b/s_H or $b/s_W = 0.0$

Figure 2.- Apparent mass ratio for various values of a/s of the existing vertical panel in the presence of a circular body with a mid horizontal surface.

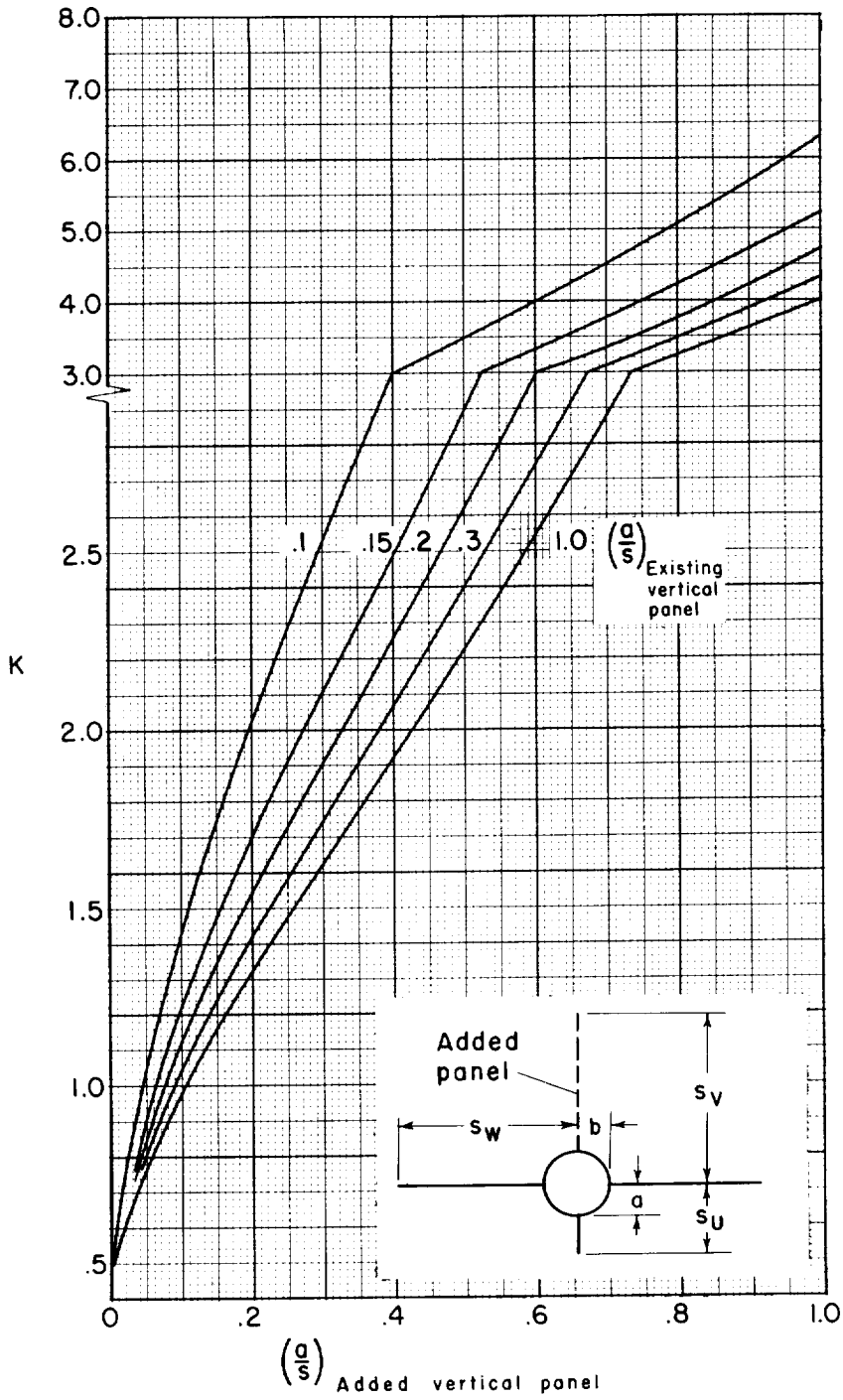

(b) b/s_H or $b/s_W = 0.2$

Figure 2.- Continued.

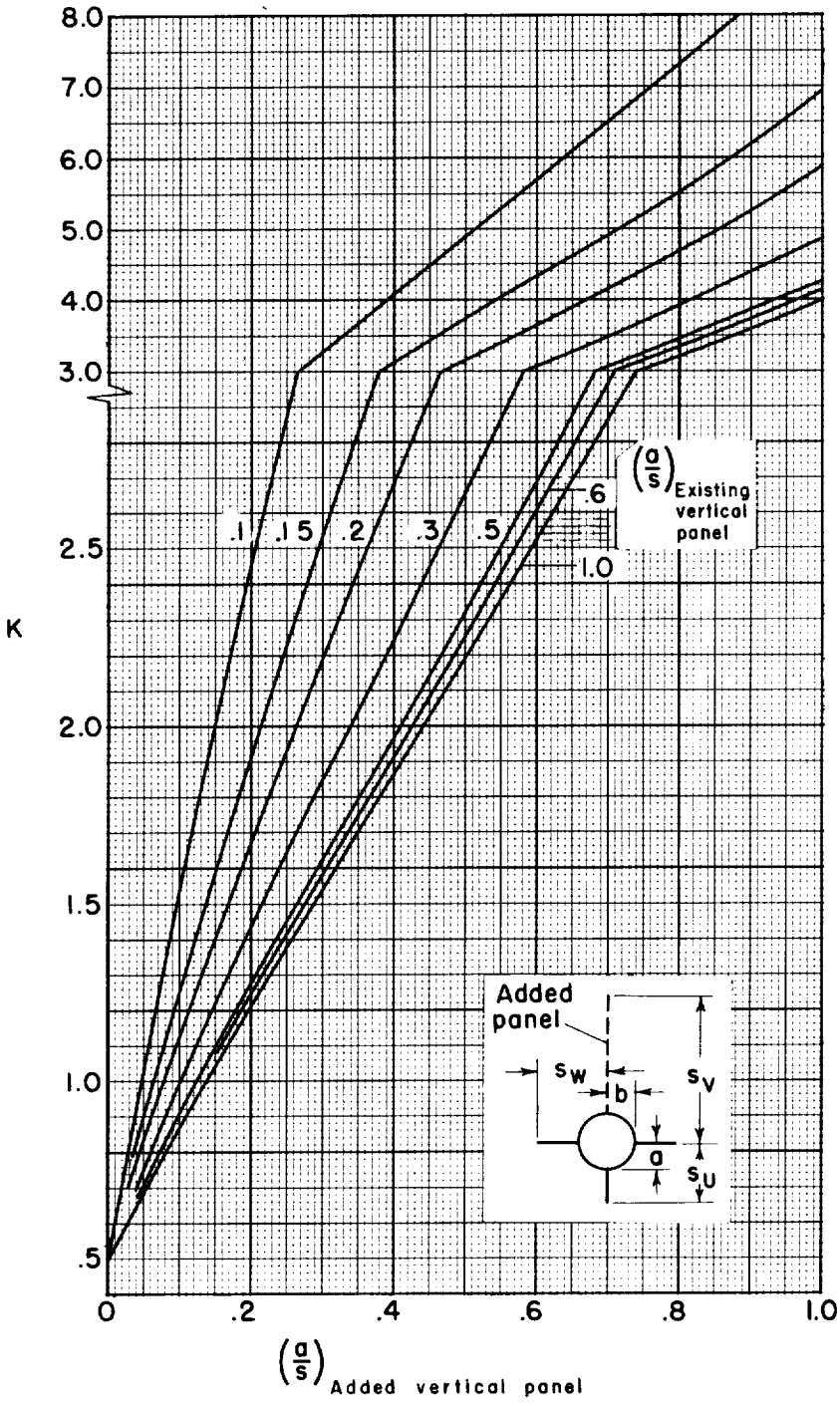

(c) b/s_H or $b/s_W = 0.4$

Figure 2.- Continued.

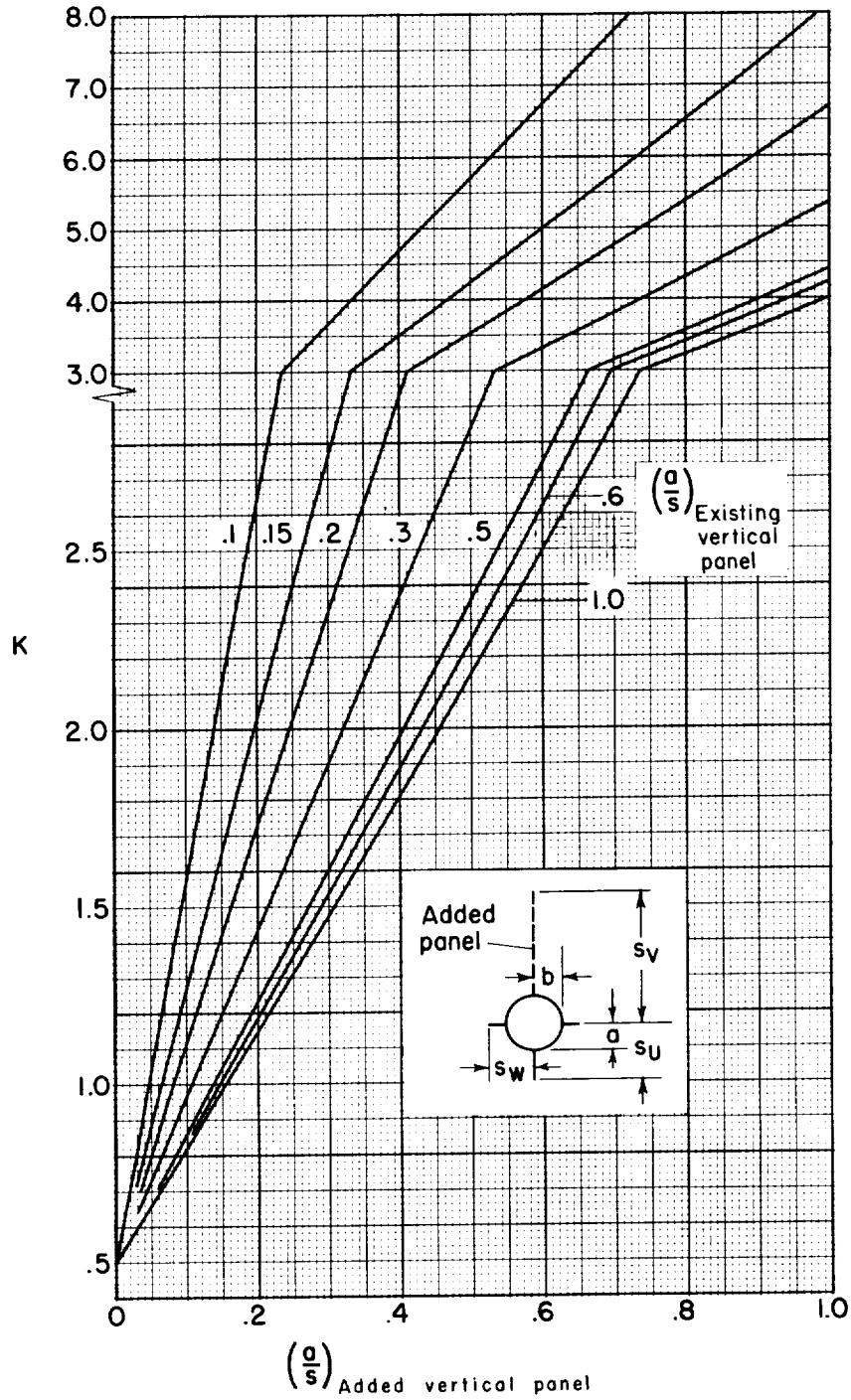

(d) b/s_H or $b/s_W = 0.6$

Figure 2.- Continued.

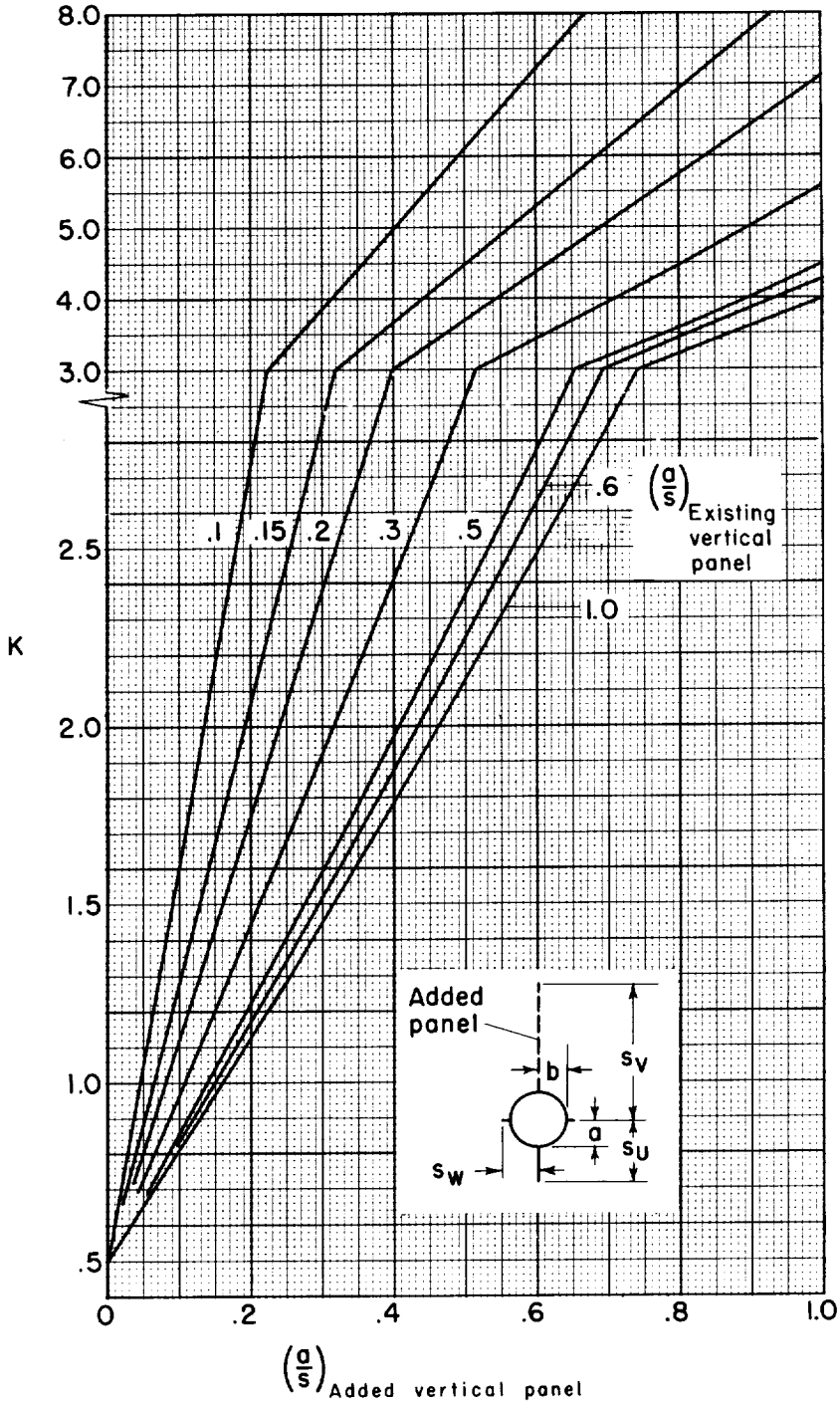

(e) b/s_H or $b/s_W = 0.8$

Figure 2.- Concluded.

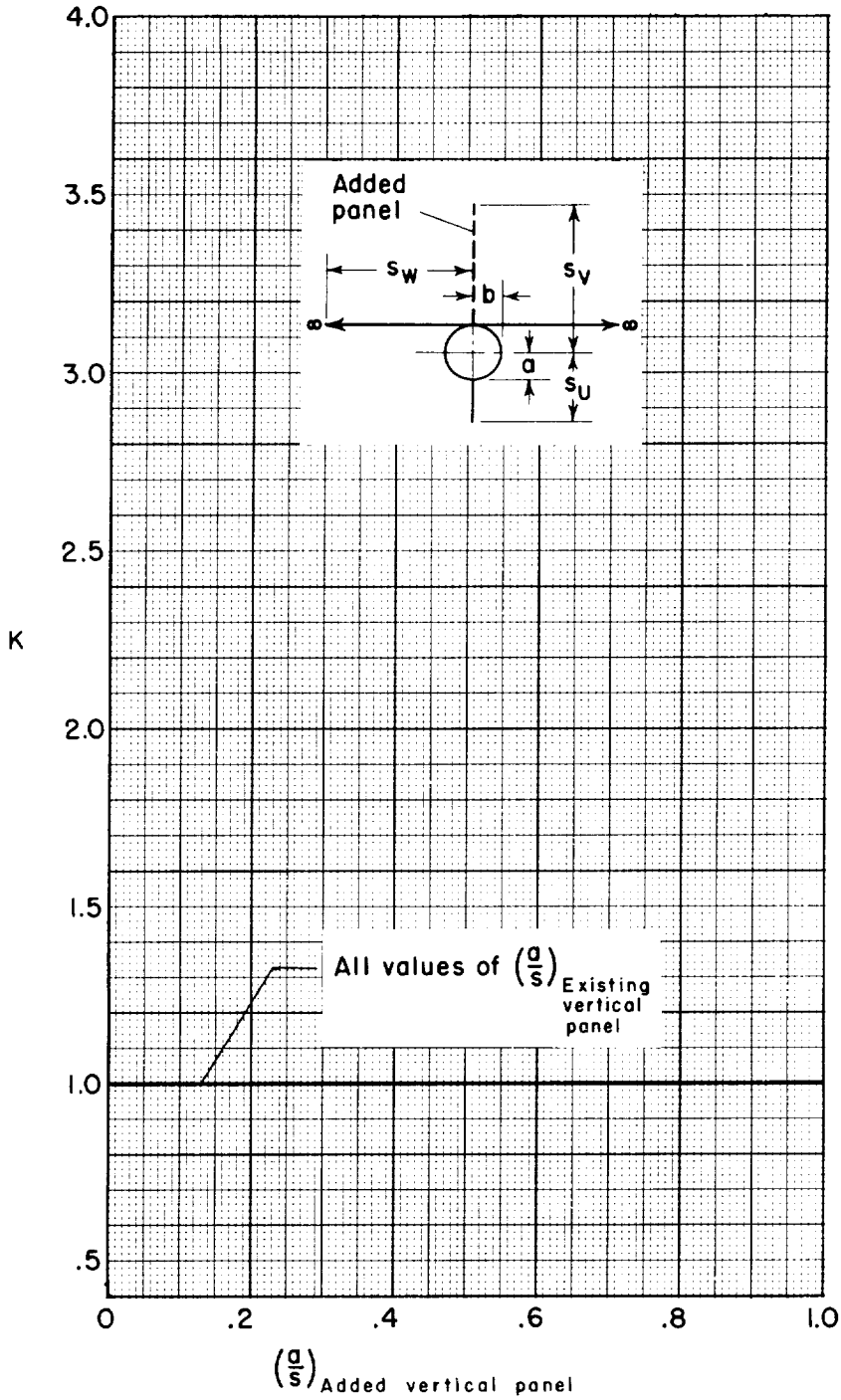

(a) b/s_H or $b/s_W = 0.0$

Figure 3.- Apparent mass ratio for various values of a/s of the existing vertical panel in the presence of a circular body with a horizontal surface mounted tangent to the body on the same side as the added panel.

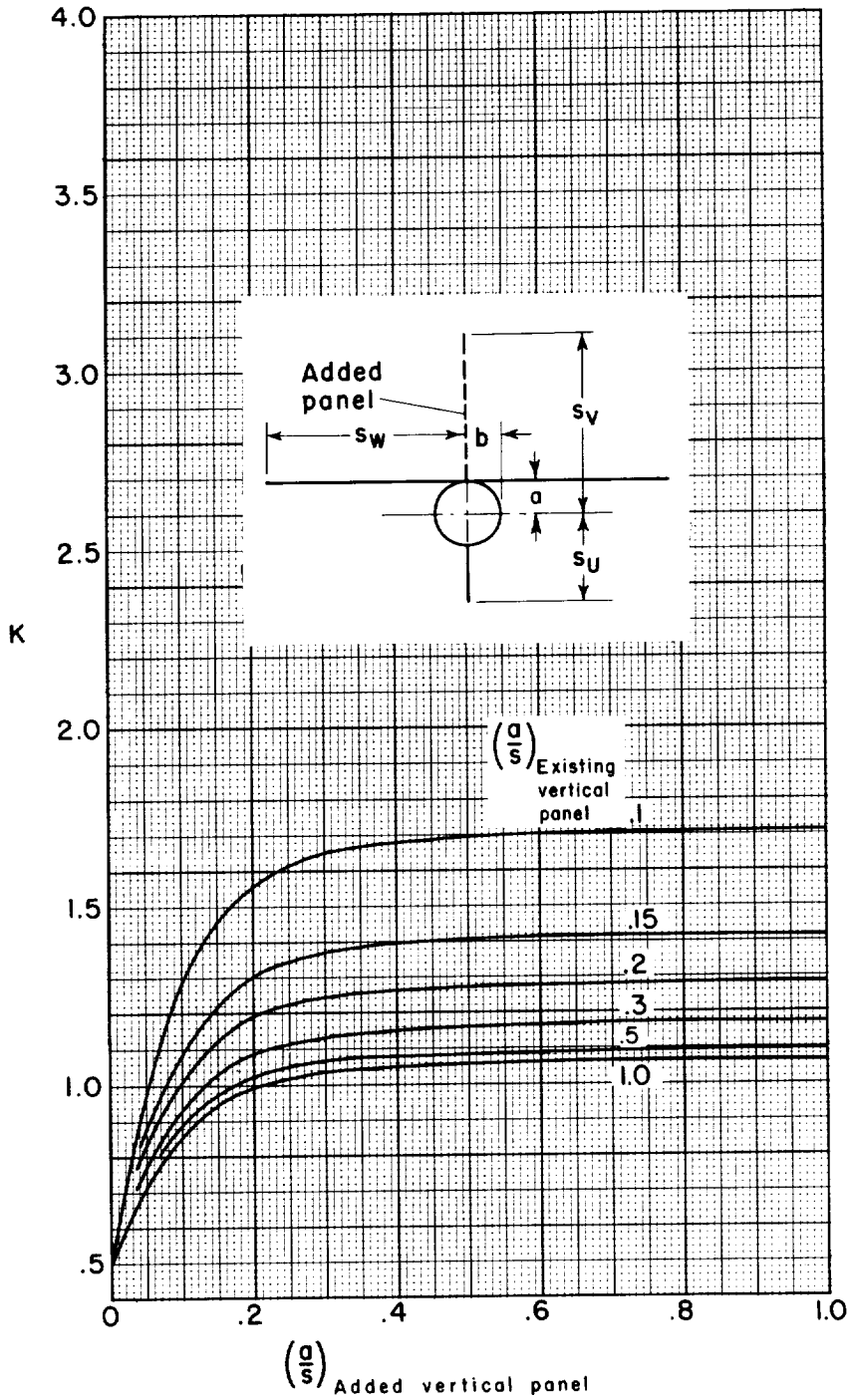

(b) b/s_H or $b/s_W = 0.2$

Figure 3.- Continued.

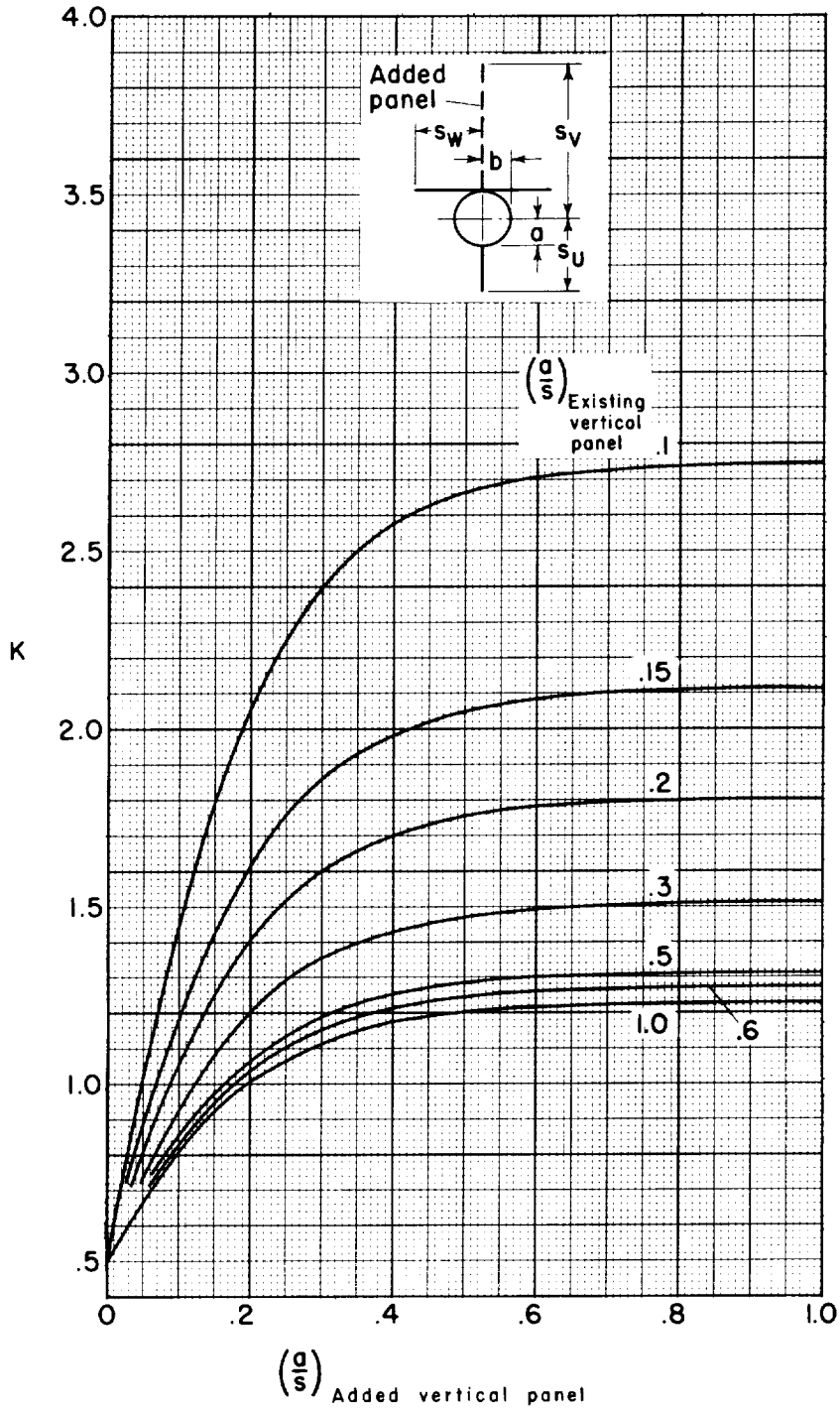

(c) b/s_H or $b/s_W = 0.4$

Figure 3.- Continued.

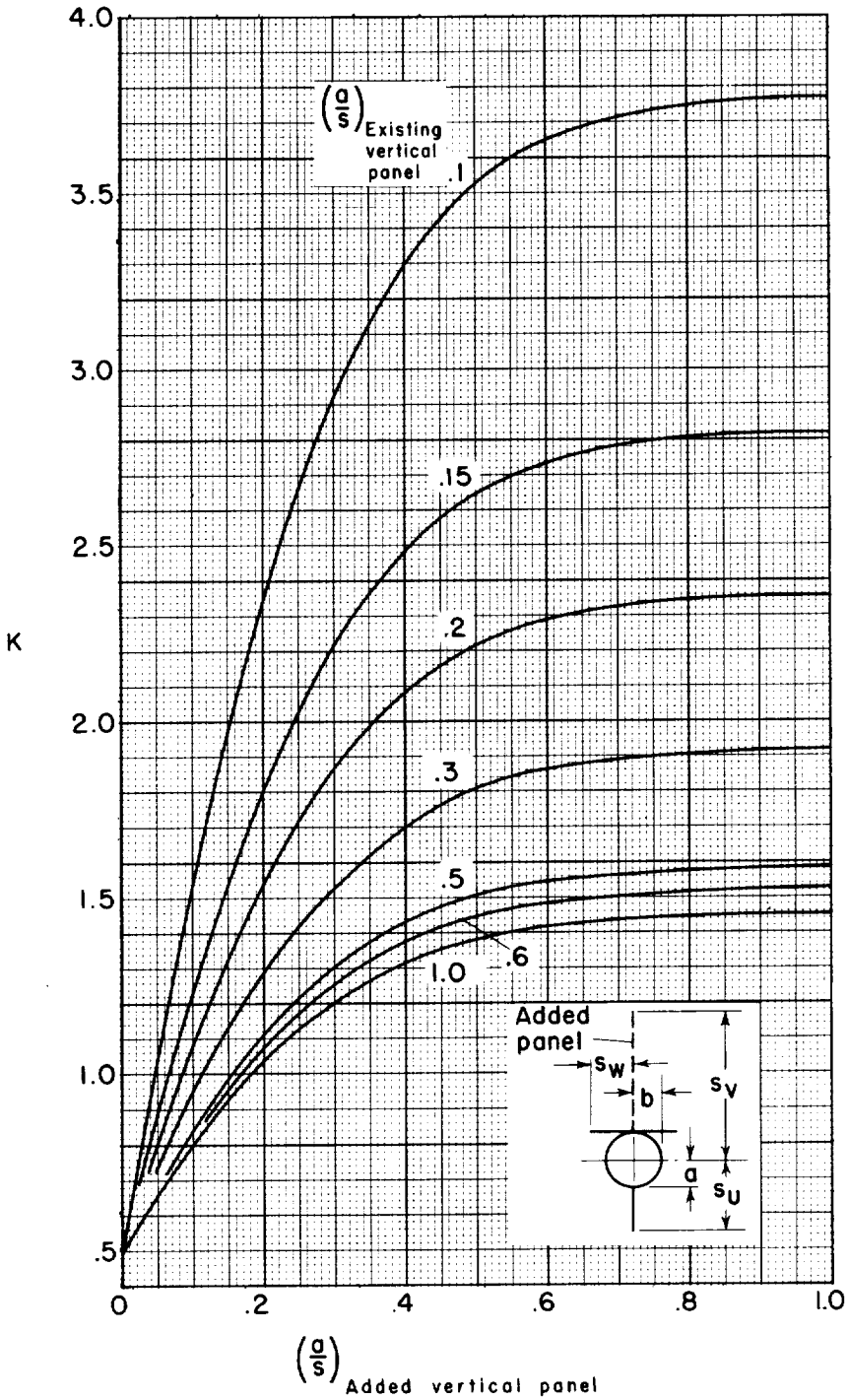

(d) b/s_H or $b/s_W = 0.6$

Figure 3.- Continued.

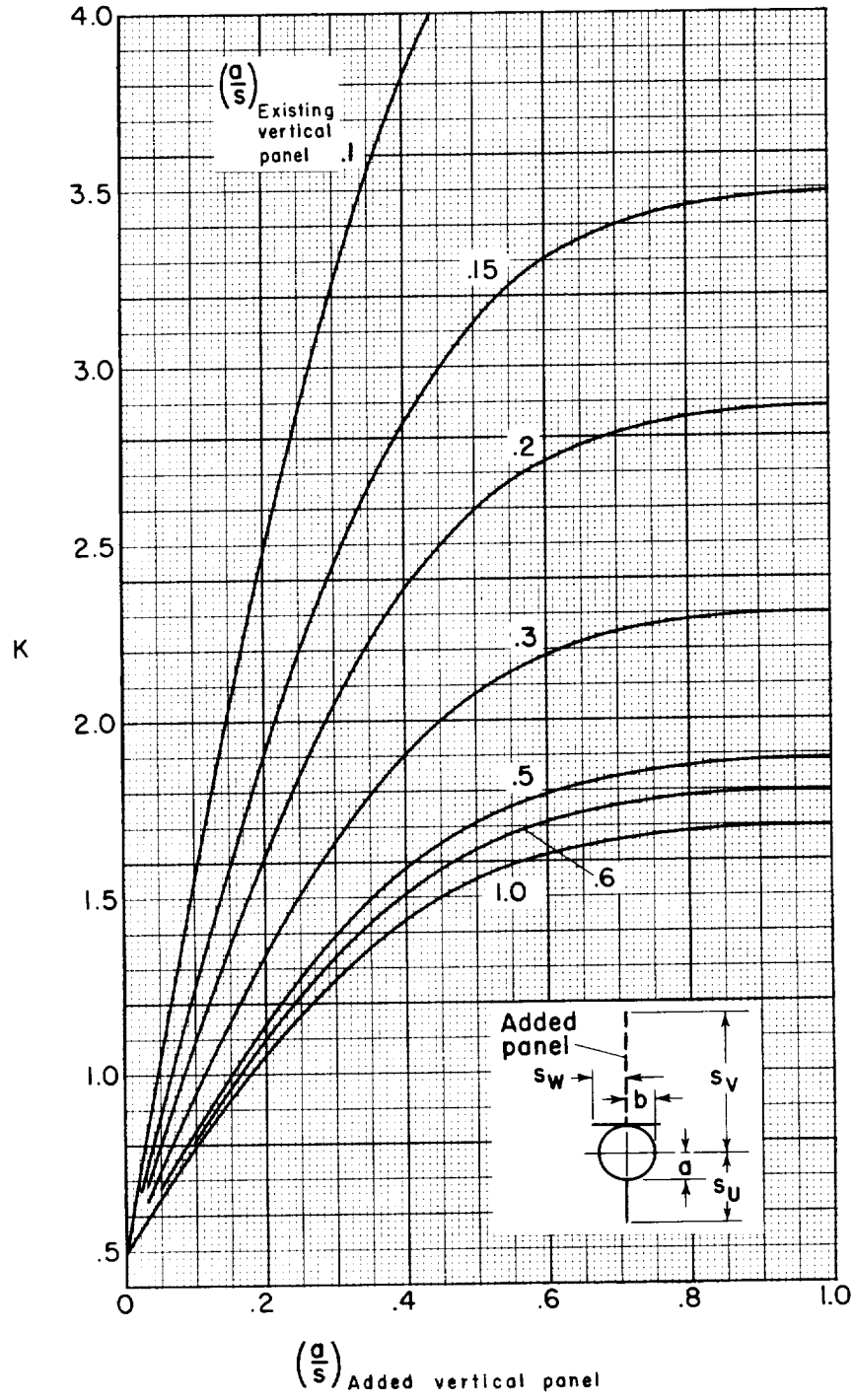

(e) b/s_H or $b/s_W = 0.8$

Figure 3.- Concluded.

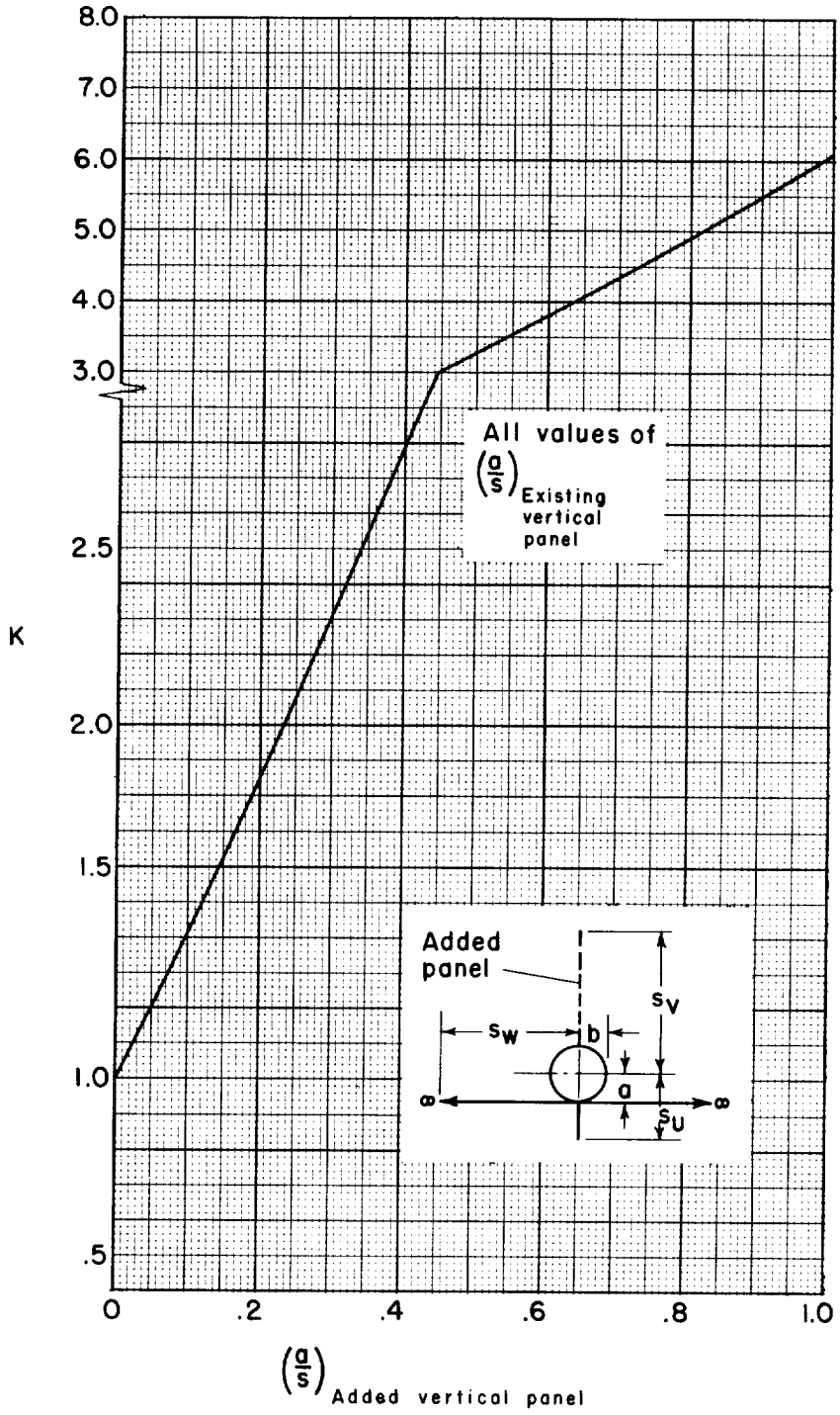

(a) b/s_H or $b/s_W = 0.0$

Figure 4.- Apparent mass ratio for various values of a/s of the existing vertical panel in the presence of a circular body with a horizontal surface mounted tangent to the body on the side opposite the added panel.

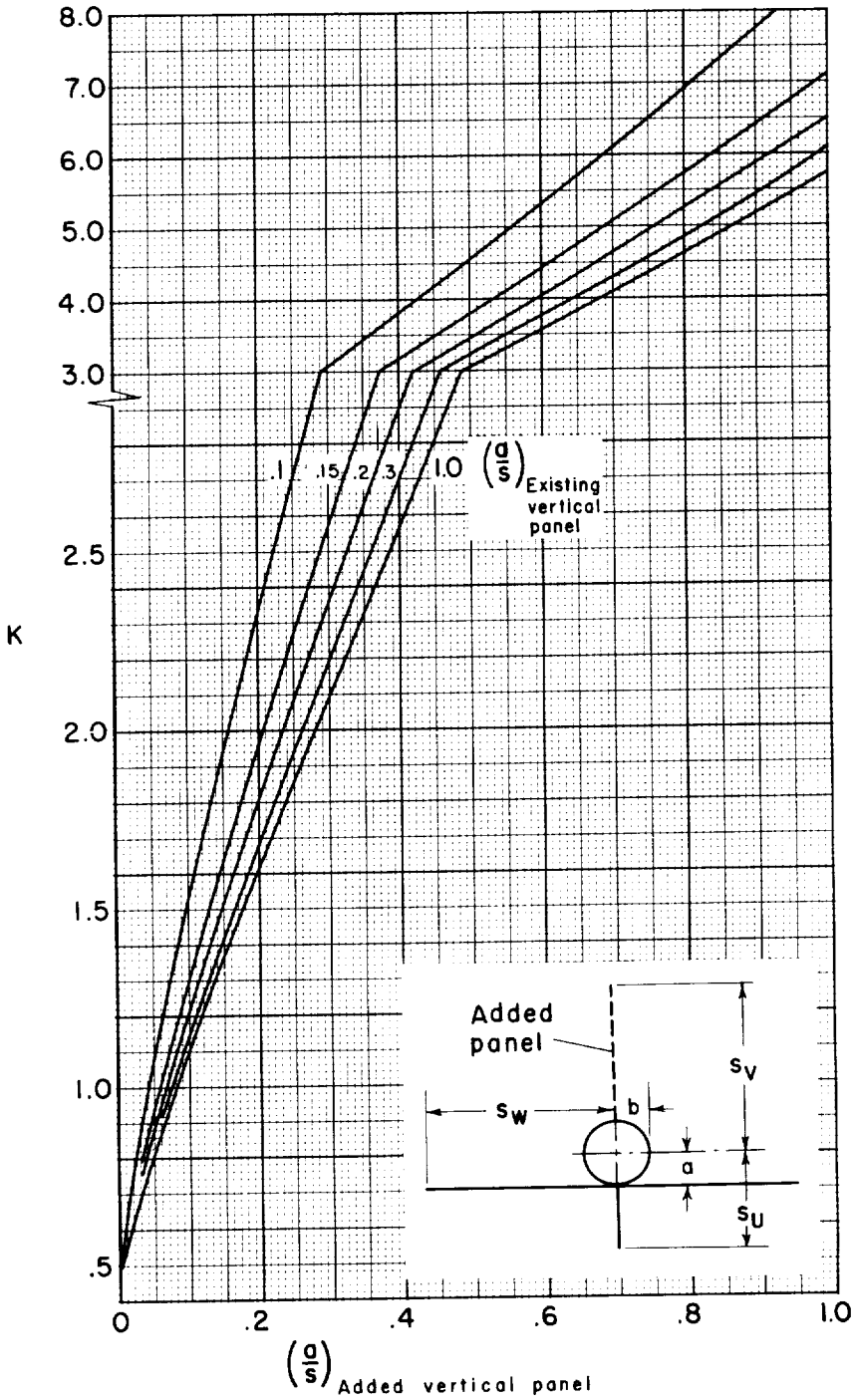

(b) b/s_H or $b/s_W = 0.2$

Figure 4.- Continued.

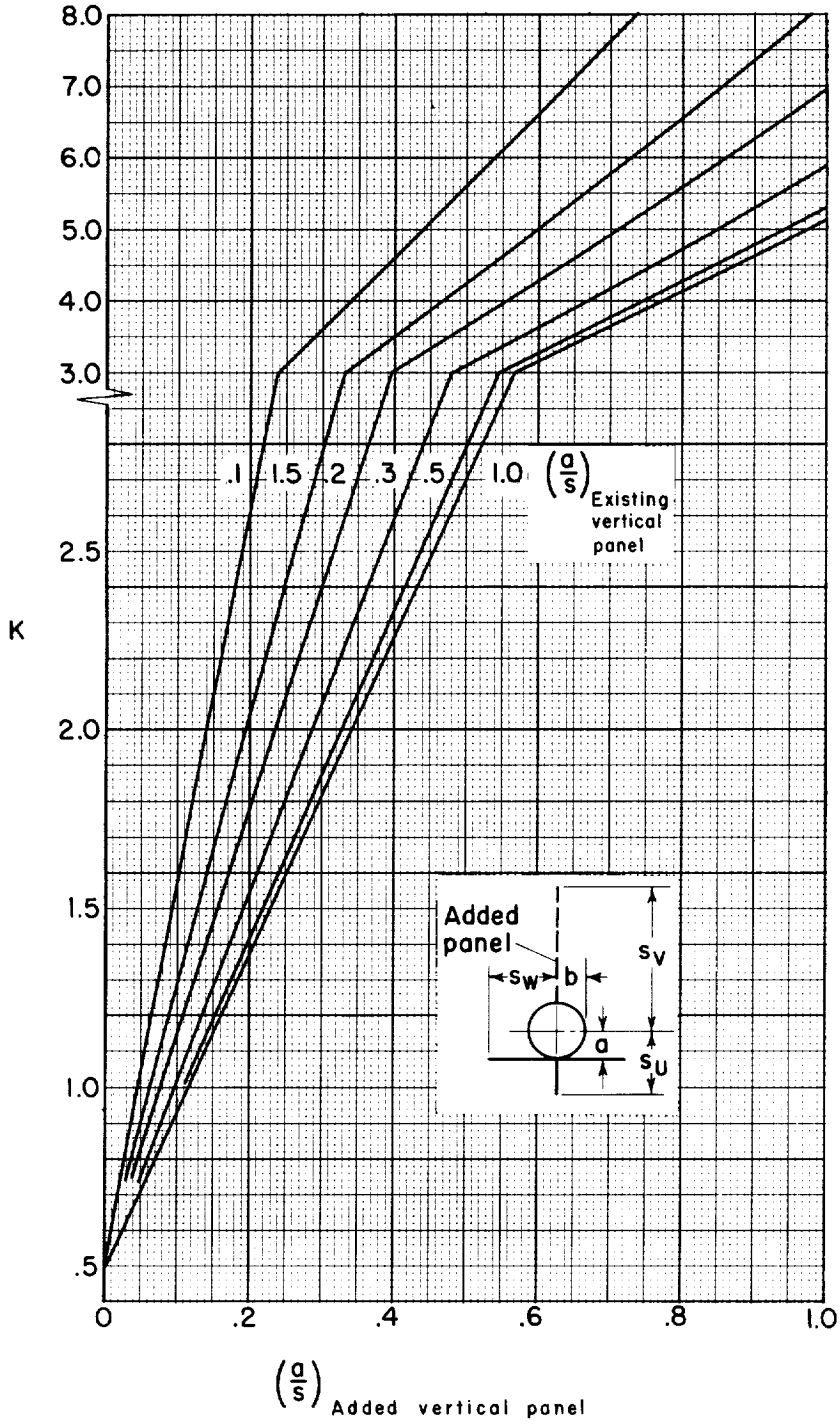

(c) b/s_H or $b/s_W = 0.4$

Figure 4.- Continued.

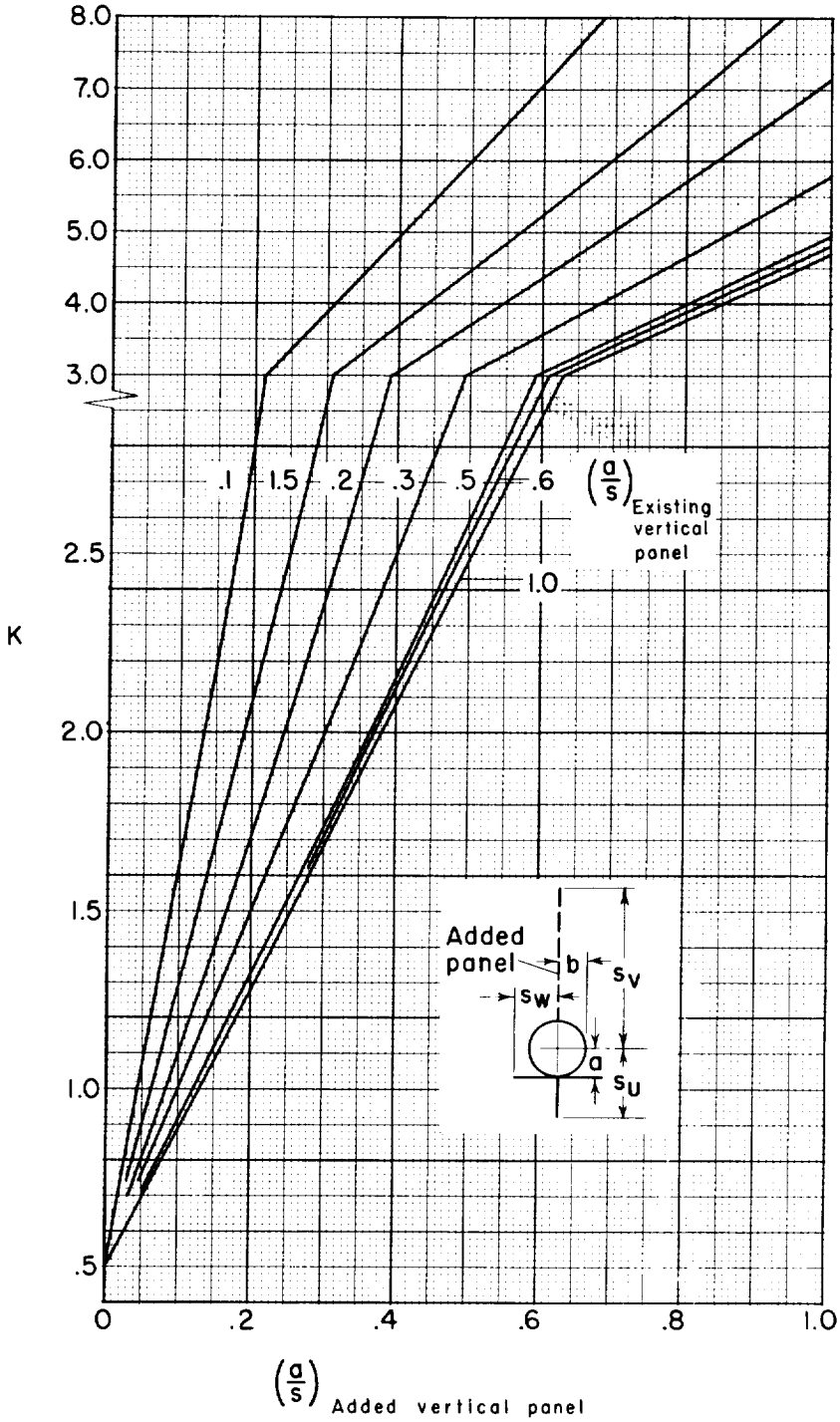

(d) b/s_H or $b/s_W = 0.6$

Figure 4.- Continued.

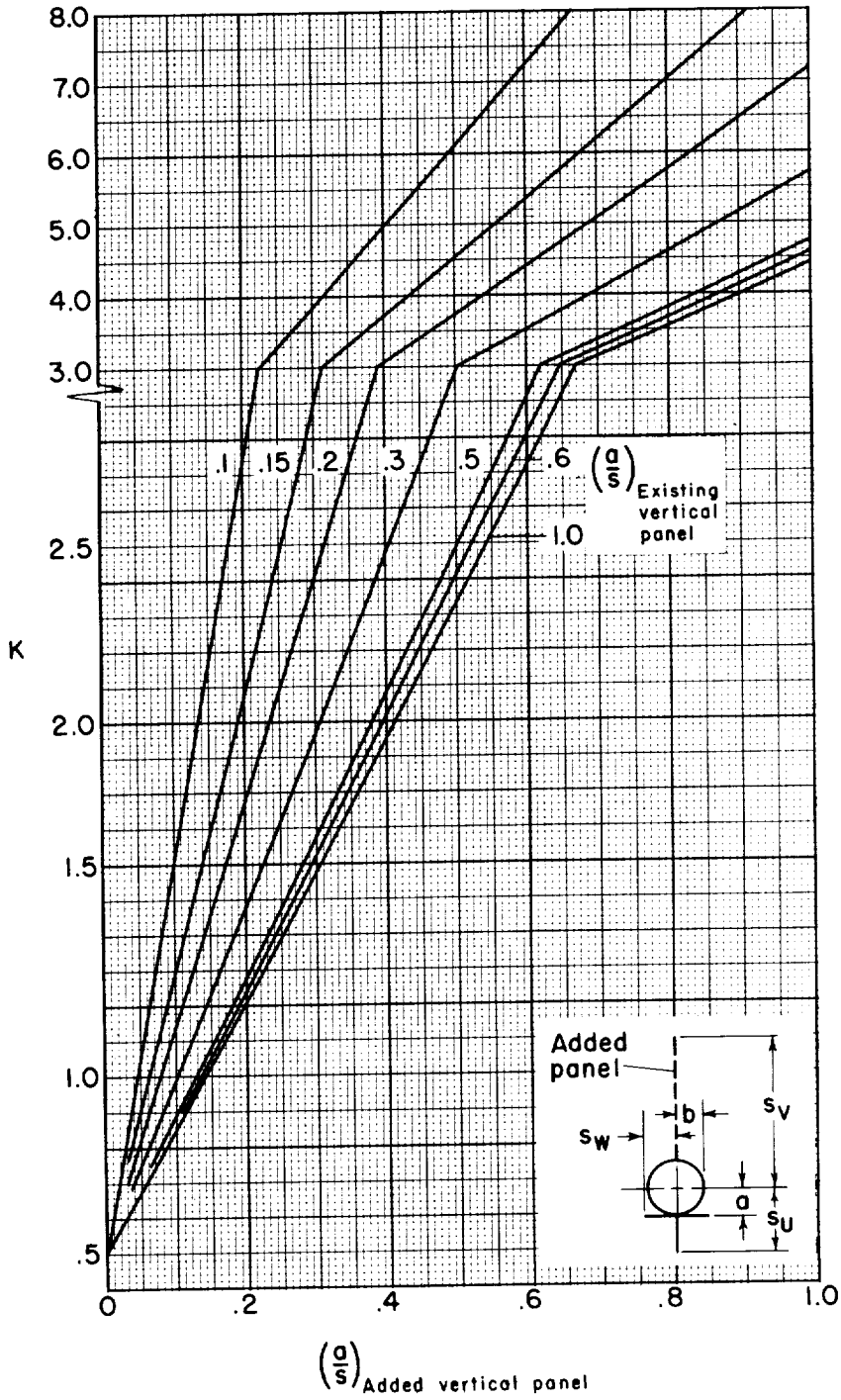

(e) b/s_H or $b/s_W = 0.8$

Figure 4.- Concluded.

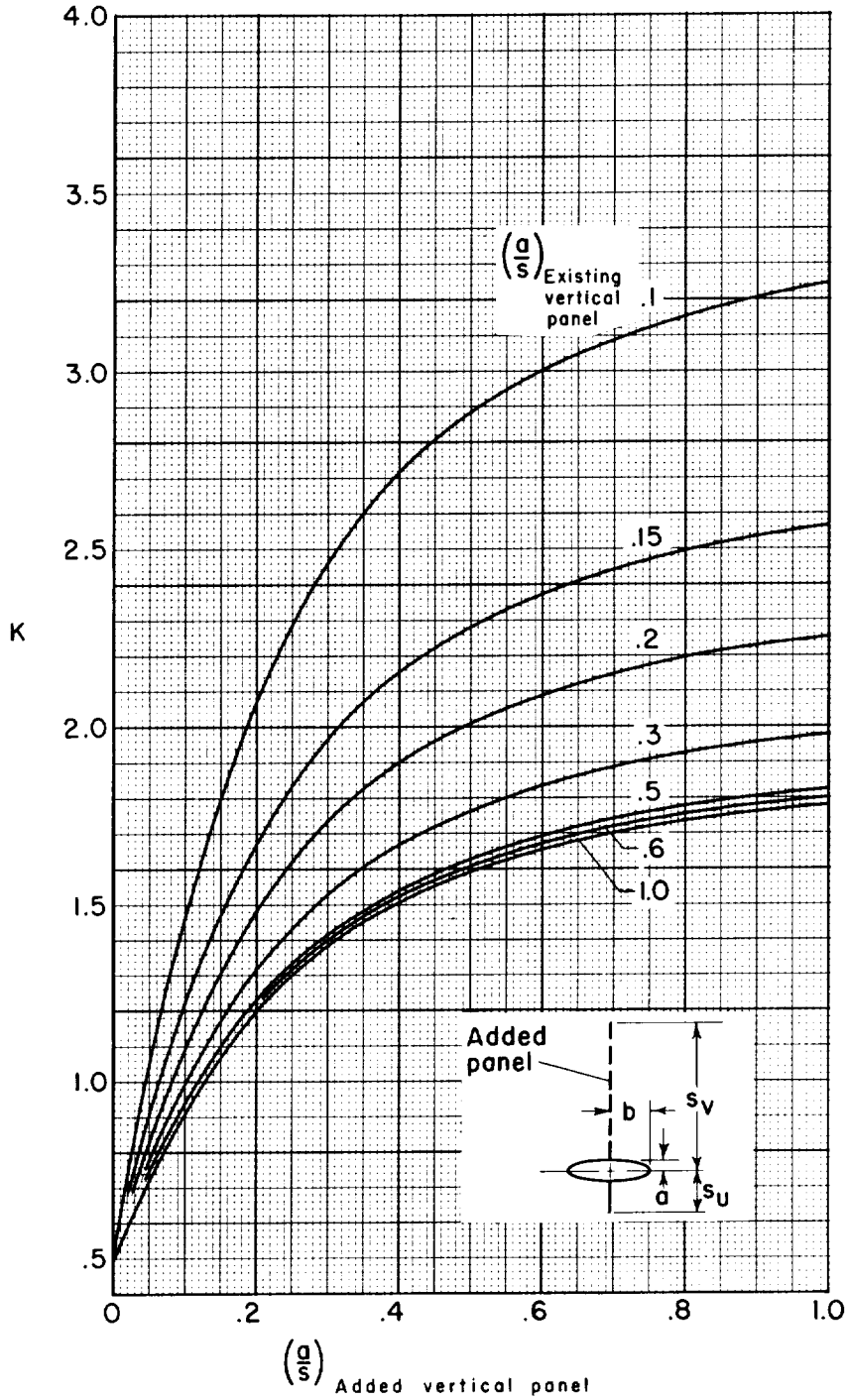

Figure 5.- Apparent mass ratio for various values of a/s of the existing vertical panel in the presence of an elliptical body (a/b = 0.333).

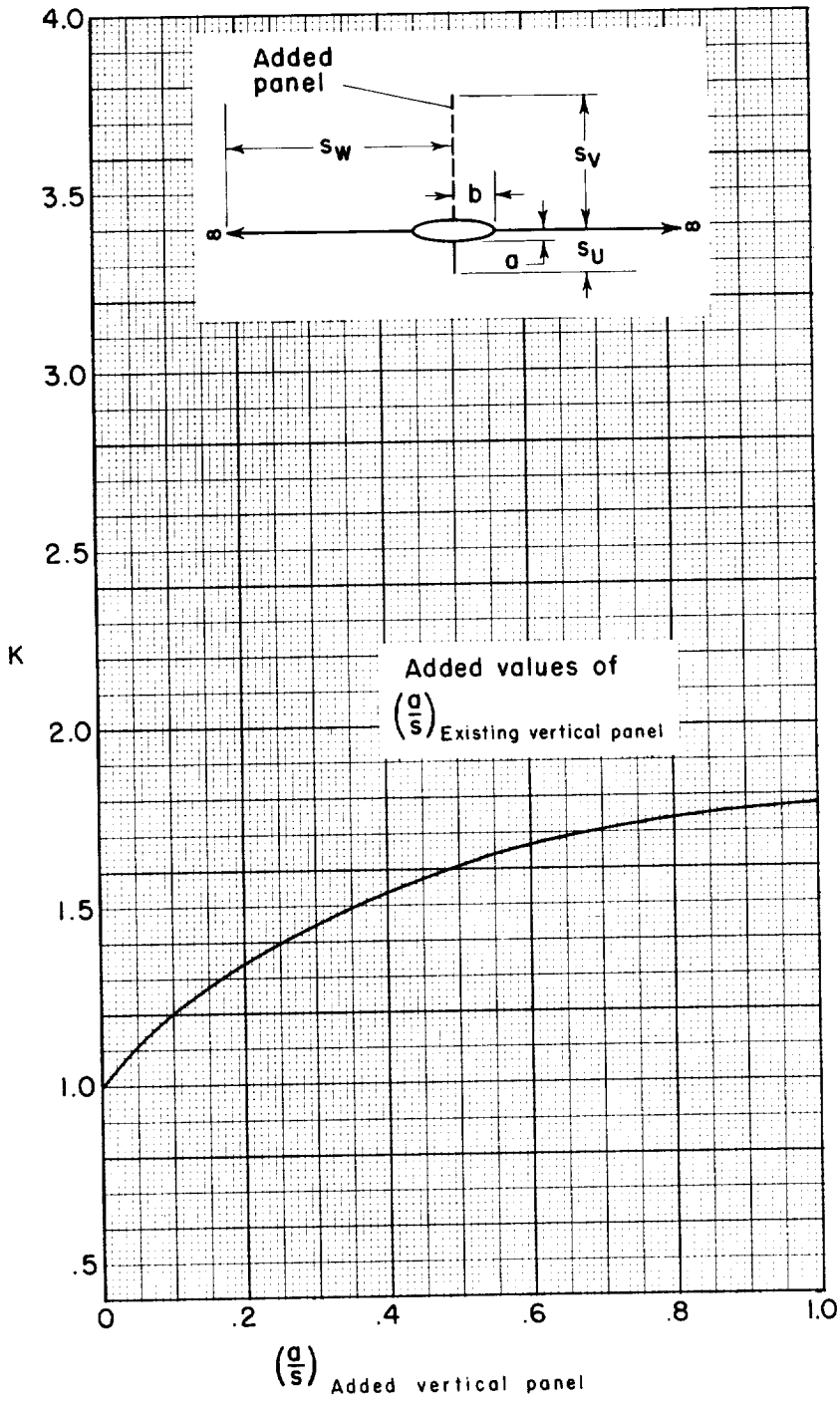

(a) b/s_H or $b/s_W = 0.0$

Figure 6.- Apparent mass ratio for various values of a/s of the existing vertical panel in the presence of an elliptical body (a/b = 0.333) with a mid horizontal surface.

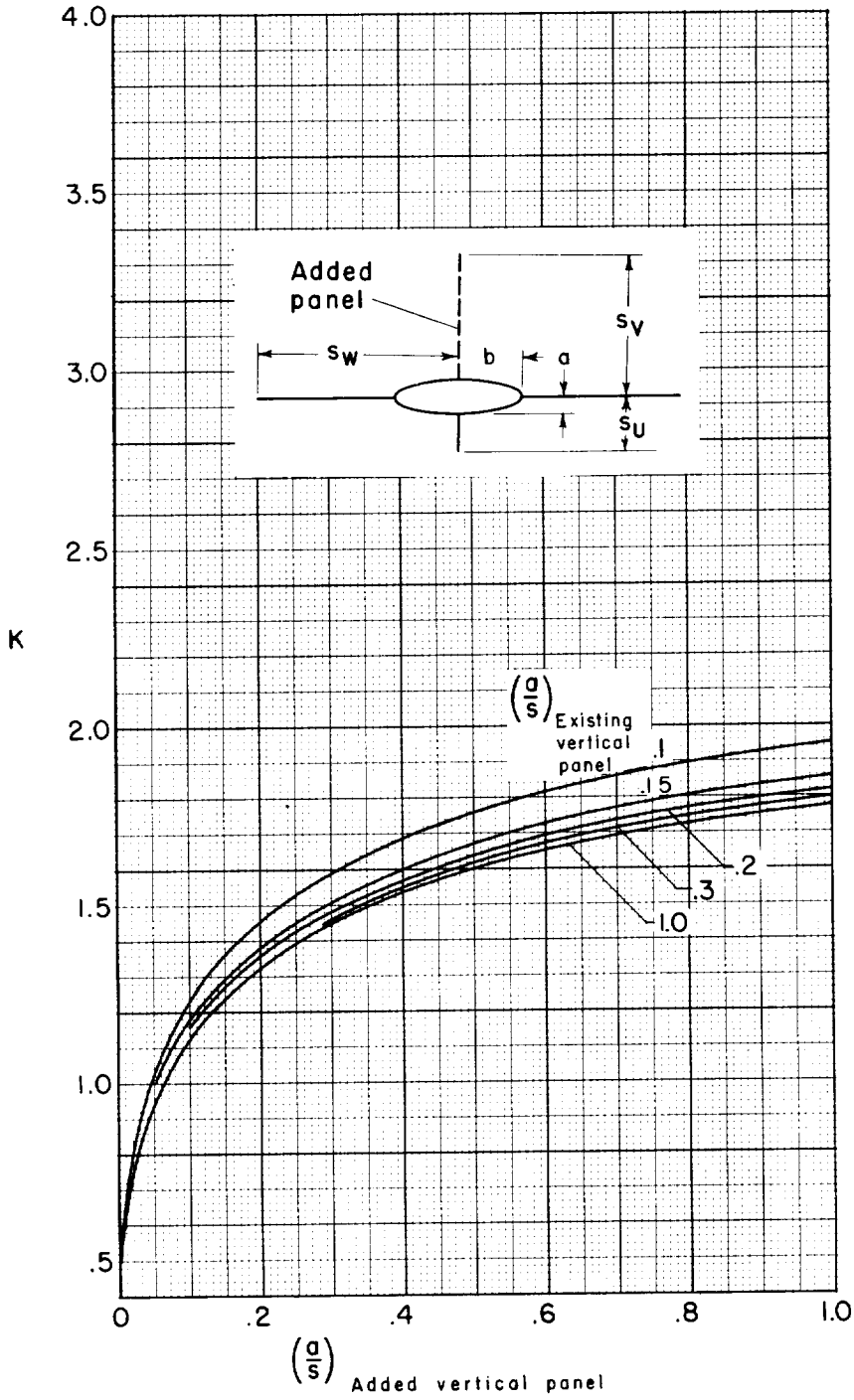

(b) b/s_H or $b/s_W = 0.2$

Figure 6.- Continued.

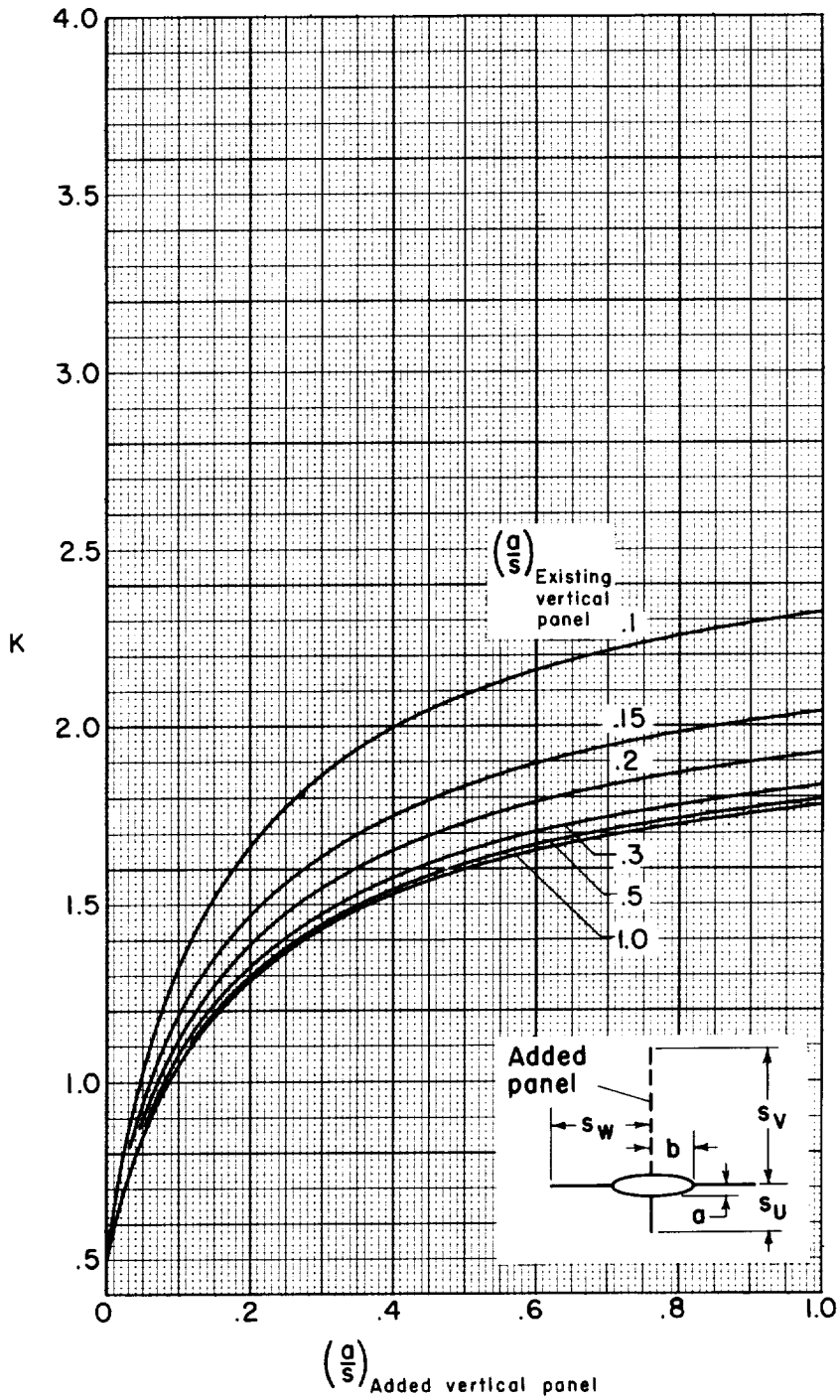

(c) b/s_H or $b/s_W = 0.4$

Figure 6.- Continued.

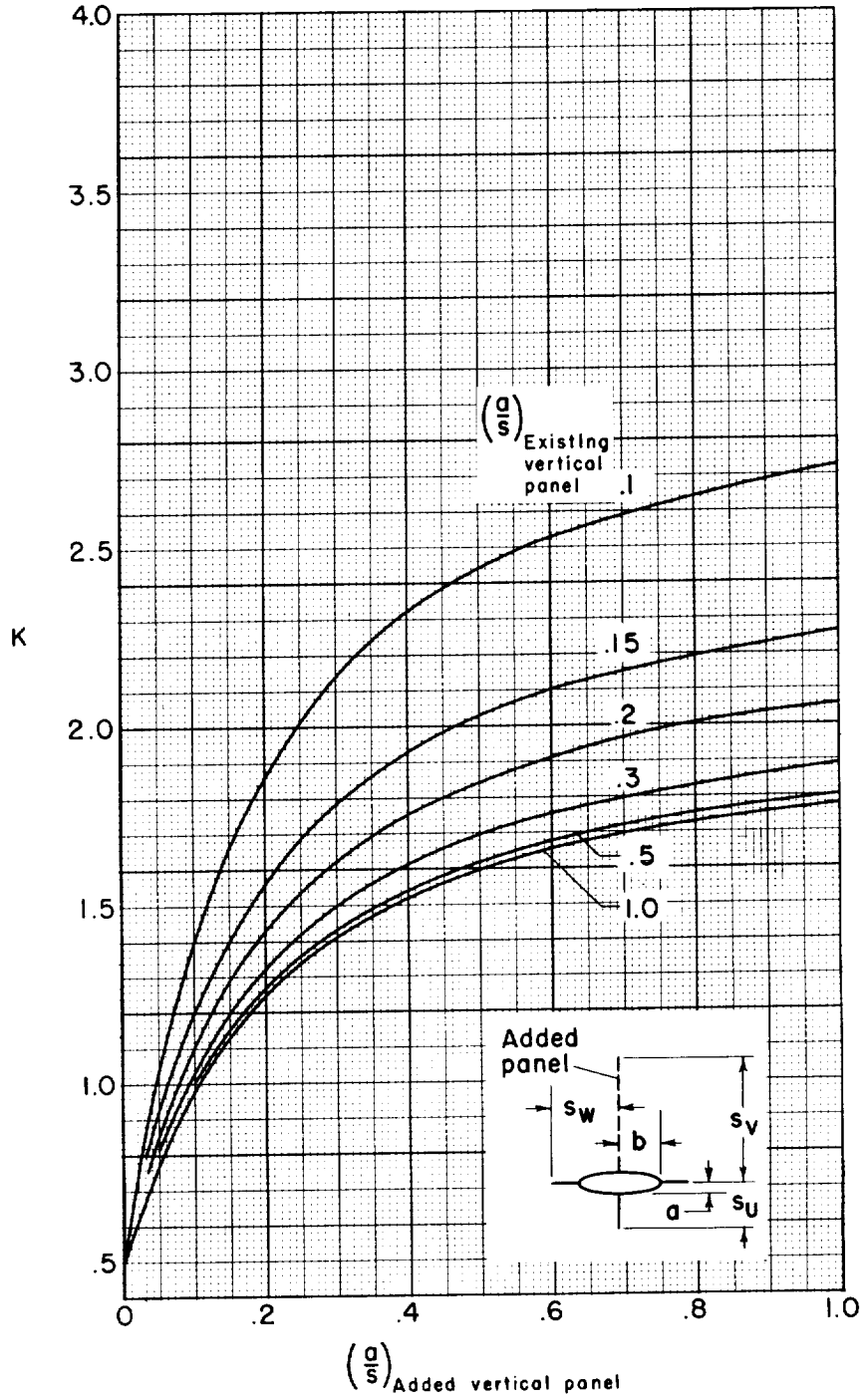

(d) b/s_H or $b/s_W = 0.6$

Figure 6.- Continued.

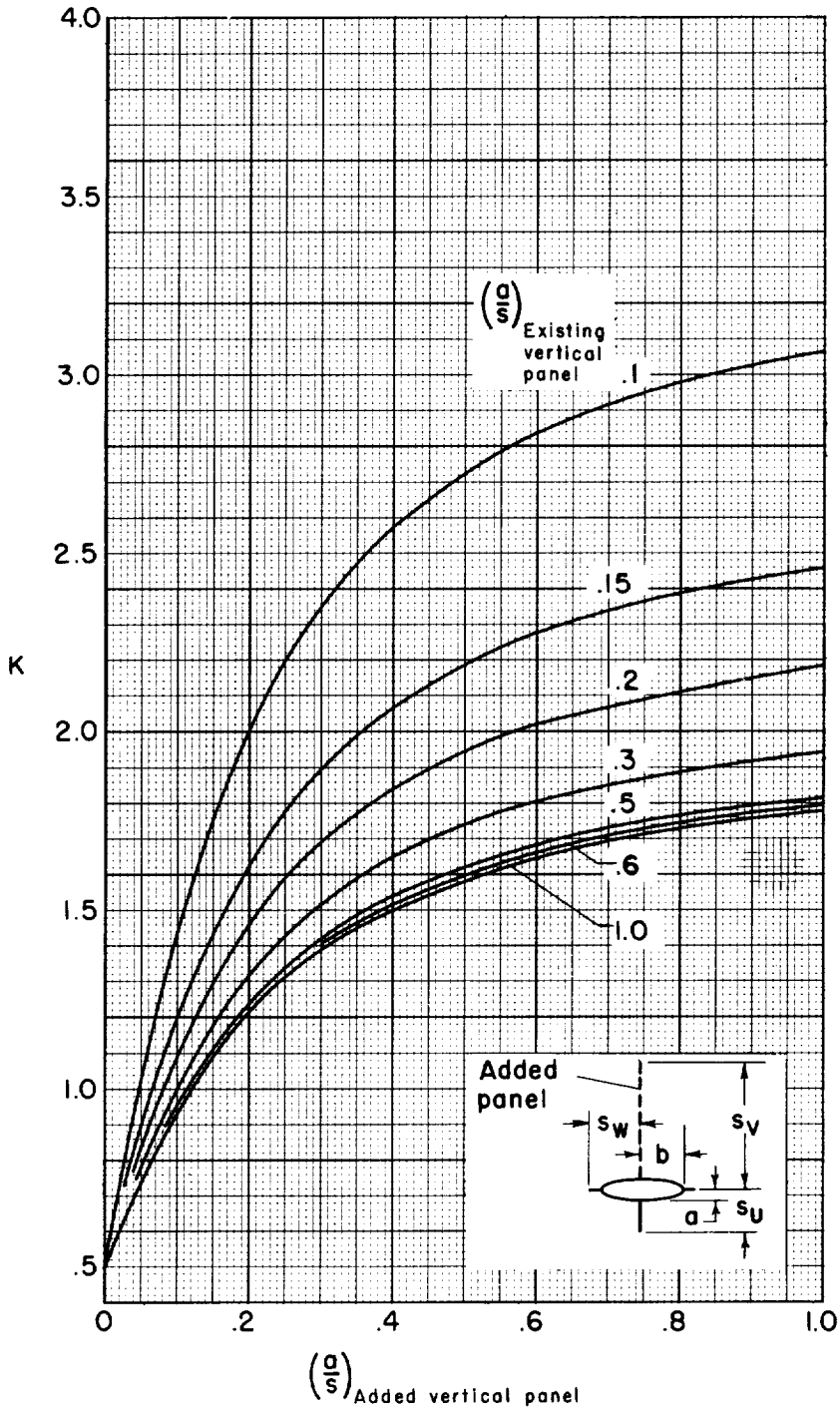

(e) b/s_H or $b/s_W = 0.8$

Figure 6.- Concluded.

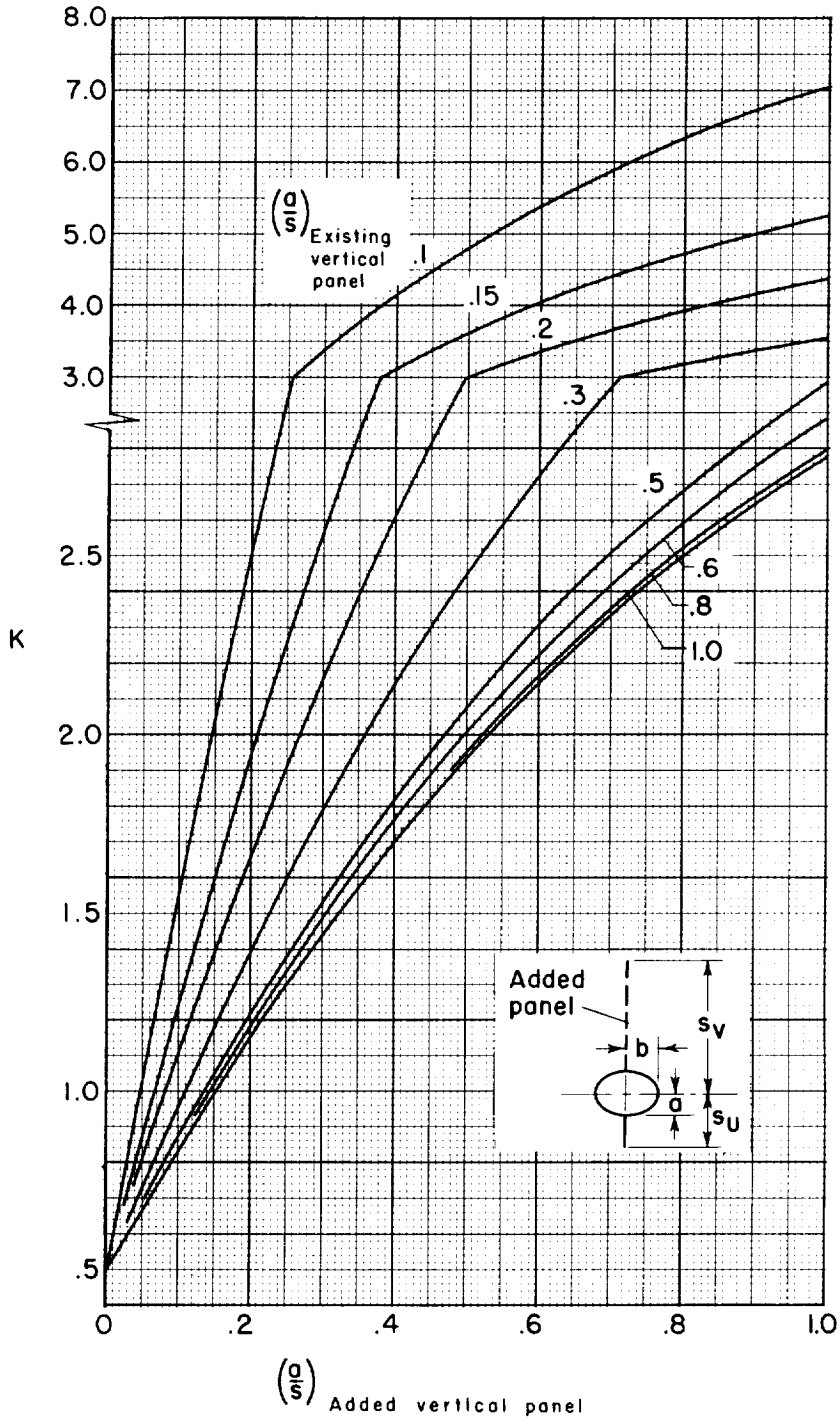

Figure 7.- Apparent mass ratio for various values of a/s of the existing vertical panel in the presence of an elliptical body (a/b = 0.667).

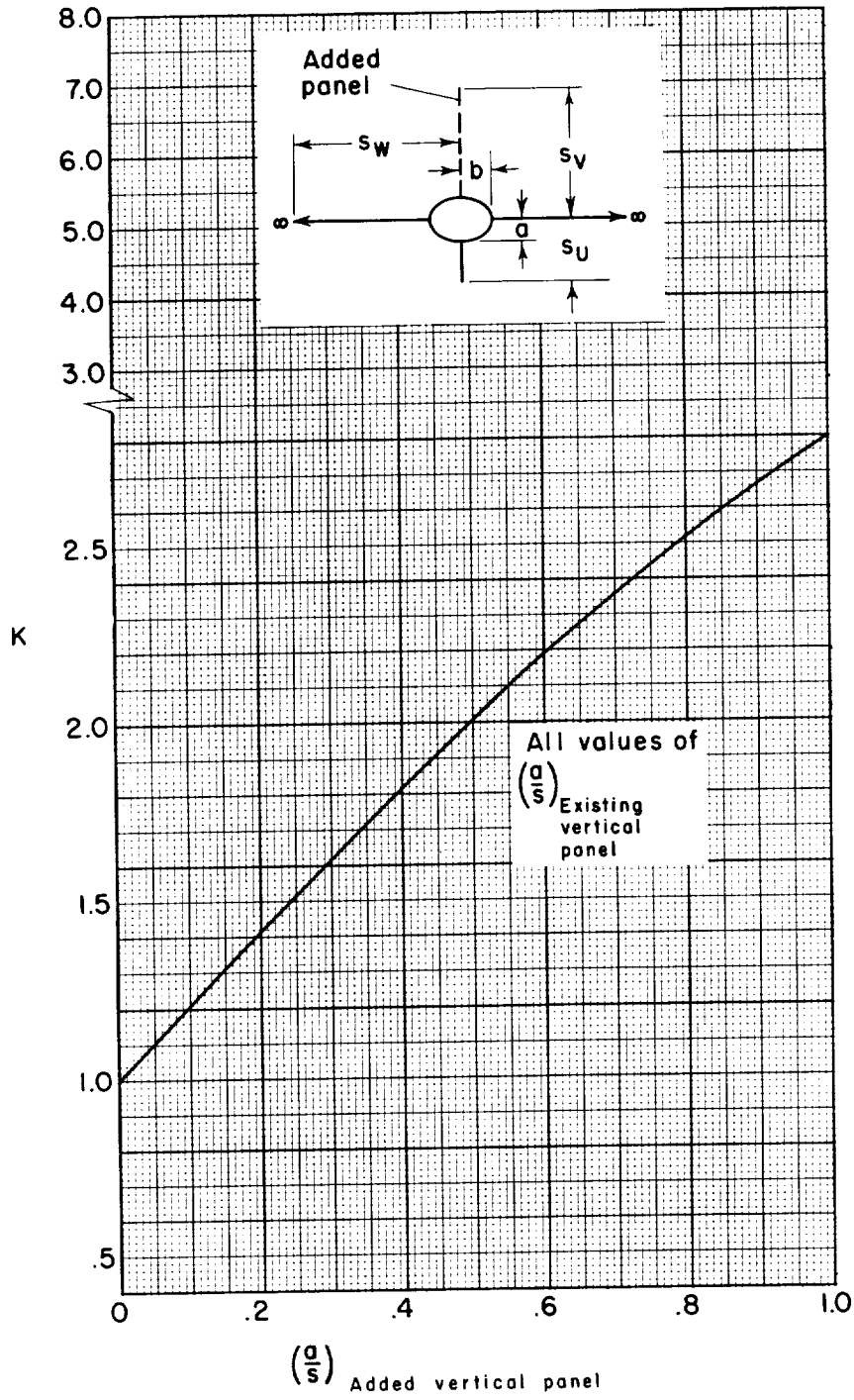

(a) b/s_H or $b/s_W = 0.0$

Figure 8.- Apparent mass ratio for various values of a/s of the existing vertical panel in the presence of an elliptical body (a/b = 0.667) with a mid horizontal surface.

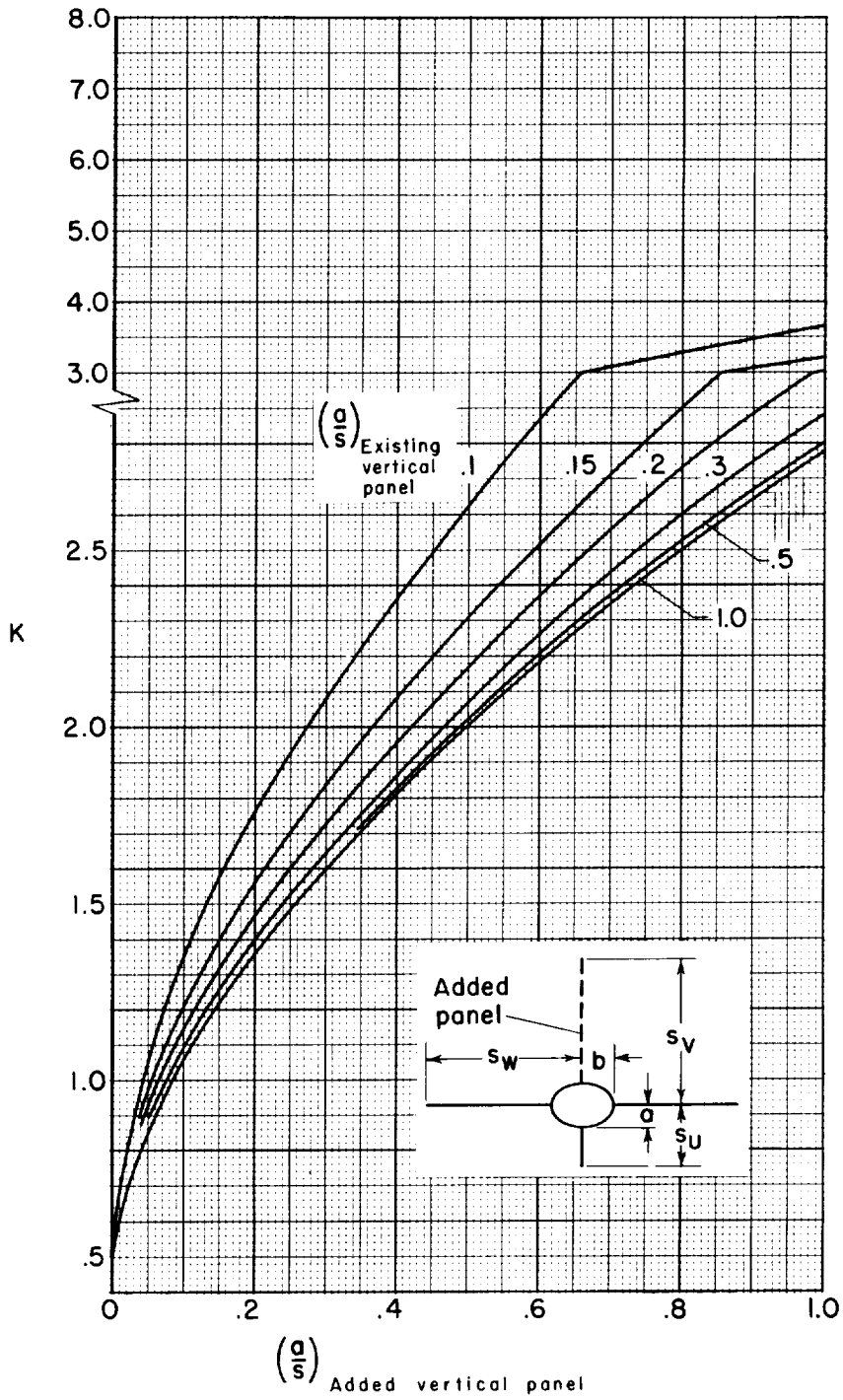

(b) b/s_H or $b/s_W = 0.2$

Figure 8.- Continued.

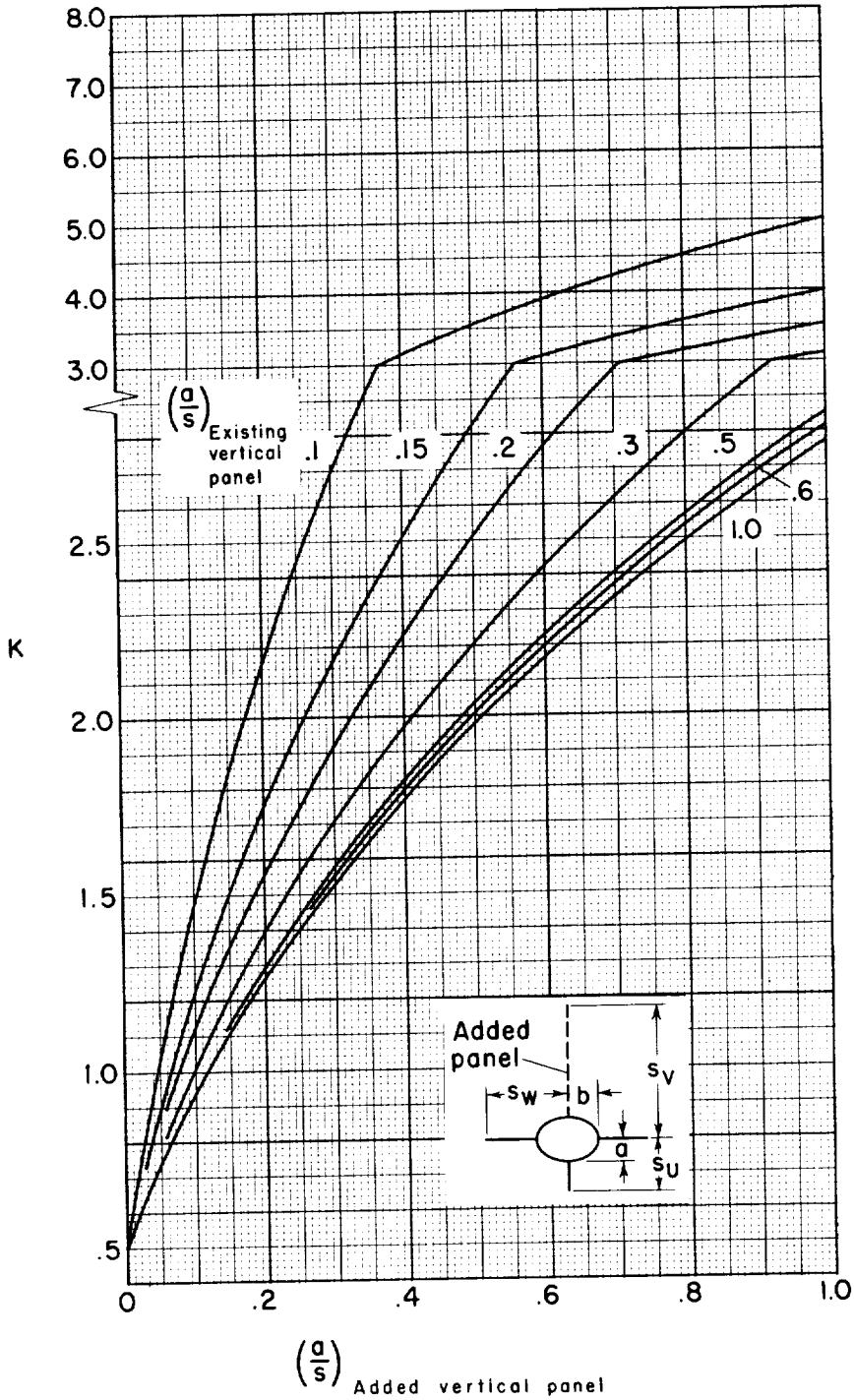

(c) b/s_H or $b/s_W = 0.4$

Figure 8.- Continued.

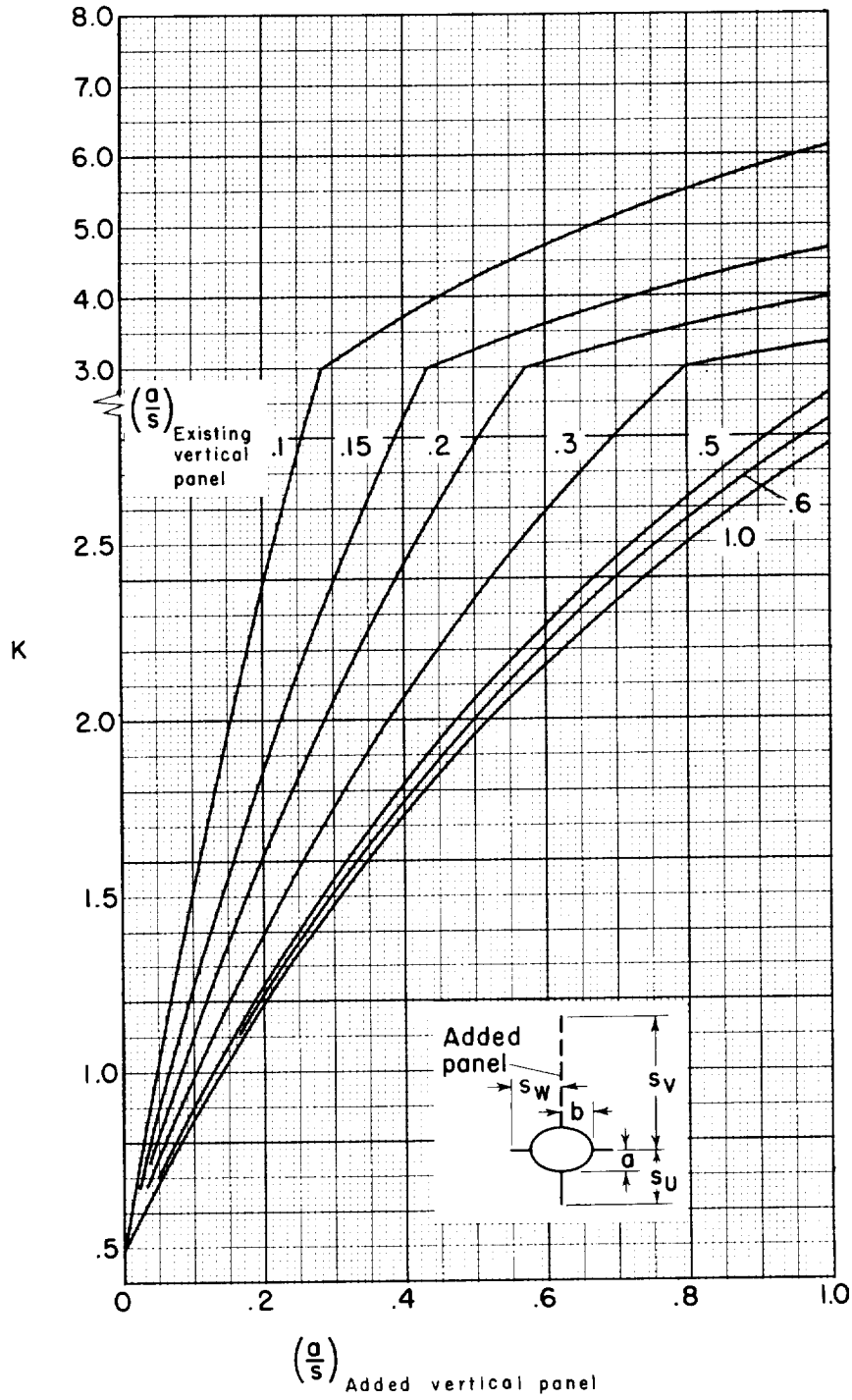

(d) b/s_H or $b/s_W = 0.6$

Figure 8.- Continued.

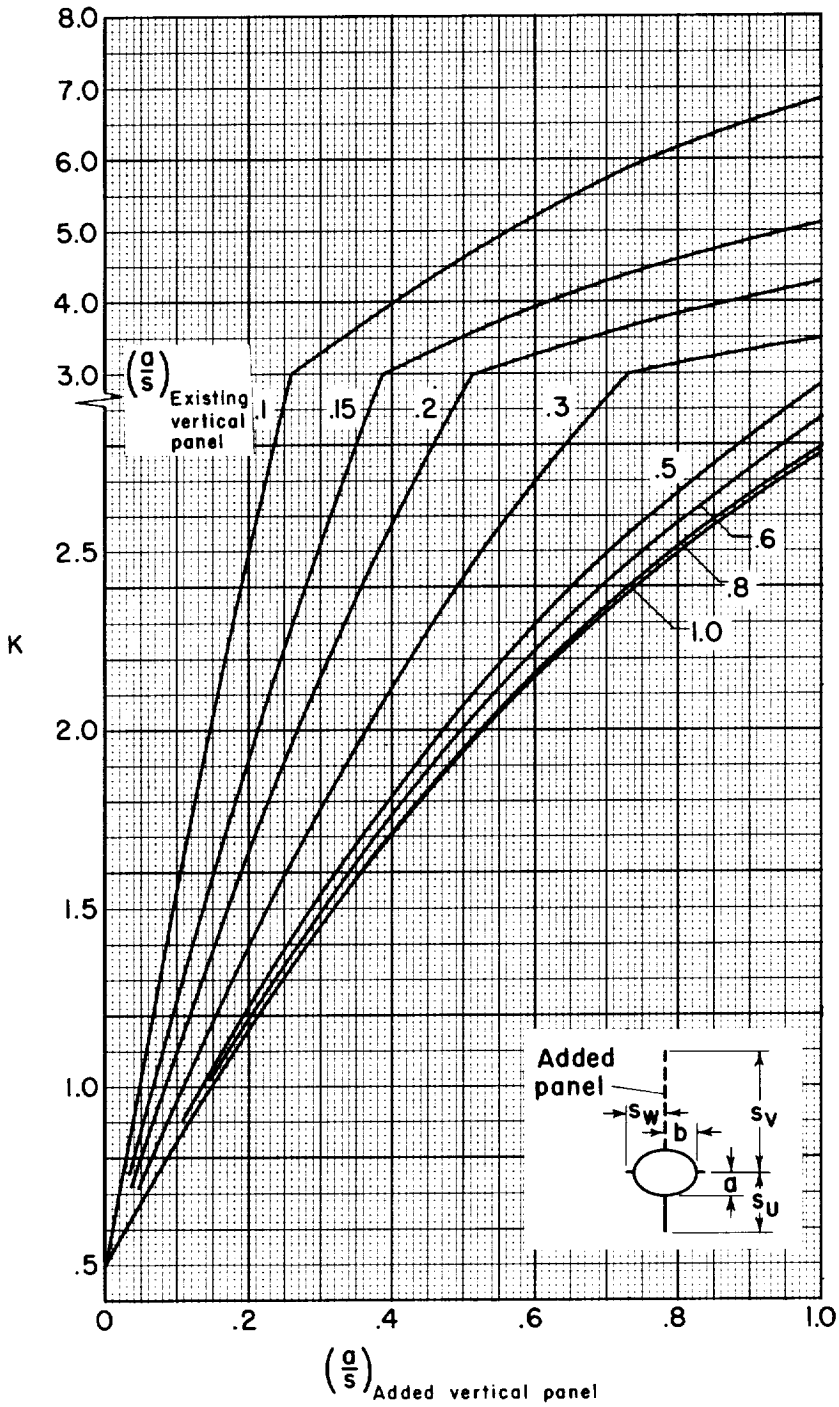

(e) b/s_H or $b/s_W = 0.8$

Figure 8.- Concluded.

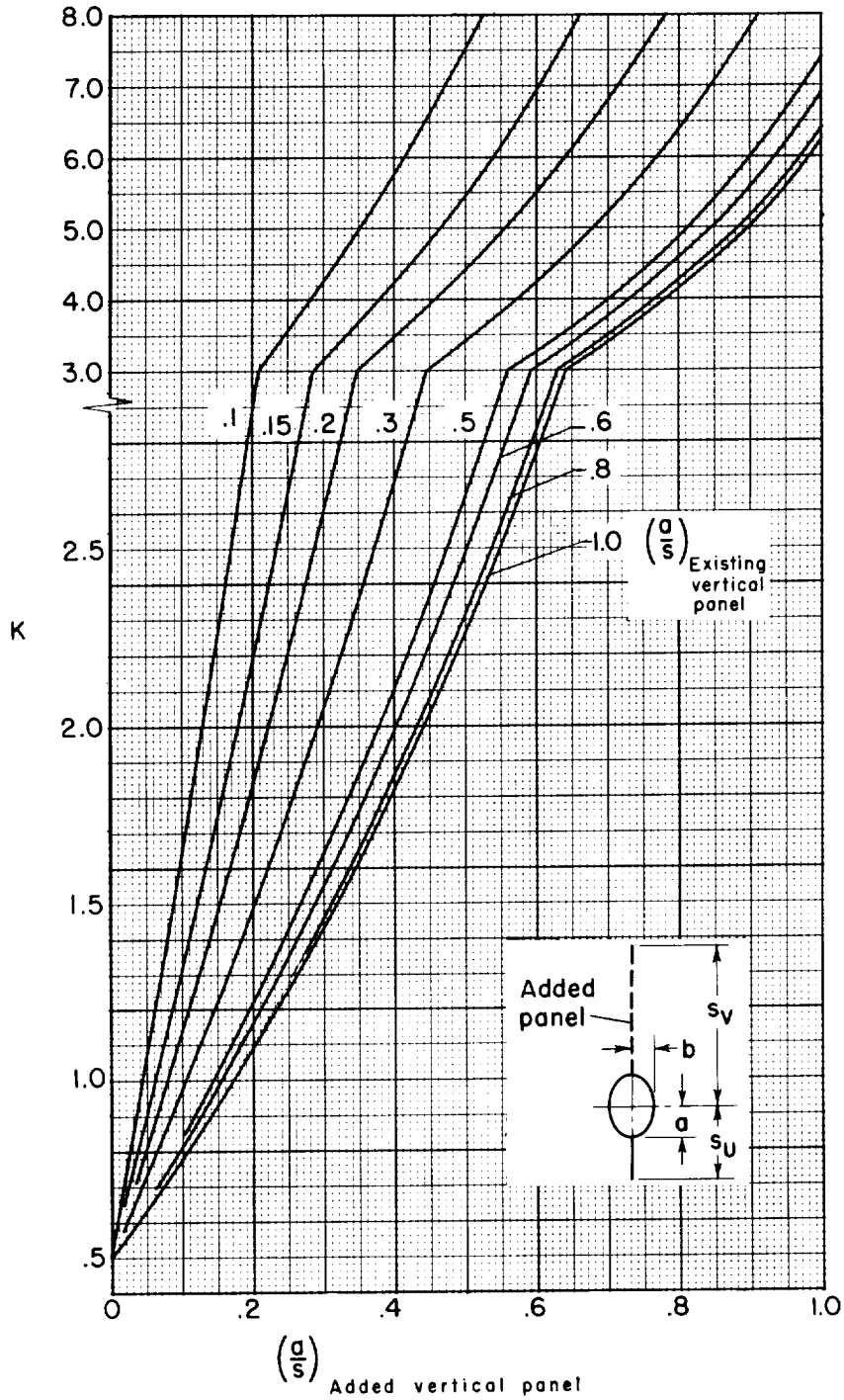

Figure 9.- Apparent mass ratio for various values of a/s of the existing vertical panel in the presence of an elliptical body (a/b = 1.500).

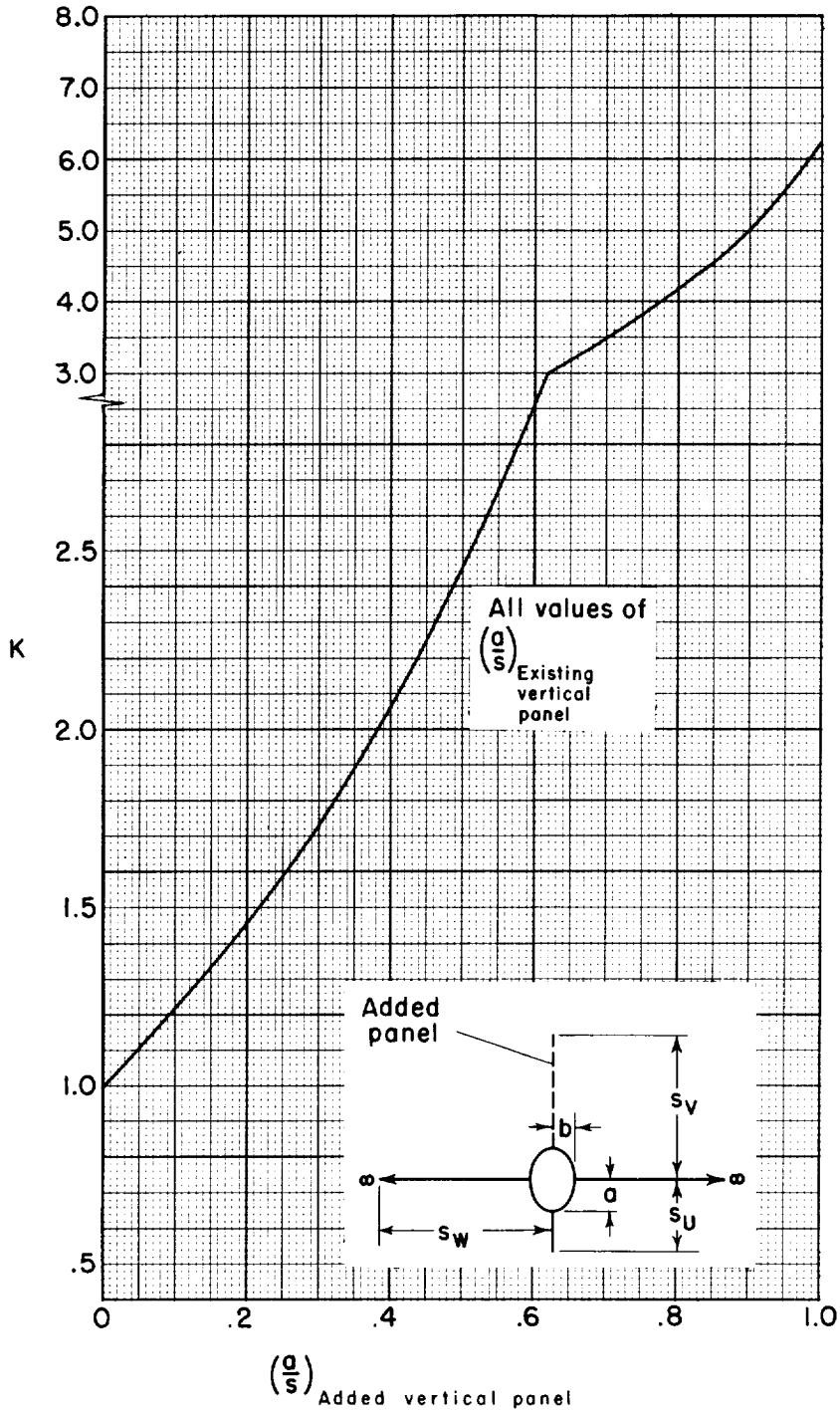

(a) b/s_H or $b/s_W = 0.0$

Figure 10.- Apparent mass ratio for various values of a/s of the existing vertical panel in the presence of an elliptical body (a/b = 1.500) with a mid horizontal surface.

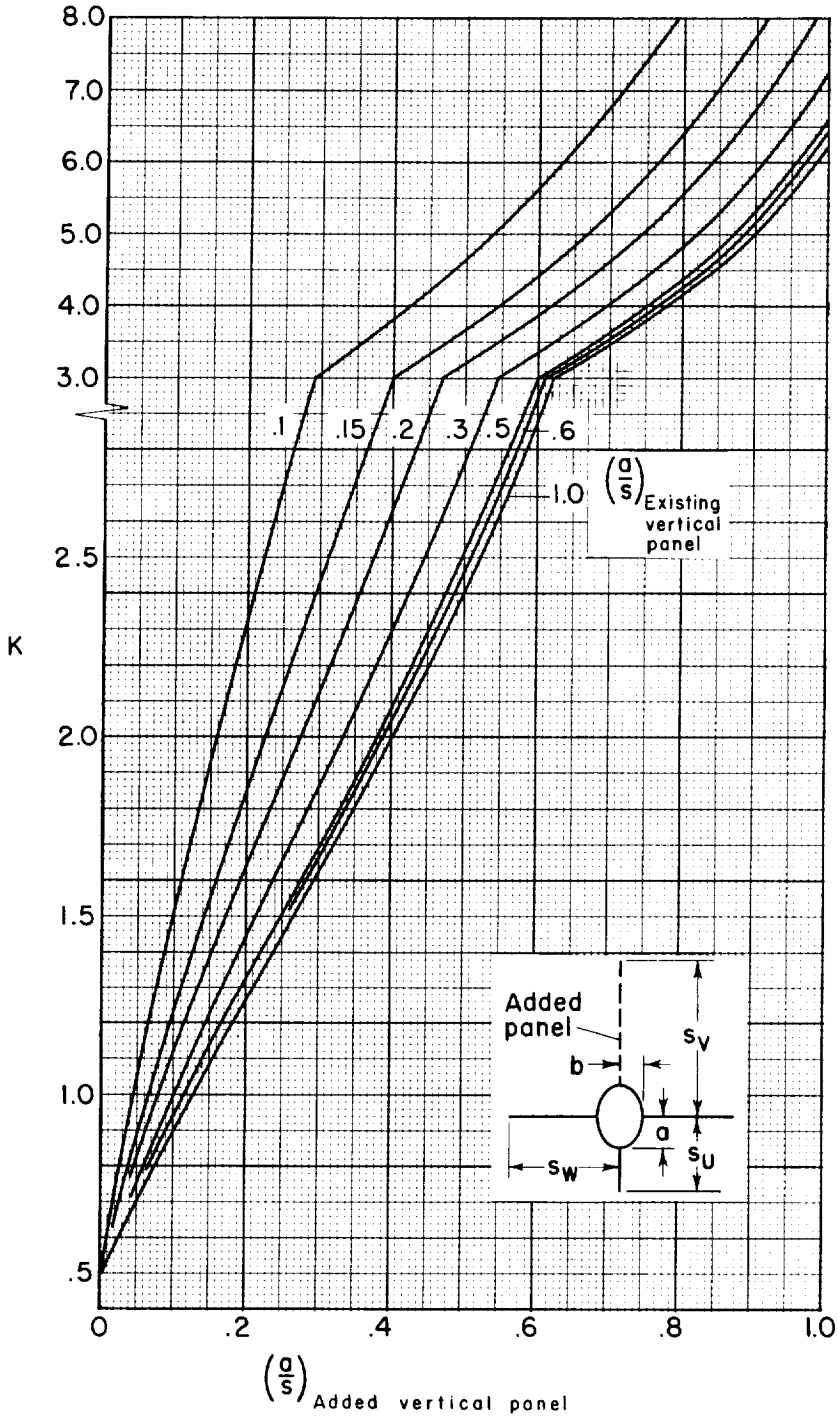

(b) b/s_H or $b/s_W = 0.2$

Figure 10.- Continued.

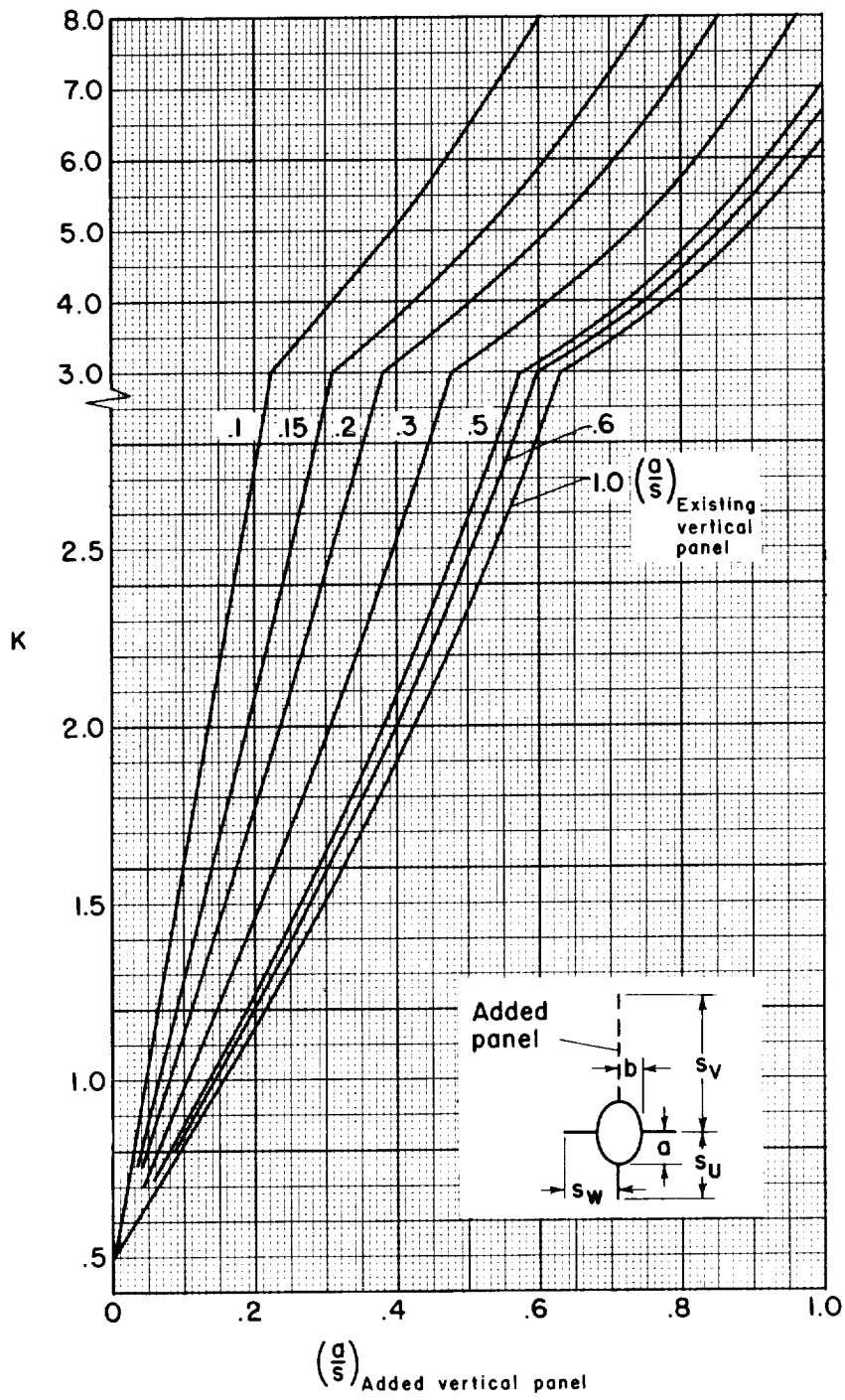

(c) b/s_H or $b/s_W = 0.4$

Figure 10.- Continued.

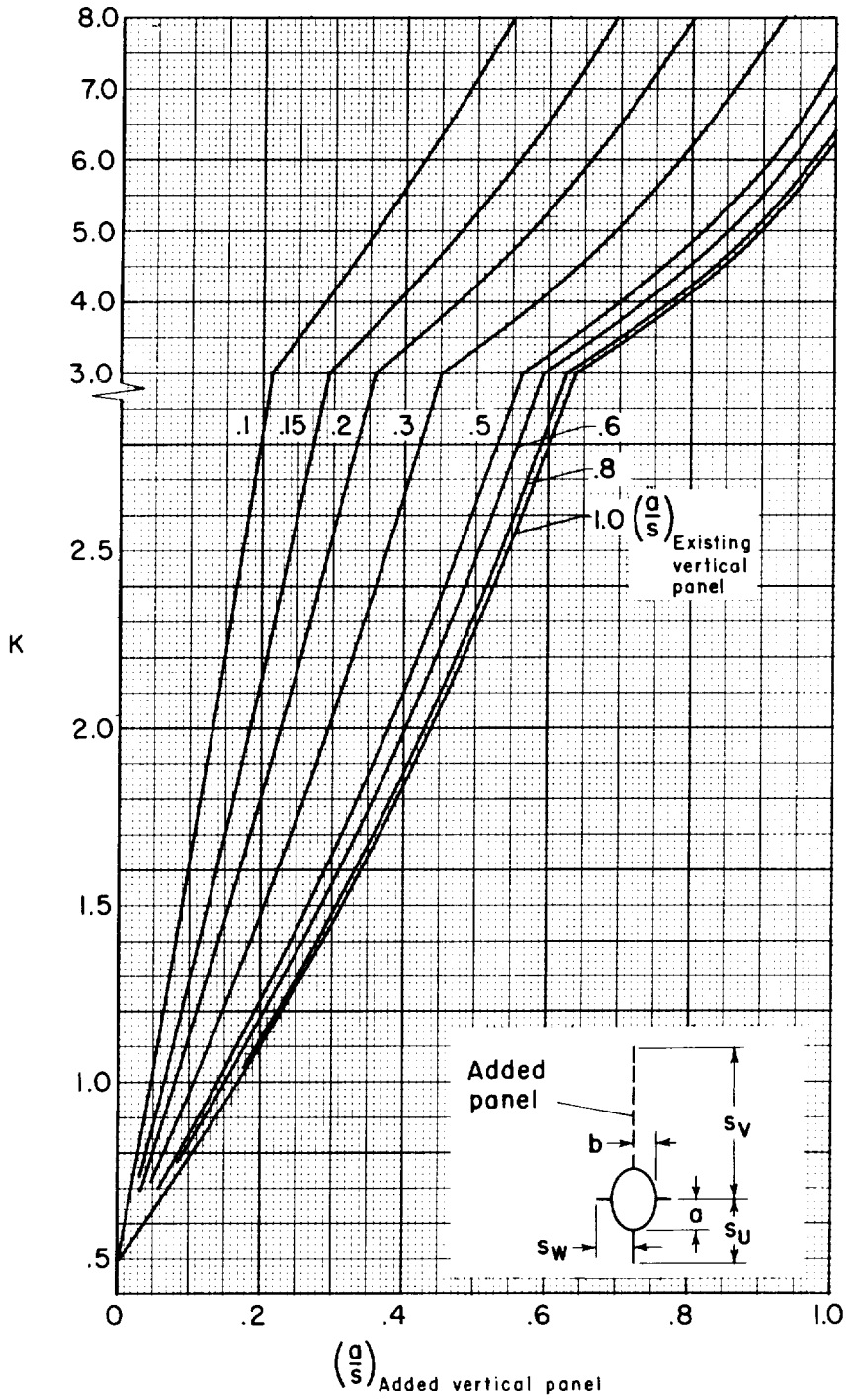

(d) b/s_H or b/s_W = 0.6

Figure 10.- Continued.

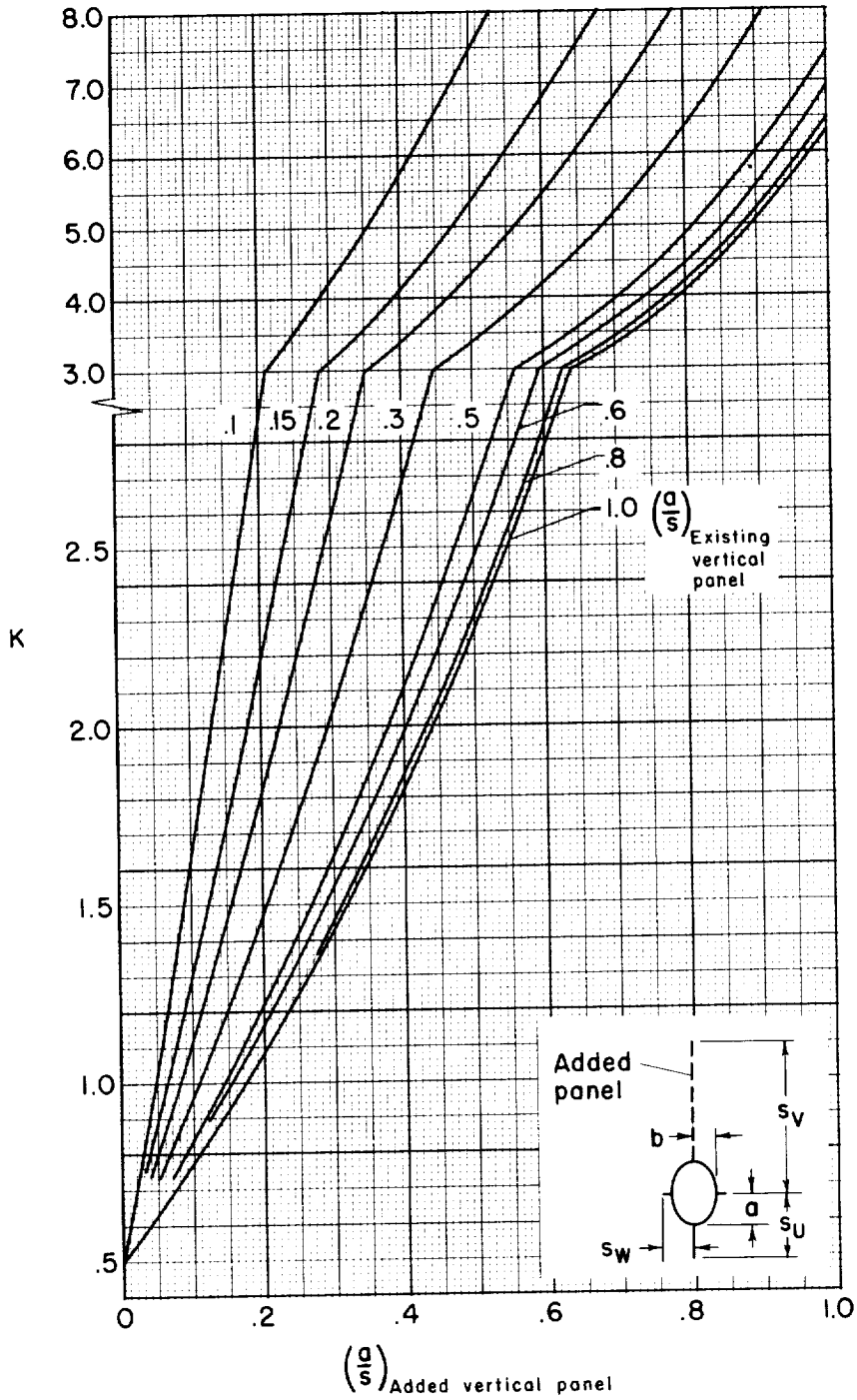

(e) b/s_H or $b/s_W = 0.8$

Figure 10.- Concluded.

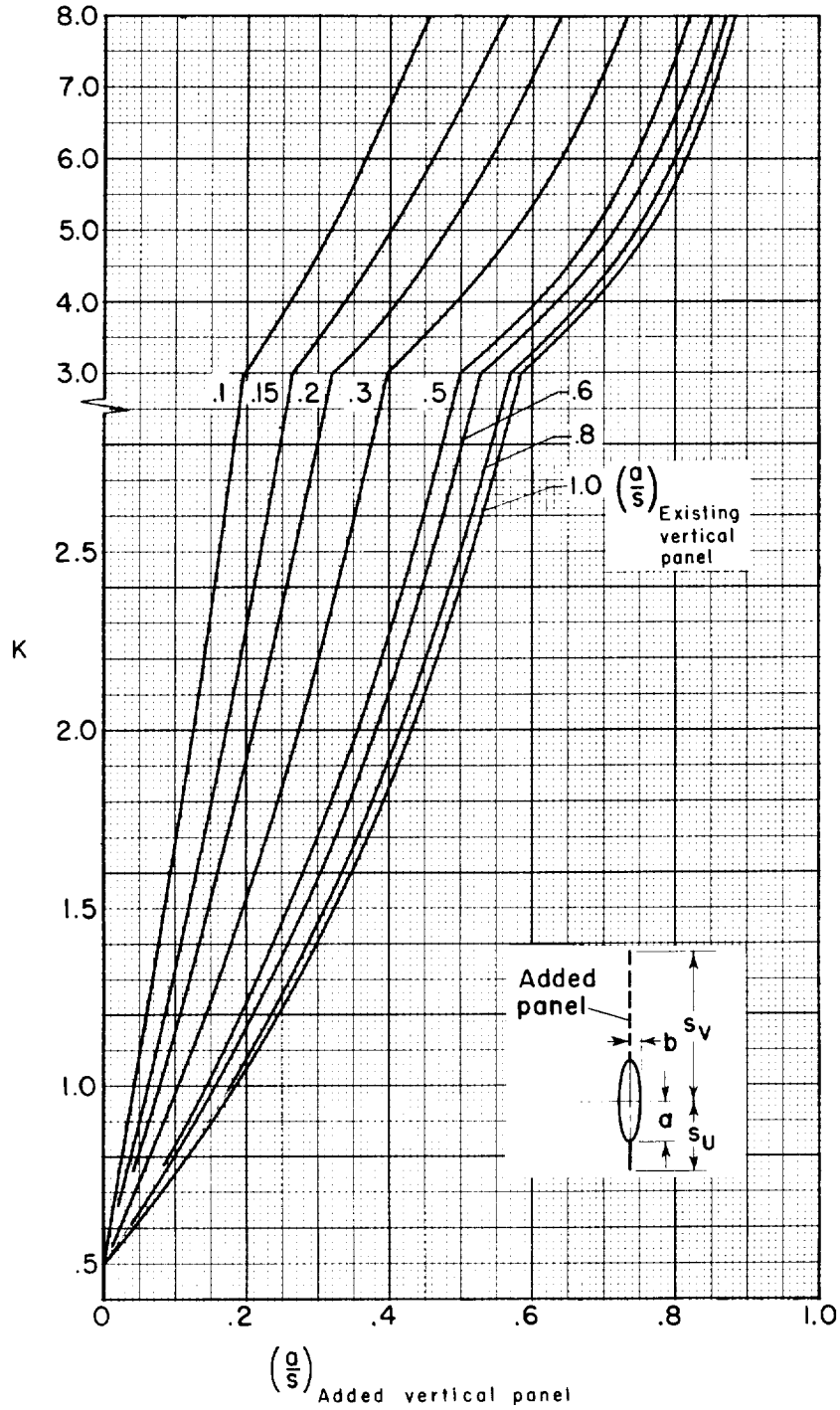

Figure 11.- Apparent mass ratio for various values of a/s of the existing vertical panel in the presence of an elliptical body (a/b = 3.000).

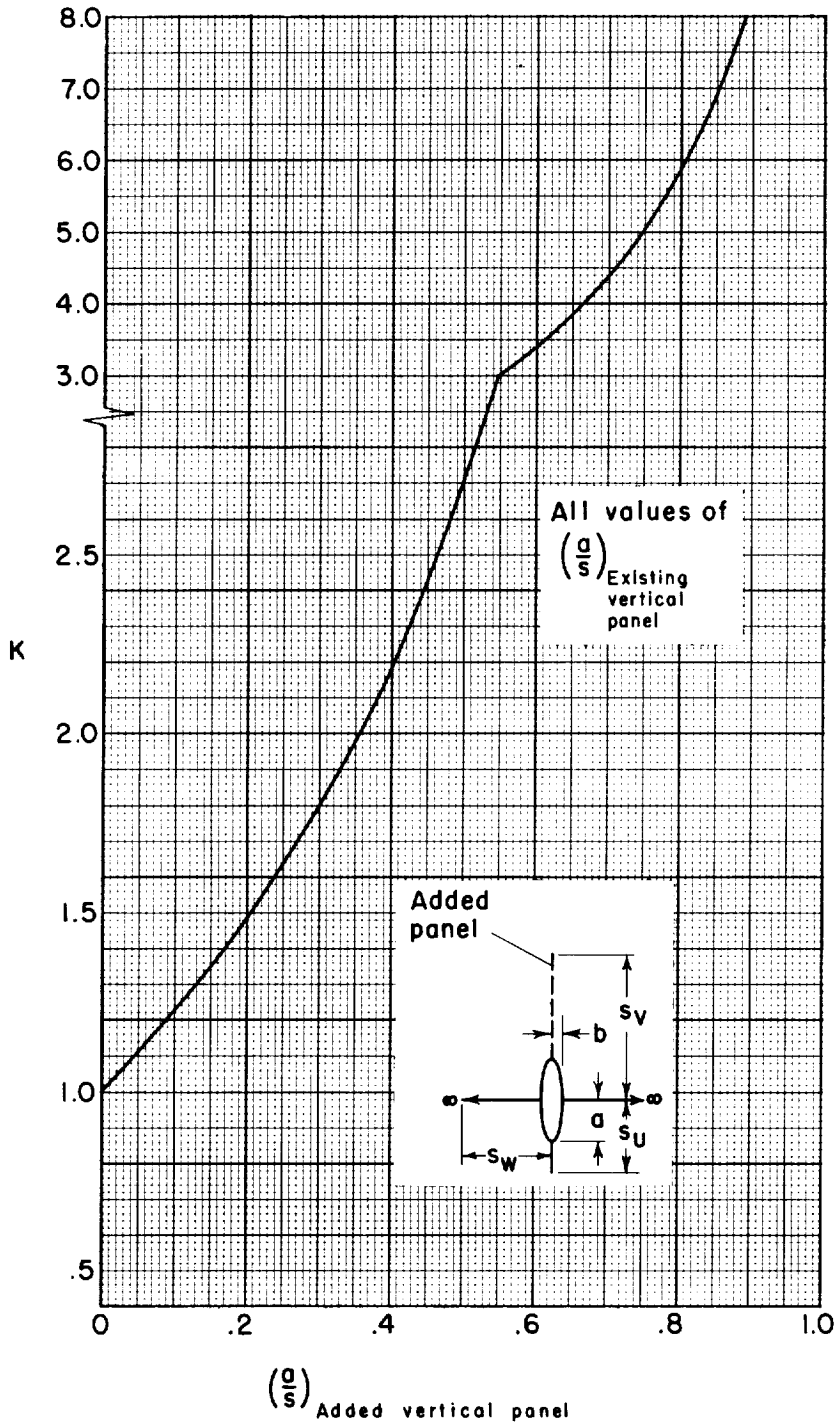

(a) b/s_H or $b/s_W = 0.0$

Figure 12.- Apparent mass ratio for various values of a/s of the existing vertical panel in the presence of an elliptical body (a/b = 3.000) with a mid horizontal surface.

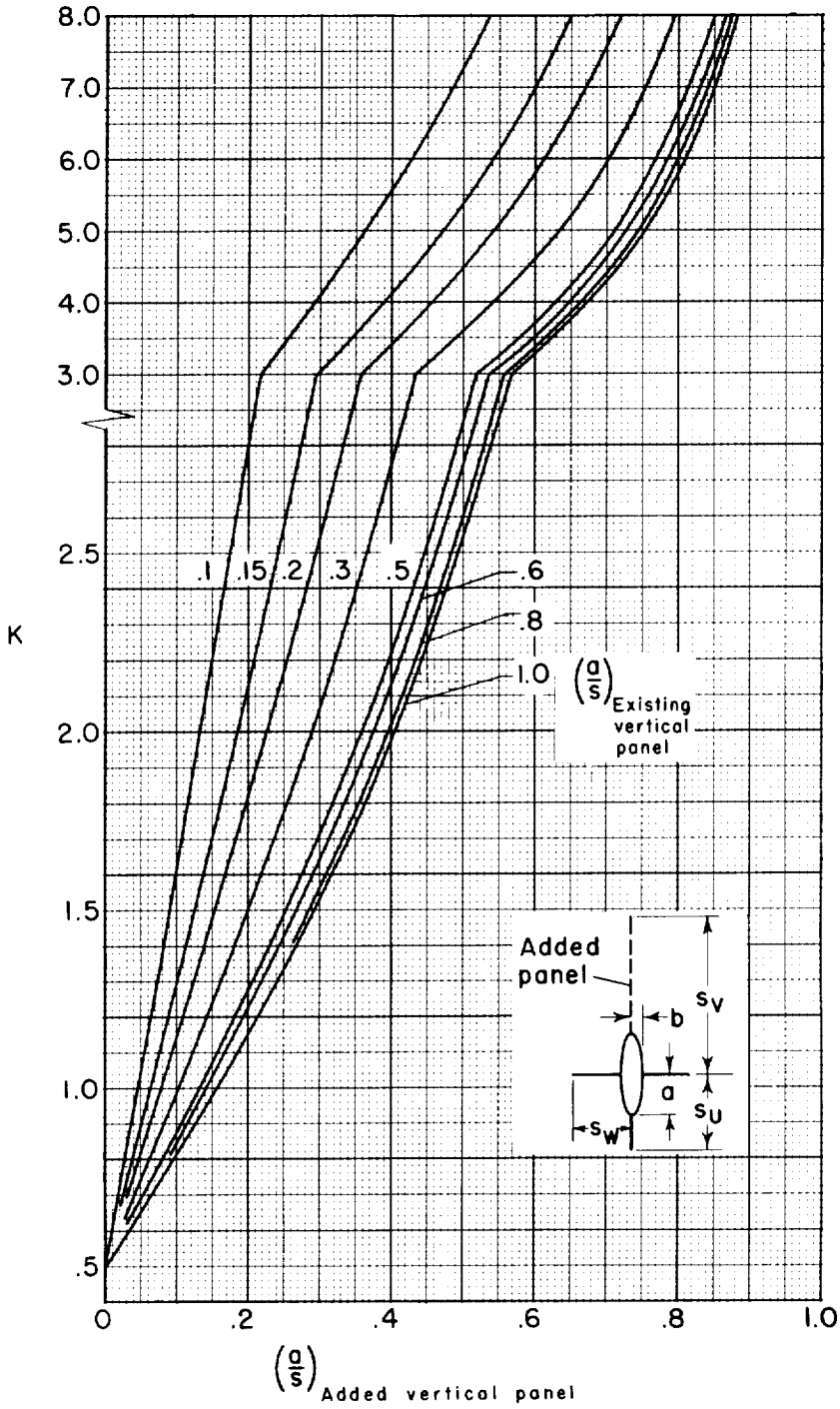

(b) b/s_H or $b/s_W = 0.2$

Figure 12.- Continued.

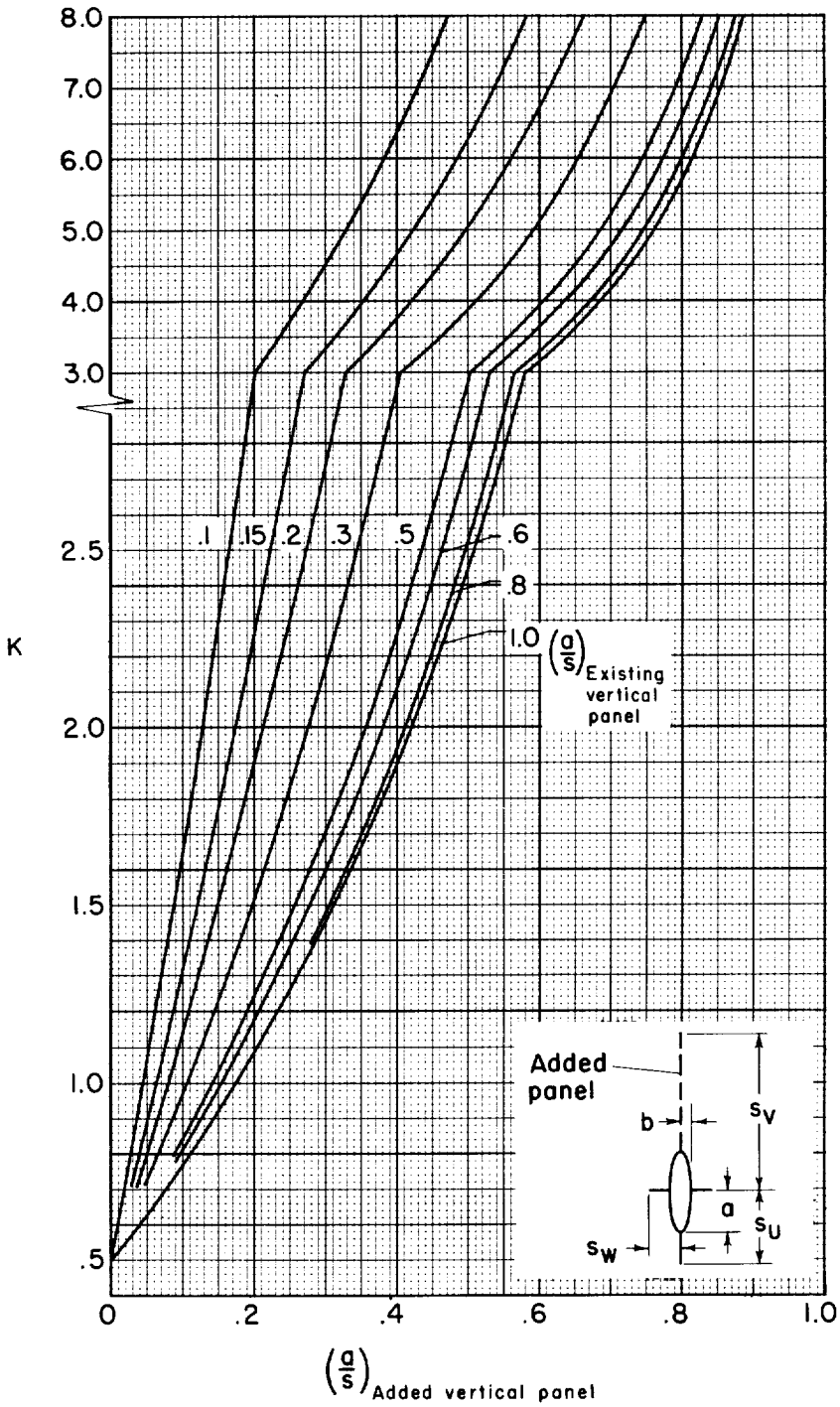

(c) b/s_H or $b/s_W = 0.4$

Figure 12.- Continued.

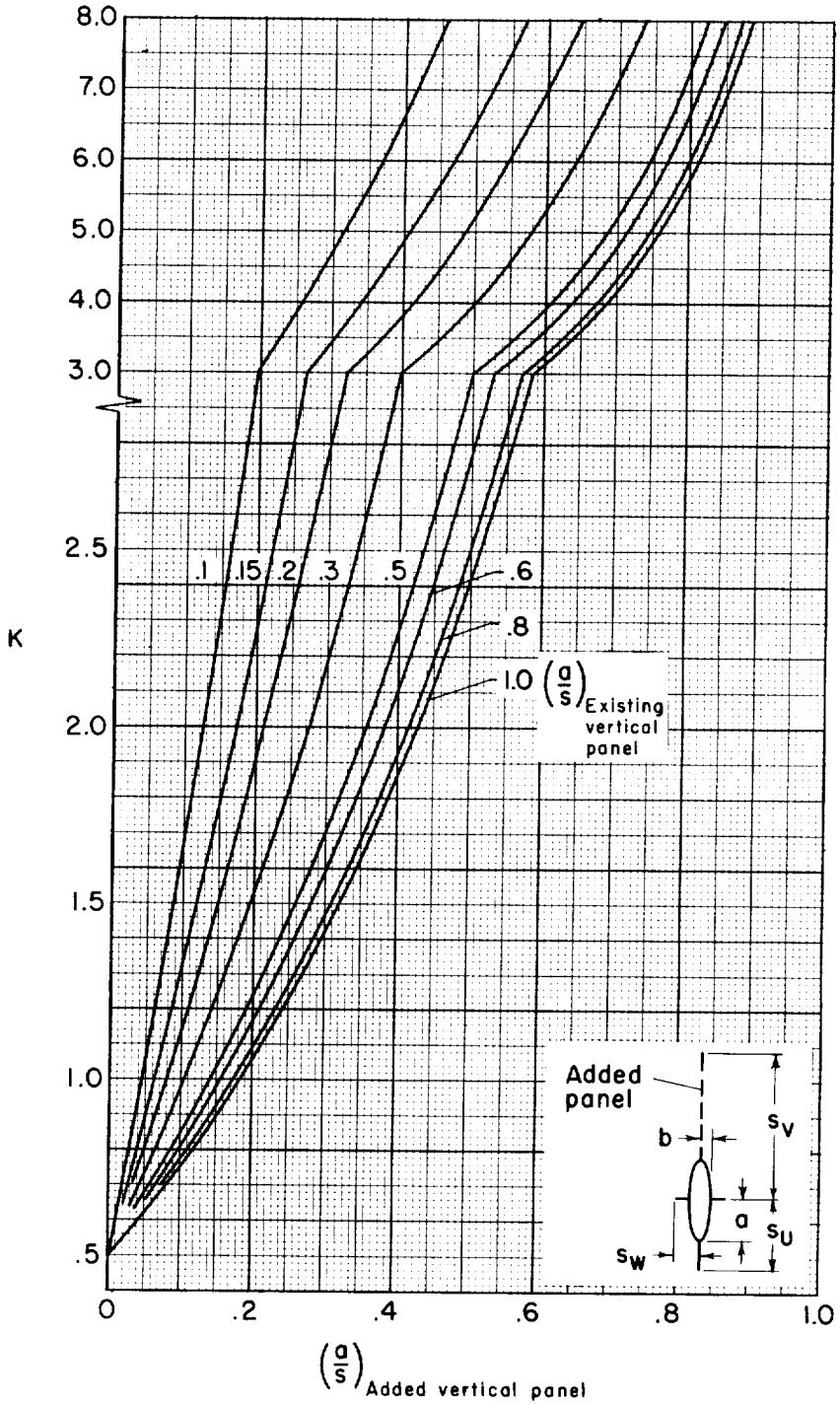

(d) b/s_H or $b/s_W = 0.6$

Figure 12.- Continued.

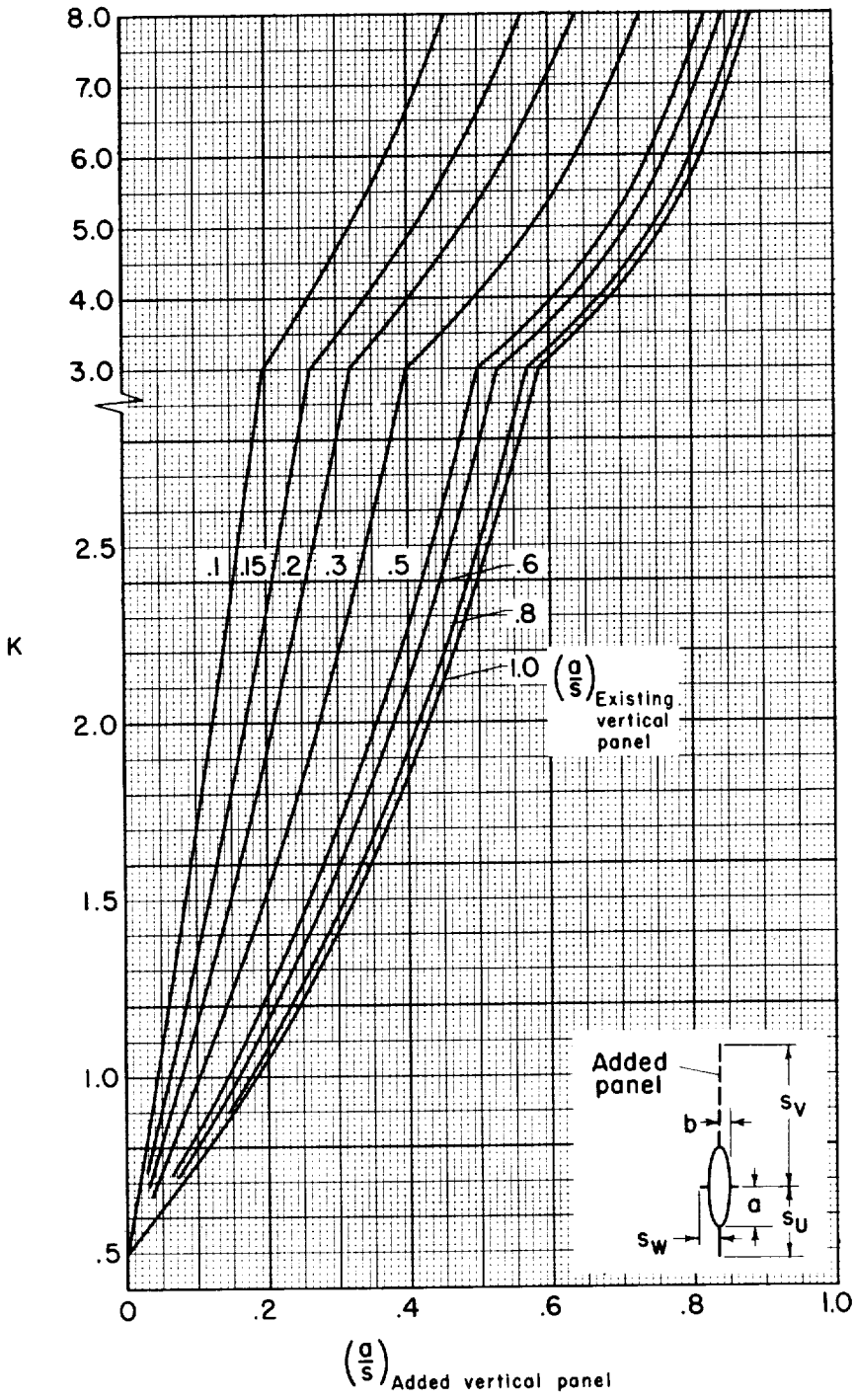

(e) b/s_H or $b/s_W = 0.8$

Figure 12.- Concluded.

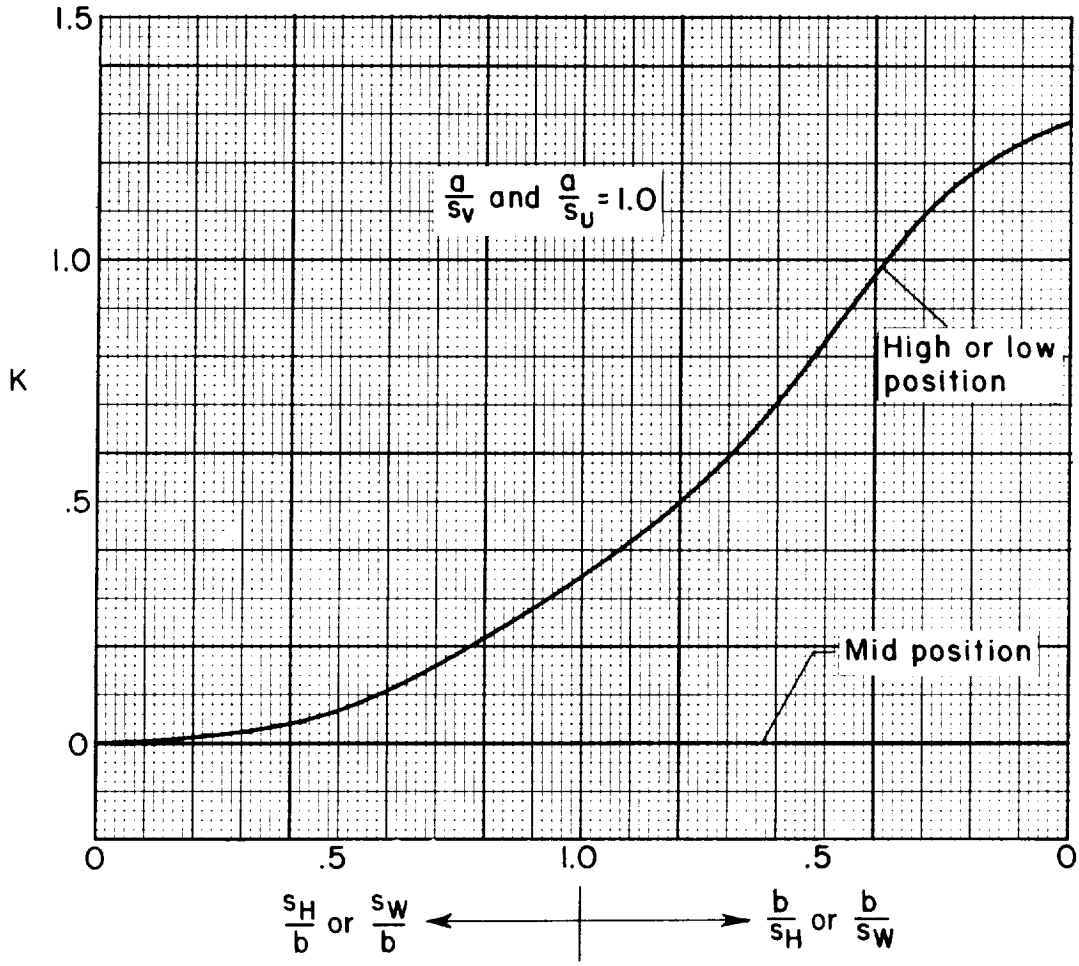

Figure 13.- Apparent mass ratio due to the addition of a horizontal surface to a circular body.

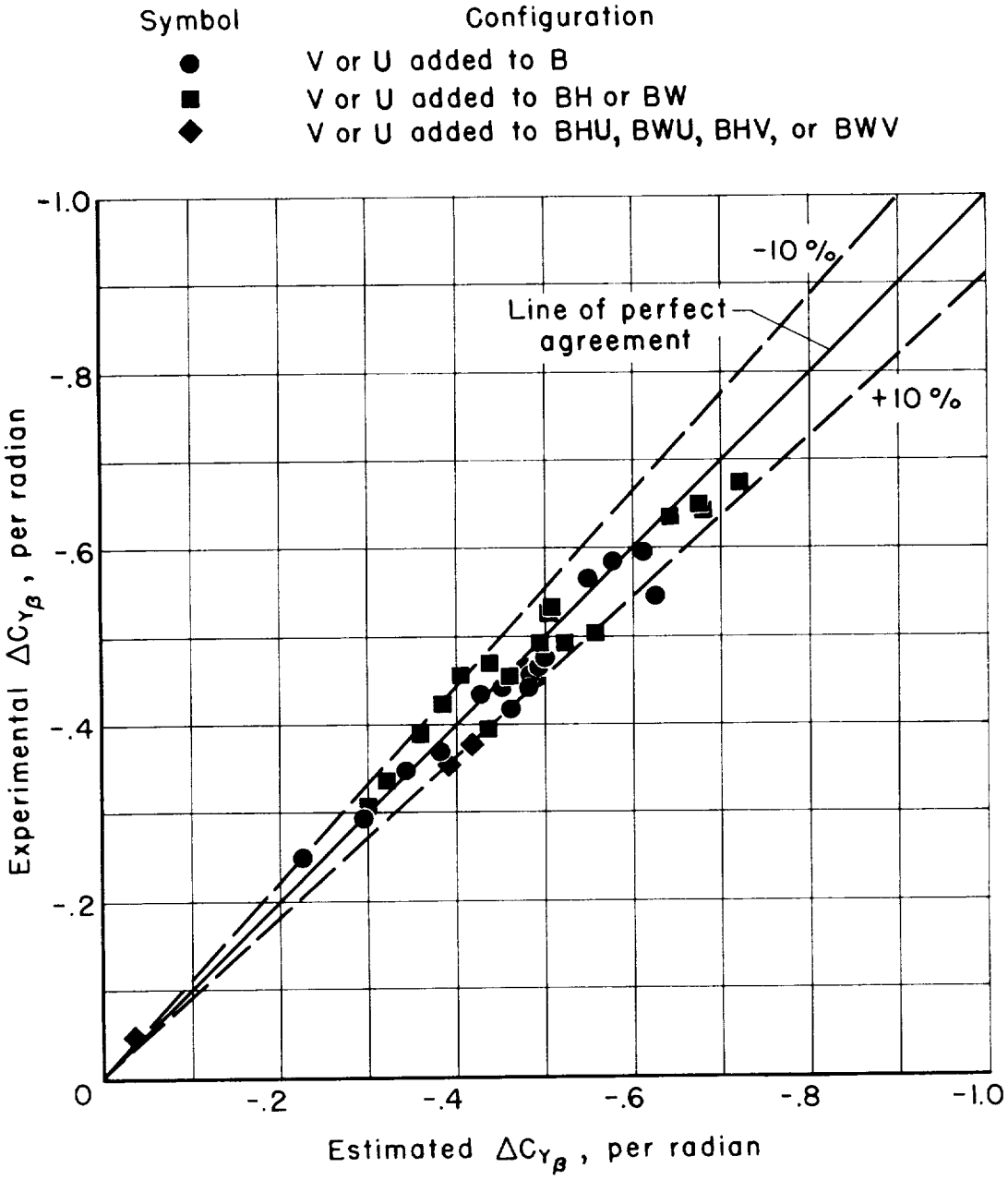

(a) Subsonic speeds.

Figure 14.- Correlation between estimated and experimental values of ΔC_{Y_β}

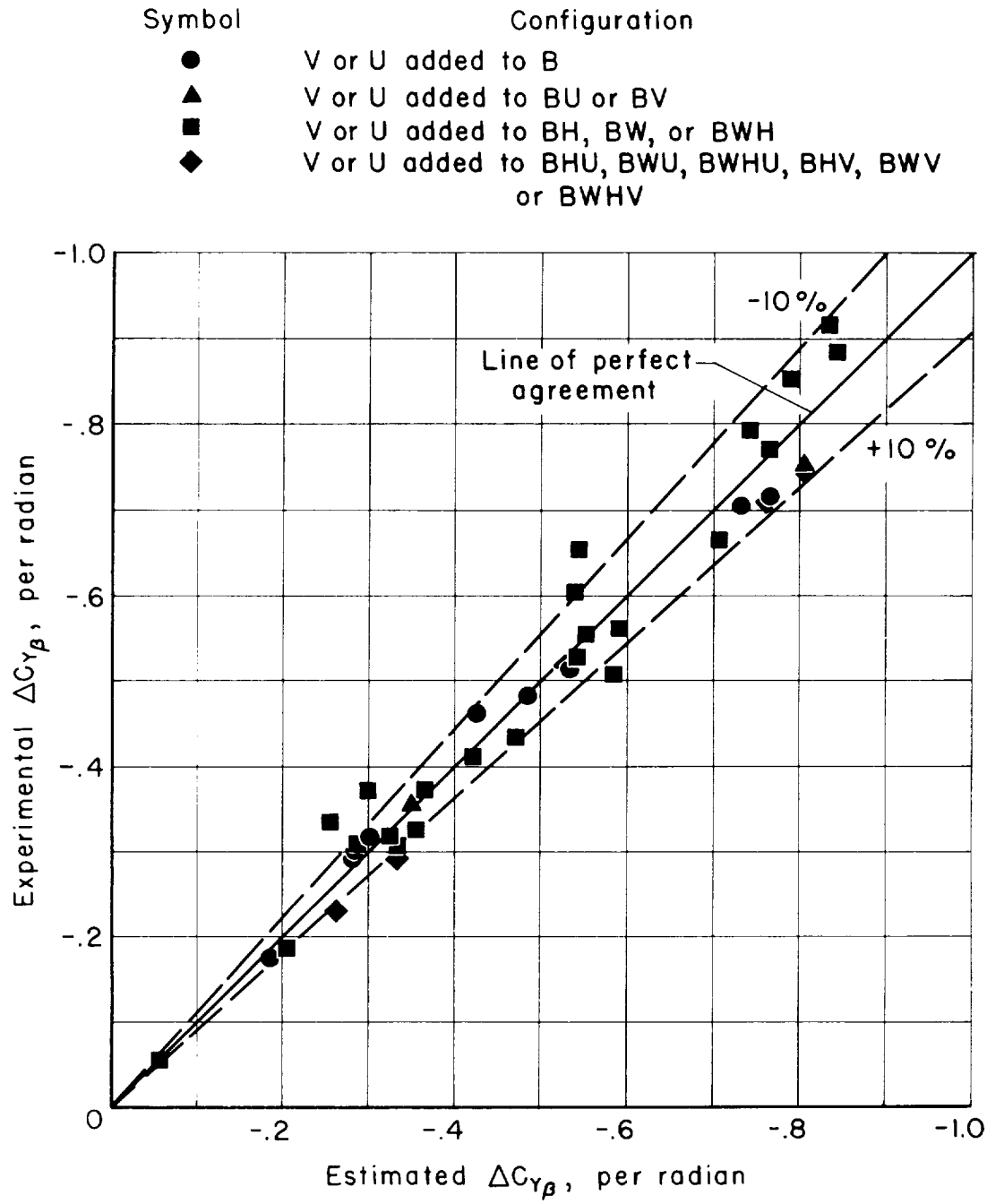

(b) Supersonic speeds.

Figure 14.- Concluded.

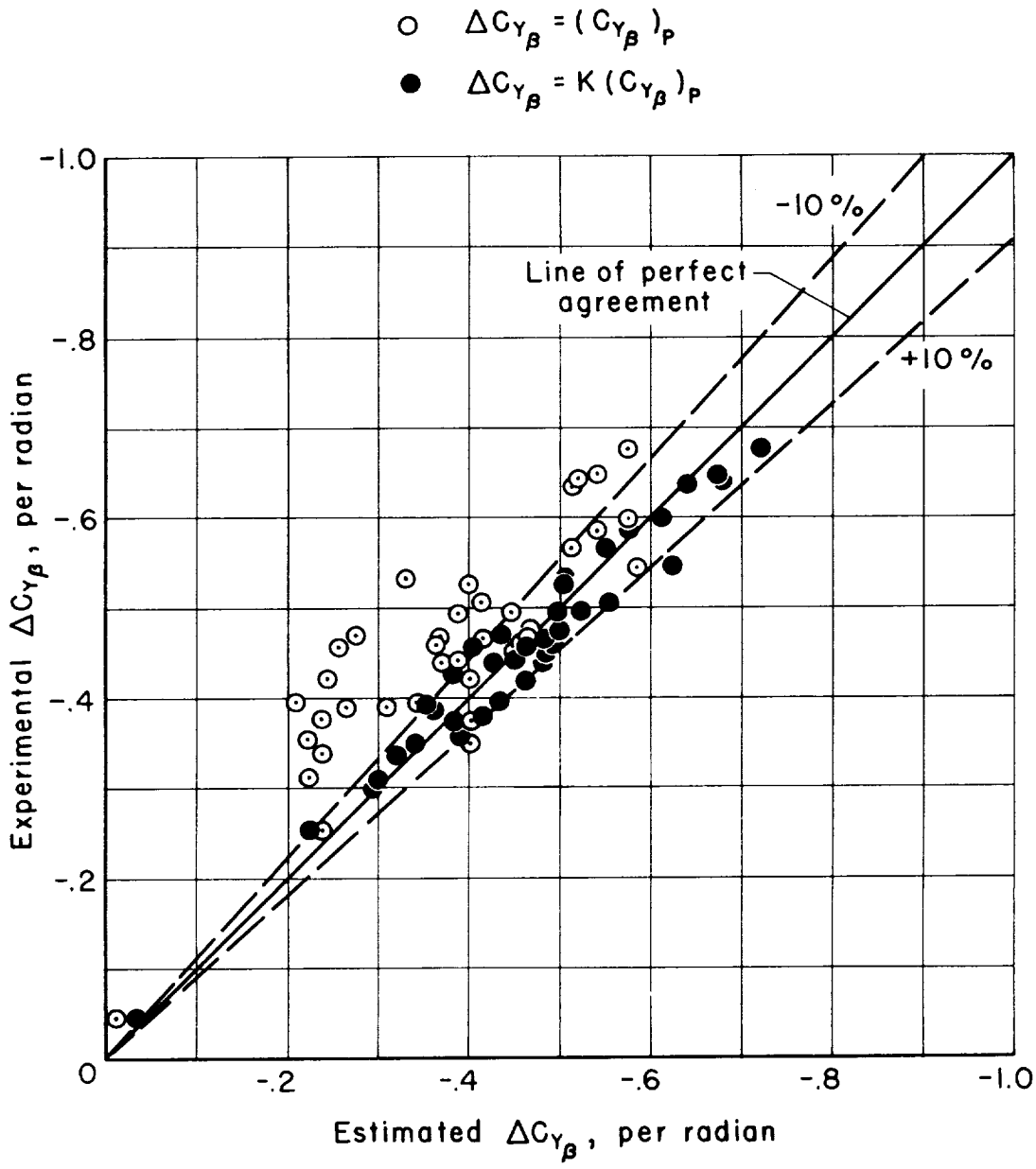

(a) Subsonic speeds.

Figure 15.- The improvement in the correlation between estimated and experimental values of ΔC_{Y_β} by the use of apparent mass ratios to account for interference.

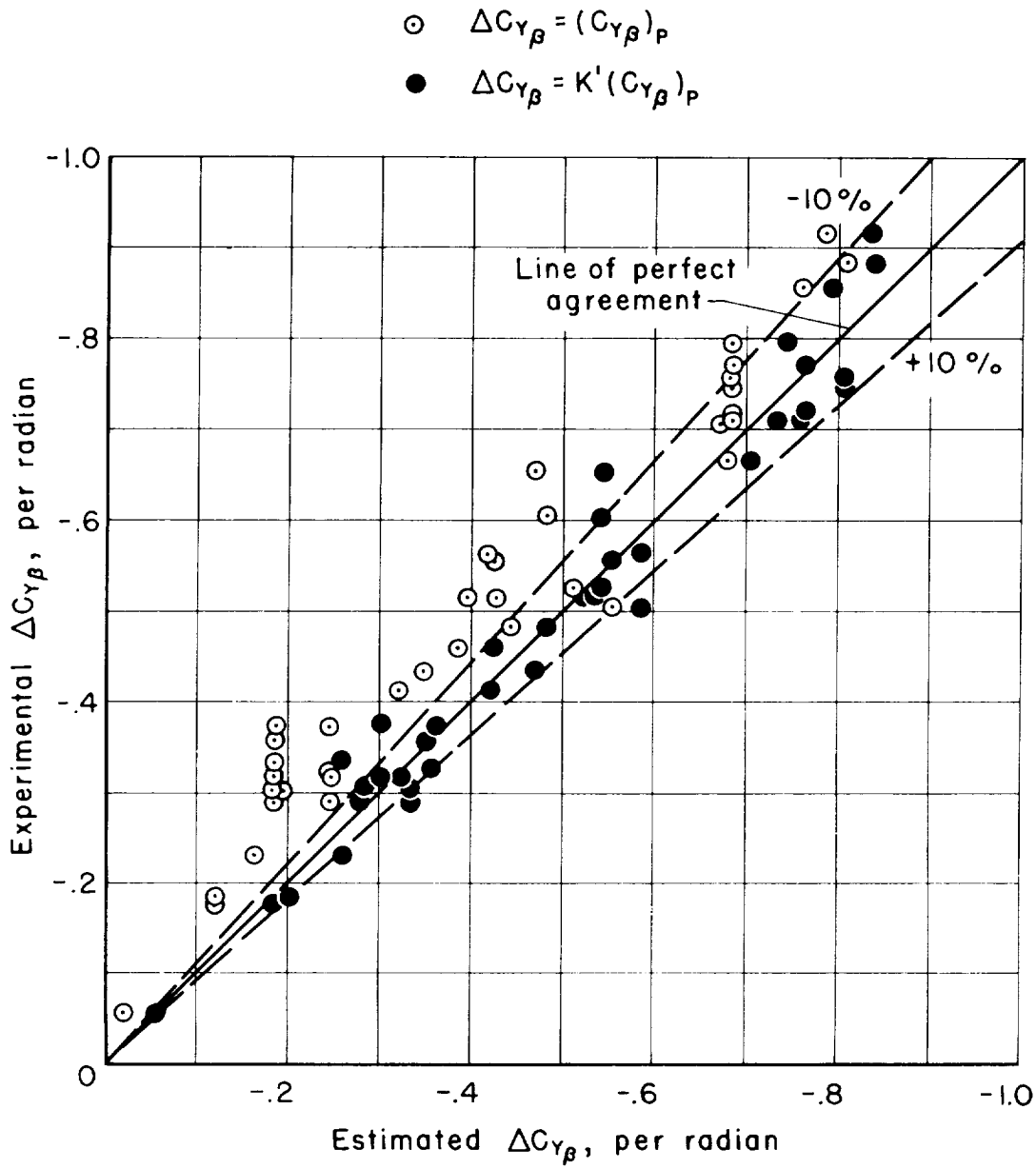

(b) Supersonic speeds.

Figure 15.- Concluded.

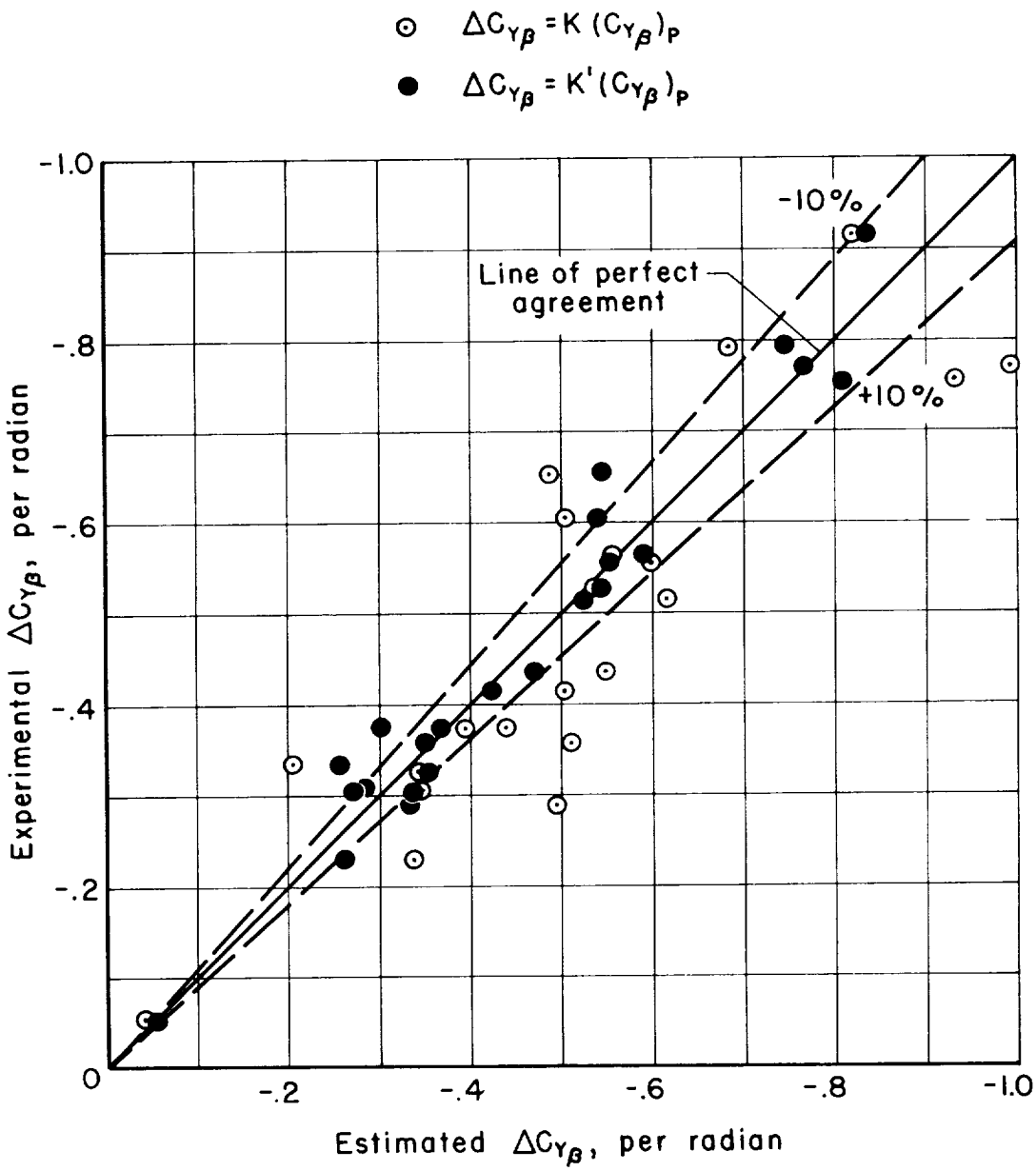

Figure 16.- The improvement in the supersonic $\Delta C_{Y\beta}$ correlation through the use of K' rather than K.

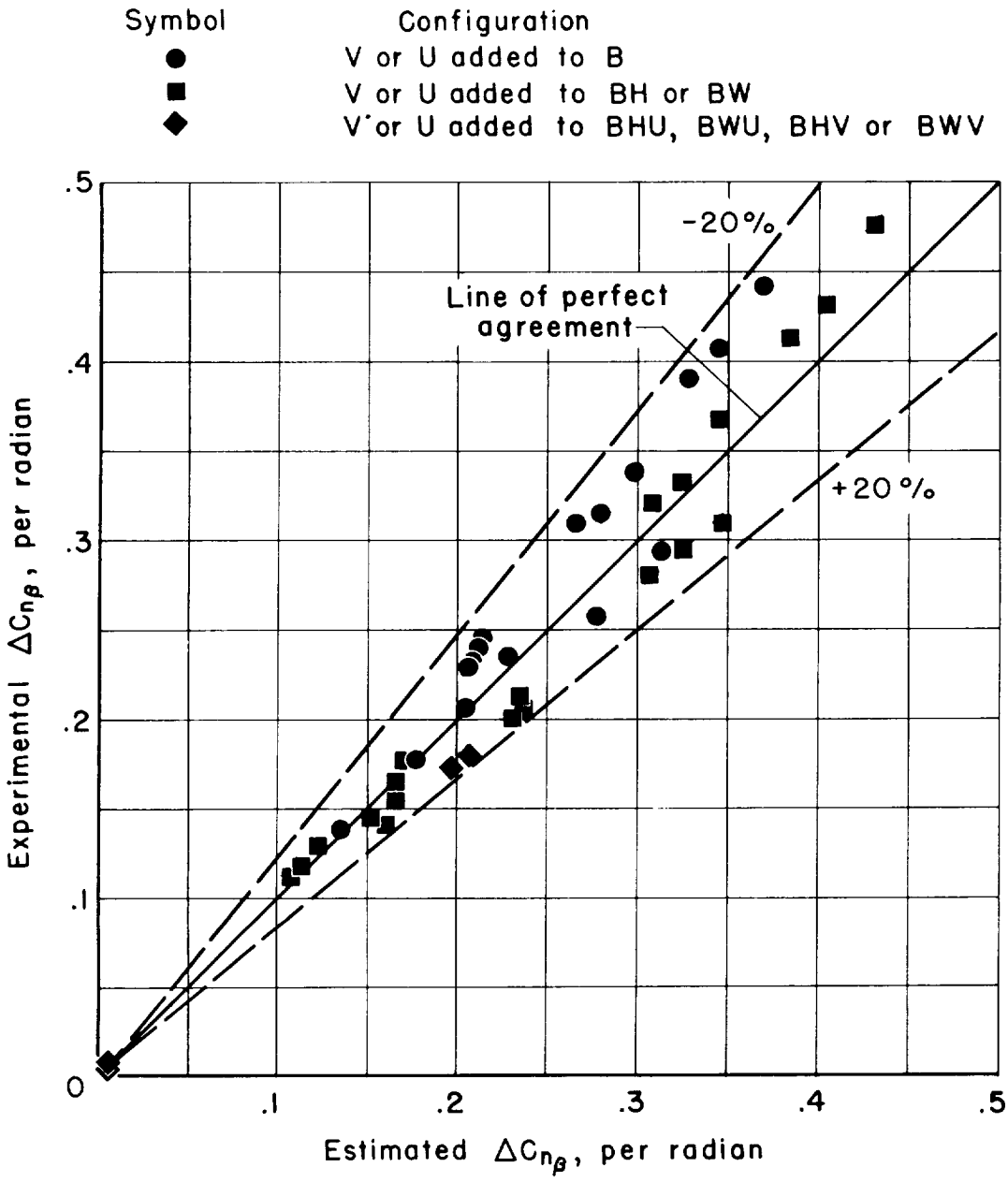

(a) Subsonic speeds.

Figure 17.- Correlation between estimated and experimental values of ΔC_{n_β}.

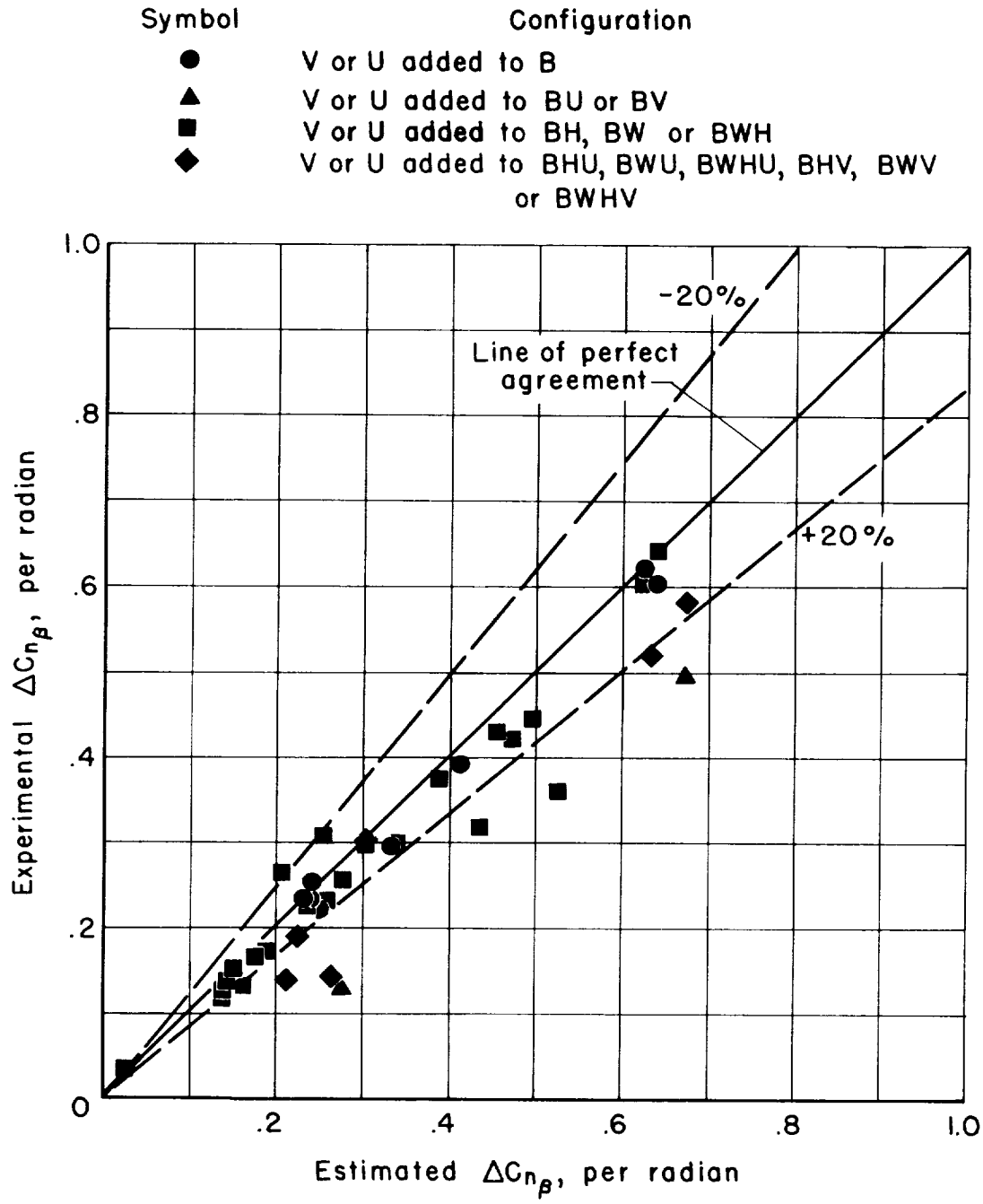

(b) Supersonic speeds.

Figure 17.- Concluded.

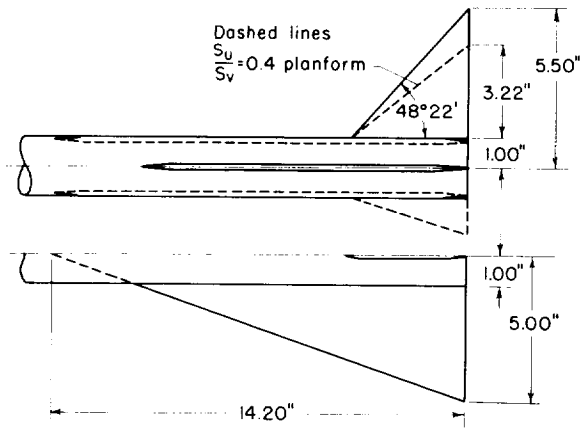

(a) Theoretical model.

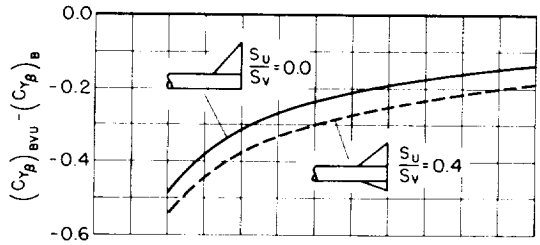

(b) Effect of shifting vertical stabilizing surface area.

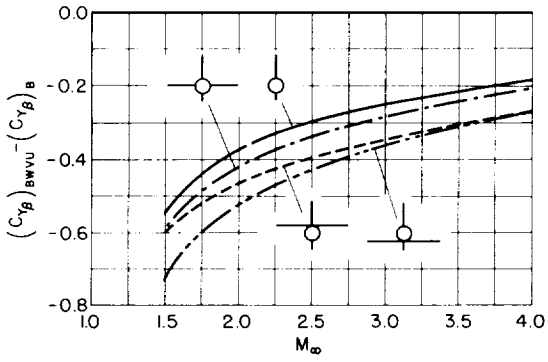

(c) Effect of adding a wing in various positions to $S_U/S_V = 0.4$ configuration.

Figure 18.- The effect of stabilizing surface arrangement on the total empennage side force. Aspect ratio of the original upper vertical tail is 4.5.

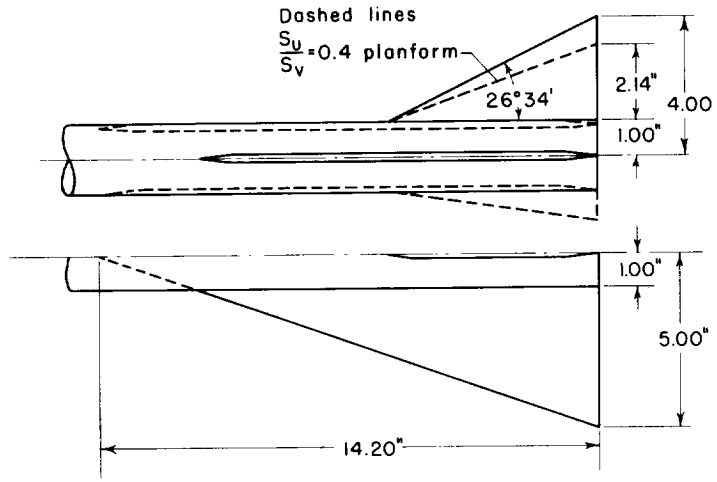

(a) Theoretical model.

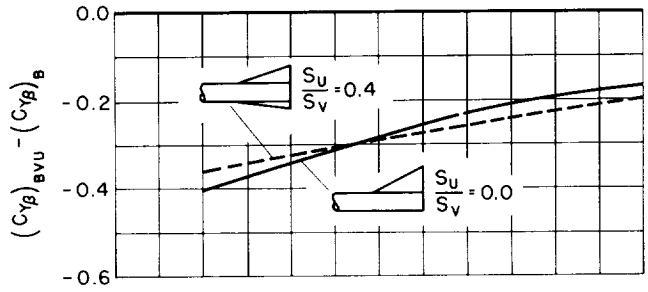

(b) Effect of shifting vertical stabilizing surface area.

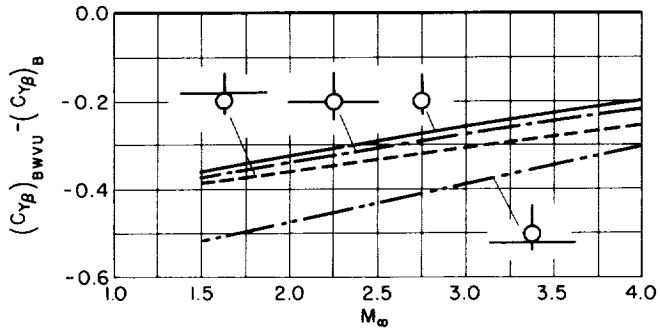

(c) Effect of adding a wing in various positions to $S_U/S_V = 0.4$ configuration.

Figure 19.- The effect of stabilizing surface arrangement on the total empennage side force. Aspect ratio of the original upper vertical tail is 2.0.